USF UNIVERSITY OF SOUTH FLORIDA

Civil and Environmental Engineering

EFFECTS OF DOWNDRAG ON PILE PERFORMANCE

BDV25-977-67

FINAL REPORT

Principal Investigator:

Gray Mullins, Ph.D., P.E.

with

Graduate Researchers

Malaak Araujo, E.I.
Tristen Mee, E.I.
Amanda Lewis, Ph.D., E.I.
and
Ruthvik Pendyala

May 2023

Disclaimer

The opinions, findings, and conclusions expressed in this publication are those of the authors and not necessarily those of the State of Florida Department of Transportation.

Approximate Conversions to SI Units

SYMBOL	WHEN YOU KNOW	MULTIPLY BY	TO FIND	SYMBOL
LENGTH				
in	inches	25.4	millimeters	mm
ft	feet	0.305	meters	m
yd	yards	0.914	meters	m
mi	miles	1.61	kilometers	km
SYMBOL	**WHEN YOU KNOW**	**MULTIPLY BY**	**TO FIND**	**SYMBOL**
AREA				
in^2	square inches	645.2	square millimeters	mm^2
ft^2	square feet	0.093	square meters	m^2
yd^2	square yard	0.836	square meters	m^2
ac	acres	0.405	hectares	ha
mi^2	square miles	2.59	square kilometers	km^2
SYMBOL	**WHEN YOU KNOW**	**MULTIPLY BY**	**TO FIND**	**SYMBOL**
VOLUME				
fl oz	fluid ounces	29.57	milliliters	mL
gal	gallons	3.785	liters	L
ft^3	cubic feet	0.028	cubic meters	m^3
yd^3	cubic yards	0.765	cubic meters	m^3
NOTE: volumes greater than 1000 L shall be shown in m^3				
SYMBOL	**WHEN YOU KNOW**	**MULTIPLY BY**	**TO FIND**	**SYMBOL**
MASS				
oz	ounces	28.35	grams	g
lb	pounds	0.454	kilograms	kg
T	short tons (2000 lb)	0.907	megagrams (or "metric ton")	Mg (or "t")

SYMBOL	WHEN YOU KNOW	MULTIPLY BY	TO FIND	SYMBOL
TEMPERATURE (exact degrees)				
°F	Fahrenheit	5 (F-32)/9 or (F-32)/1.8	Celsius	°C

SYMBOL	WHEN YOU KNOW	MULTIPLY BY	TO FIND	SYMBOL
ILLUMINATION				
fc	foot-candles	10.76	lux	lx
fL	foot-Lamberts	3.426	candela/m^2	cd/m^2
SYMBOL	**WHEN YOU KNOW**	**MULTIPLY BY**	**TO FIND**	**SYMBOL**
FORCE and PRESSURE or STRESS				
lbf	poundforce	4.45	newtons	N
lbf/in²	poundforce per square inch	6.89	kilopascals	kPa
kip	kilopound	4.45	kilonewtons	kN

SYMBOL	WHEN YOU KNOW	MULTIPLY BY	TO FIND	SYMBOL
LENGTH				
mm	millimeters	0.039	inches	in
m	meters	3.28	feet	ft
m	meters	1.09	yards	yd
km	kilometers	0.621	miles	mi
SYMBOL	**WHEN YOU KNOW**	**MULTIPLY BY**	**TO FIND**	**SYMBOL**
AREA				
mm^2	square millimeters	0.0016	square inches	in^2
m^2	square meters	10.764	square feet	ft^2
m^2	square meters	1.195	square yards	yd^2
ha	hectares	2.47	acres	ac
km^2	square kilometers	0.386	square miles	mi^2

SYMBOL	WHEN YOU KNOW	MULTIPLY BY	TO FIND	SYMBOL
VOLUME				
mL	milliliters	0.034	fluid ounces	fl oz
L	liters	0.264	gallons	gal
m^3	cubic meters	35.314	cubic feet	ft^3
m^3	cubic meters	1.307	cubic yards	yd^3

SYMBOL	WHEN YOU KNOW	MULTIPLY BY	TO FIND	SYMBOL
MASS				
g	grams	0.035	ounces	oz
kg	kilograms	2.202	pounds	lb
Mg (or "t")	megagrams (or "metric ton")	1.103	short tons (2000 lb)	T

SYMBOL	WHEN YOU KNOW	MULTIPLY BY	TO FIND	SYMBOL
TEMPERATURE (exact degrees)				
°C	Celsius	1.8C+32	Fahrenheit	°F
SYMBOL	**WHEN YOU KNOW**	**MULTIPLY BY**	**TO FIND**	**SYMBOL**
ILLUMINATION				
lx	lux	0.0929	foot-candles	fc
cd/m^2	candela/m^2	0.2919	foot-Lamberts	fl
SYMBOL	**WHEN YOU KNOW**	**MULTIPLY BY**	**TO FIND**	**SYMBOL**
FORCE and PRESSURE or STRESS				
N	newtons	0.225	poundforce	lbf
kPa	kilopascals	0.145	poundforce per square inch	lbf/in^2
kN	kilonewtons	0.225	kilopound	kip

*SI is the symbol for the International System of Units. Appropriate rounding should be made to comply with Section 4 of ASTM E380.

Technical Report Documentation Page

1. Report No.	2. Government Accession No.	3. Recipient's Catalog No.
4. Title and Subtitle EFFECTS OF DOWNDRAG ON PILE PERFORMANCE		5. Report Date March 2023
		6. Performing Organization Code
7. Author(s) G. Mullins, M. Araujo, T. Mee, A. Lewis and R. Pendyala		8. Performing Organization Report No.
9. Performing Organization Name and Address University of South Florida Department of Civil and Environmental Engineering 4202 E. Fowler Avenue, ENB 118s Tampa, FL 33620		10. Work Unit No. (TRAIS) 11. Contract or Grant No. BDV25-977-67
12. Sponsoring Agency Name and Address Florida Department of Transportation 605 Suwannee Street, MS 30 Tallahassee, FL 32399		13. Type of Report and Period Covered Final Report 02/01/20-05/31/23 14. Sponsoring Agency Code
15. Supplementary Notes FDOT Project Manager: Larry Jones		

Regardless of the soil type, density, or consistency, all soils settle under the weight of newly constructed embankments. The magnitude and rate of the settlement is largely affected by the site-specific soil properties and layer thicknesses. Embankments are the most common and cost-effective method of transitioning grade separation or over-water bridges to the roadway grades on either side of the bridge. The most common construction sequence is to drive piles prior to embankment construction. In these cases, settlement of the soils beneath the embankment begins after pile installation and hence the downward movement of the existing soils induces downward side shear loads on the piles called downdrag. Upper portions of the pile therefore contribute to the top of pile structural load all of which must be resisted by lower portions of the pile which resist downdrag and bridge loads. The transition point between downward and upward pile forces defines a neutral point where the highest pile load is experienced.

Prior to this study, the effects of loose compressible sandy soils have been largely disregarded with respect to downdrag largely due to the immediate nature of the settlement and those effects are not seen later as a service-related maintenance problem. However, forces caused by downdrag from compressible sands are present, nonetheless.

This study instrumented piles in end bents and the soil beneath the embankments at three bridge sites to monitor the progression of construction-induced loads in the piles with focus on downdrag forces in the piles. Sites were selected where loose sandy soils were anticipated to produce a measurable amount of settlement. Results showed downdrag was among the highest permanent loads on the pile and that transient loads thought to not superimpose with downdrag were additive. Findings suggest that downdrag should be evaluated for all piles where embankments are constructed after pile installation.

17. Key Words	18. Distribution Statement
Driven piles, settlement in sands, embankments, downdrag force	No restrictions.

19. Security Classif. (of this report)	20. Security Classif. (of this page)	21. No. of Pages	22. Price
Unclassified.	Unclassified.	137	

Form DOT F 1700.7 (8-72) Reproduction of completed page authorized

Acknowledgments

The authors would like to acknowledge the Florida Department of Transportation for funding this project, with specific thanks to Larry Jones, Juan Castellanos, Dr. David Horhota, Rodrigo Herrera, and the entire FDOT review team for their insightful contributions. Similarly, the following companies and entities are acknowledged for their contributions to the successful completion of the project: CDS Manufacturing, Inc., EXP U.S. Services, Inc., FDOT District Engineers, FDOT SMO Drill Crew, Foundation & Geotechnical Engineering, LLC, GRL Engineers, Inc., HNTB Corporation (special thanks to John Bosnoian), Prince Construction, SACYR Construccion, and Southern Concrete Products.

Executive Summary

Regardless of the soil type, density, or consistency, all soils settle under the weight of newly constructed embankments. The magnitude and rate of the settlement is largely affected by the site-specific soil properties and layer thicknesses. Embankments are the most common and cost-effective method of transitioning grade separation or over-water bridges to the roadway grades on either side of the bridge. The most common construction sequence is to drive piles prior to embankment construction. In these cases, settlement of the soils beneath the embankment begins after pile installation and hence the downward movement of the existing soils induces downward side shear loads on the piles called downdrag. Upper portions of the pile therefore contribute to the top of pile structural load all of which must be resisted by lower portions of the pile which resist downdrag and bridge loads. The transition point between downward and upward pile forces defines a neutral point where the highest pile load is experienced.

Prior to this study, the effects of loose compressible sandy soils have been largely disregarded with respect to downdrag largely due to the immediate nature of the settlement and to effects that are not seen later as a service-related maintenance problem. However, forces caused by downdrag from compressible sands are present, nonetheless.

This study instrumented piles in end bents and the soil beneath the embankments at three bridge sites to monitor the progression of construction-induced loads in the piles with focus on downdrag forces in the piles. Sites were selected where loose sandy soils were anticipated to produce a measurable amount of settlement. Results showed the downdrag forces were among the highest permanent loads on the pile and that transient loads (thought to not superimpose with downdrag forces) were additive. Findings suggest that downdrag should be evaluated for all piles where embankments are constructed after pile installation.

Table of Contents

List of Figures

List of Tables

Chapter One: Introduction

1.1 Background

Regardless of the soil type, density, or consistency, all soils settle under the weight of newly constructed embankments. The magnitude of the settlement, however, is largely affected by the site-specific soil properties and layer thicknesses. Embankments are the most common and cost-effective method of transitioning grade separation or over-water bridges to the roadway grades on either side of the bridge. In Florida, mechanically stabilized earth (MSE) walls have become the bridge approach embankment of choice due to the smaller footprint (compared to slope-sided embankments). Figure 1.1 shows the exterior face of an MSE wall under construction along I-75 in Sarasota County (left) and a completed embankment at the time of pile cutoff in Naples, Florida (right).

Figure 1.1 Early stages of embankment filling and MSE wall construction (left); final stages behind MSE wall (right).

Construction sequencing dictates how embankment settlement interacts with piles located behind the wall. The most common construction practice is to drive piles prior to embankment construction and where the MSE wall straps can be negotiated around the pile locations. In these cases, settlement of the existing soils begins after pile installation, and hence the downward movement of the existing soils will induce downward side shear loads on the piles called downdrag (DD). While the magnitude of embankment settlement is not thought to be significantly reduced by the presence of the piles, the magnitude of downdrag forces transferred into the piles is minimized by preventing friction between the newly placed backfill material and the piles. Methods of eliminating or drastically reducing the pile-backfill side shear vary, but a common method entails double wrapping the pile with plastic sheeting above the natural ground after pile installation and before placing fill. This creates a slick interface between the plastic sheets. Other methods include coating the pile with bituminous material to create a weak bond or a combination of the two approaches.

Regardless of whether the fill material bonds with the pile, there is always some downward movement of the existing soil that contributes to downdrag, and it is important to identify the depth at which no significant settlement occurs: a neutral point of zero side shear. Pile embedment below that depth contributes to withstanding all downward loads and movements; the pile length above that depth contributes to downdrag and does not resist downward loads from the bridge. Depending on the

amount of embankment settlement and the depth to the neutral side shear resistance, there can be a significant portion of the upper pile length experiencing negative side shear (Figure 1.2).

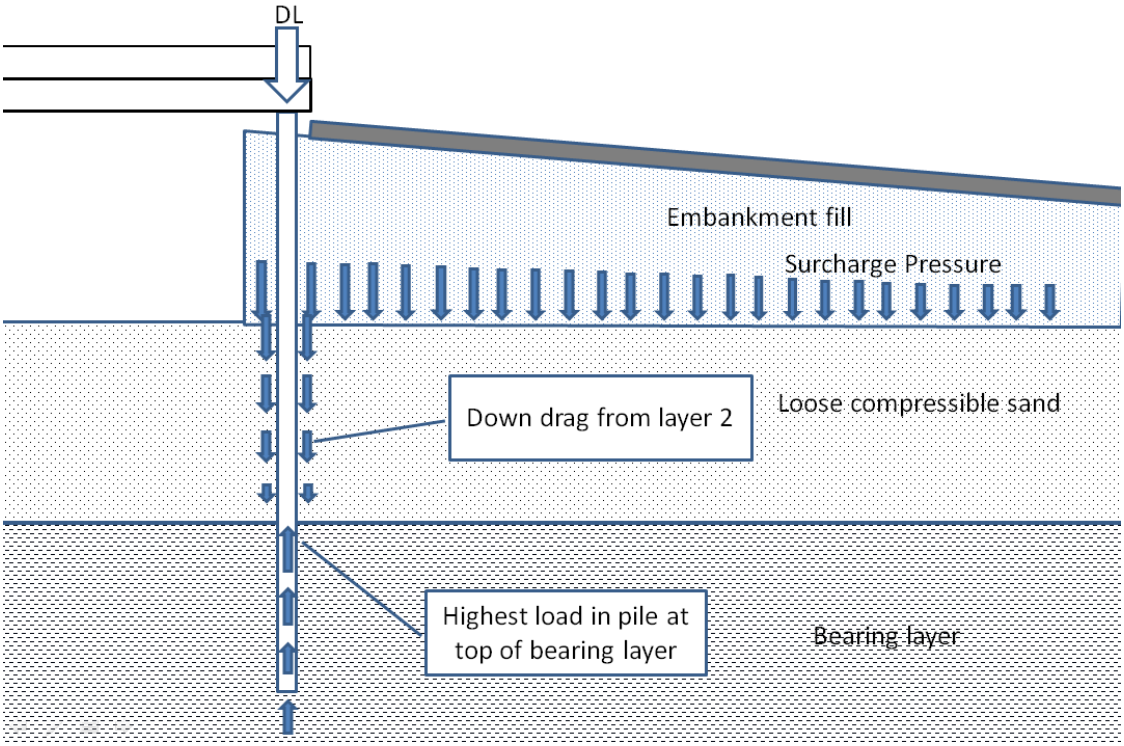

Figure 1.2 Side shear reversal near or at the interface between compressible soil and bearing layer.

AASHTO treats downdrag, DD, as a permanent load in all load combinations including when there is live load, LL (Table 1.1). The general approach in designing for downdrag is to simply add it to all other downward loads (i.e., bridge dead load + live load + downdrag, etc.) when in fact these loads do not necessarily add; they do however superimpose.

Superposition of displacements suggest that additional temporary loads not shown in Figure 1.2 and which do not add to the surcharge pressure on the compressible layer reduce the amount of negative side shear. This is possible by way of temporary elastic shortening of the pile which in turn reduces the amount of negative side shear strain in the compressible layer contributing to downdrag. It is further conceivable that live load may not add load to the pile in the bearing layer region under some circumstances. The parameters that affect this phenomenon include: the magnitude of the downdrag and the magnitude of the live load; downdrag is further dependent on the compressible layer thickness, soil type, soil density or consistency, the height of the embankment which in turn affects the length of the pile and the magnitude of elastic shortening. While the motivation for this study stems from driven concrete pile performance, drilled shafts and now augered cast-in-place piles are also vulnerable to settlement-induced downdrag in bridge embankments.

A primary motivation for this study was to identify scenarios where downdrag can and cannot be ignored.

Table 1.1 AASHTO load cases where live loads (LL) are always combined with downdrag (DD).

Load Combination Limit State	*DC DD DW EH EV ES EL PS CR SH*	*LL IM CE BR PL LS*	*WA*	*WS*	*WL*	*FR*	*TU*	*TG*	*SE*	Use One of These at a Time				
										EQ	*BL*	*IC*	*CT*	*CV*
Strength I (unless noted)	γ_p	1.75	1.00	—	—	1.00	0.50/1.20	γ_{TG}	γ_{SE}	—	—	—	—	—
Strength II	γ_p	1.35	1.00	—	—	1.00	0.50/1.20	γ_{TG}	γ_{SE}	—	—	—	—	—
Strength III	γ_p	—	1.00	1.00	—	1.00	0.50/1.20	γ_{TG}	γ_{SE}	—	—	—	—	—
Strength IV	γ_p	—	1.00	—	—	1.00	0.50/1.20	—	—	—	—	—	—	—
Strength V	γ_p	1.35	1.00	1.00	1.00	1.00	0.50/1.20	γ_{TG}	γ_{SE}	—	—	—	—	—
Extreme Event I	1.00	γ_{EQ}	1.00	—	—	1.00	—	—	—	1.00	—	—	—	—
Extreme Event II	1.00	0.50	1.00	—	—	1.00	—	—	—	—	1.00	1.00	1.00	1.00
Service I	1.00	1.00	1.00	1.00	1.00	1.00	1.00/1.20	γ_{TG}	γ_{SE}	—	—	—	—	—
Service II	1.00	1.30	1.00	—	—	1.00	1.00/1.20	—	—	—	—	—	—	—
Service III	1.00	γ_{LL}	1.00	—	—	1.00	1.00/1.20	γ_{TG}	γ_{SE}	—	—	—	—	—
Service IV	1.00	—	1.00	1.00	—	1.00	1.00/1.20	—	1.00	—	—	—	—	—
Fatigue I— *LL, IM & CE* only	—	1.75	—	—	—	—	—	—	—	—	—	—	—	—
Fatigue II— *LL, IM & CE* only	—	0.80	—	—	—	—	—	—	—	—	—	—	—	—

The primary objective of this study was to instrument, monitor and collect data from piles behind embankments that are anticipated to have measurable amounts of downdrag and settlement (new construction) with the motivation of determining under what circumstances downdrag is a critical load and when it is not. A secondary objective focused on refining the FDOT design criteria for the inclusion of downdrag computations.

1.2 Organization of the Report

This report includes five ensuing chapters presenting the efforts undertaken to assess the effects of downdrag on pile performance. Chapter 2 provides background from past studies. Chapter 3 presents the review of various sites scrutinized for inclusion in the study. Chapter 4 presents initial instrumentation and Chapter 5 the data collection and presentation of the data. Chapter 6 concludes with recommendations stemming from the study findings.

Chapter Two: Literature Review

This chapter provides a synopsis of 36 references [articles, reports, specifications, and guidelines] on the topic of pile downdrag where they have been categorized under the following general topics:

- Codes and Specifications
- Reports and Guidelines
- Field and Lab Measurements
- Load Transfer
- Neutral Plane Method
- Pile Groups
- Bituminous Coatings, and
- Finite Element Modeling.

A section on Future Work is also provided which includes preparations for Task 2 measurements and Task 3 in the form of preliminary finite element modeling.

2.1 Introduction

The design and construction of driven piles is an interdisciplinary and iterative process that involves the roles of structural, geotechnical, and construction engineers. Upon determining the need for a deep foundation, the geotechnical engineer chooses candidate piles (or other foundation elements) for the structural engineer to evaluate. The structural engineer and geotechnical engineer collaborate to calculate structural and geotechnical capacities of the proposed piles, respectively. After performing pile drivability analyses, the geotechnical engineer estimates the size of the pile foundation and produces pile loads for every limit state. An iterative design process ensues where the geotechnical engineer estimates embedment depth for both vertical and lateral loads and checks group efficiency. Service limit states are then checked by performing settlement analyses. Following the determination of the depth of the neutral plane and calculation of the resulting drag force, the structural strength limit state is checked. Economic evaluation is performed, and the preliminary substructure design is complete. After refinement of the superstructure design and load analyses by the structural engineer, the geotechnical engineer reevaluates the substructure design, and refines if necessary. If all limit states are satisfied, the structural engineer designs the pile cap. The geotechnical engineer then finalizes the substructure design and coordinates production of the plans and specifications with the structural engineer. After evaluating the contractor's equipment, the geotechnical engineer establishes the final pile lengths and driving criteria. The information gathered from the test piles is evaluated and the construction plan is revised, as necessary. The construction engineer then monitors the installation process. Finally, the geotechnical engineer conducts post-construction evaluation (Hannigan et al. 2016).

Shaft resistance (side shear) forces develop when there is relative movement between the piles and the soil surrounding the piles. In cases of recently filled embankments surrounding previously driven piles, the settlement of the soil is larger relative to the settlement of the piles. The soil settlement creates friction alongside the piles, resulting in a downward force dragging the piles down. This

downward force on the piles is known as downdrag. Other instances in which downdrag can be induced include lowering of the water table (increases effective stresses), liquefaction, or consolidation of recently filled or compressible soil. Some mitigation techniques for reducing downdrag include preloading the site to consolidate the surrounding soil before driving the piles, as well as minimizing friction through use of bitumen coating or polyethylene wrap.

Determination of the neutral plane and computation of the magnitude of the downdrag developed is a substantial step in the design process of driven piles. When the surrounding soil moves downward relative to the piles, the downward side shear resistance is known as negative shaft resistance, or previously known as negative skin friction. The neutral plane is the location where the negative shaft resistance transitions to positive shaft resistance and where relative pile-soil settlement is zero. Above this plane, soil settlement is greater than pile settlement, resulting in negative shaft resistance. Below this plane, the pile settlement is greater than the soil settlement and the frictional forces act in a positive (upward) direction. Briaud and Tucker (1997) provide some clues (Table 2.1) as to when downdrag may cause potential problems and should be considered in design. A warning that downdrag may occur even if the listed conditions are not met was placed below the table.

Table 2.1 Indicators for potential downdrag problems (Briaud and Tucker 1997)

1.	The total settlement of the ground surface will be larger than 100 mm (4 in)
2.	The settlement of the ground surface after the piles are driven will be larger than 10 mm (0.4 in)
3.	The height of the embankment to be placed on the ground surface exceeds 2 m (6.5 ft)
4.	The thickness of the soft compressible layer is larger than 10 m (33 ft)
5.	The water table will be a drawn down by more than 4 m (13 ft)
6.	The piles will be longer than 25 m (82 ft)

There have been various documented structural failures of deep foundations due to the presence of downdrag. Johannessen and Bjerrum (1965) reported the failure of driven steel piles embedded in clay and bearing on rock in Norway. Settlement of the clay under the weight of over 30 feet (10 m) of fill led to high stresses, elastic shortening, and ultimately failure of the pile. The downdrag reportedly caused the pile to penetrate the underlying rock layer. Brand and Luangdilok (1975) tracked the history and structural failure of a concrete building in Southeast Asia due to downdrag forces. The building, which was supported by piles driven through soft clay, was reported to experience differential settlements of 3.9 to 12 inches (10 to 30 cm). Davisson (1993) presented various unpublished cases of pile foundation failures caused by negative skin friction. All the structures settled excessively and in some instances the structures collapsed. Some of the errors that led to these failures included failure to anticipate the effect of future dewatering and the effect of adjacent ground loading, improper downdrag analysis, and failure to drive the pile adequately into the bearing layer.

There has been much published on the effects of downdrag on piles embedded in soft clay. The literature on downdrag in cohesionless granular soils is sparse; of the citations listed herein, 18 explicitly dealt with soft clays, two with sands, one with silt, and nine with multiple soil profiles. The

objective of this study is to investigate the influence of downdrag and subsequent drag force on driven piles embedded in compressible sands.

2.2 Codes and Specifications

Appendix C of FDOT (2020) Soils and Foundation Manual lists a procedure for downdrag analysis of a driven pile. The first steps involve determining the soil profile and corresponding soil properties, as well as determining the surcharge pressure from the embankment fill. Next is to determine settlement of the pile and of the surrounding soil. The total surrounding soil settlement is determined by summing the settlement for each soil layer along the embedded pile length. The portion of the pile that experiences downdrag is then determined by comparing the settlement between the pile and surrounding soil. Thus, the next step involves determining the magnitude of negative shaft resistance along the upper length of the pile which experiences 0.5 inches or greater of relative settlement. The ultimate pile capacity is then computed by summing the toe resistance with the positive shaft resistance developed along the lower portion of the pile. The net ultimate pile capacity is calculated by taking the difference between the ultimate pile capacity and the negative shaft resistance. The value of downdrag is determined by summing the negative shaft resistance with the driving resistance of the soil inducing the negative shaft resistance. The driving resistance for sand and silty sand is approximately 75% of the ultimate skin friction. It may be higher for clean sands. The nominal pile resistance is then the sum of the factored design load, net scour, and downdrag, all of which are divided by a resistance factor.

While FDOT states that the relative movement needed to mobilize downdrag is 0.5 in, AASHTO (2017) states 0.4 in of movement is needed. AASHTO treats the downdrag as a load to be included in the geotechnical strength limit state design analysis. AASHTO presents four cases in which downdrag can occur. In the cases where mitigation techniques are not implemented to prevent downdrag development, the deep foundation must be designed to resist the additional load. AASHTO allows for the neutral plane method for downdrag analysis. It is stated that it is conservative to combine the transient loads with downdrag. Both FDOT and AASHTO reference NCHRP Report 393 (Briaud and Tucker 1997) for downdrag analysis.

The FHWA *Design and Construction of Driven Pile Foundations* (Hannigan et al. 2016) states that downdrag does not ultimately affect geotechnical capacity, because as a pile approaches nominal geotechnical capacity, all shaft resistance is in the upward direction (meaning no downdrag in that state). As there have been relatively few transportation structures with downdrag related problems, the AASHTO current approach of a geotechnical strength limit state has been conservative (Hannigan et al. 2016). Instead, an approach that considers downdrag in the geotechnical service limit state and pile structural strength limit state is recommended and presented.

2.3 Reports and Guidelines

Meyerhof (1976) states that while negative skin friction may be insignificant for friction piles, it may be more consequential for end bearing piles. It is noted that the negative skin friction mobilized in clay generally increases linearly with depth (even though relative movement decreases with depth). Additionally, in clay, the long-term negative skin friction can be estimated from the drained shear

strength. It was concluded that settlement of pile groups in homogenous sand not underlain by more compressible soil can be estimated using Equivalent Pier Foundation Method.

In his report for the design of pile foundations, Vesic (1977) describes the mechanism of load transfer and discusses the phenomenon of residual loads experienced by driven piles. These residual loads affect the foundation load-settlement response. It is stated that downdrag is a function of effective vertical stress. Additionally, it is concluded that the damaging effect of negative skin friction on pile performance is minimized so long as the live load is larger than the downdrag force.

When describing the mechanisms of pile resistance, the author referenced his earlier work (Vesic 1969) and stated only 0.4 inches of relative movement are needed to mobilize skin friction in sand, regardless of the foundation size and length. The introduction to the negative skin friction section of the report stated that previous discussion was related to load transfer between pile and soil in normal circumstances. "Normal" referring to relative settlement induced by the pile itself, rather than by downdrag related circumstances. The author then suggested that a relative movement of 0.6 inches may be adequate to fully mobilize negative skin friction Based on observations and results from investigations on multiple continents, Fellenius (1989) states that Vesic's suggestion of "rather large" relative settlement is an exception. Instead, extremely small movement needed to mobilize negative skin friction is the rule. Fellenius then states that Vesic's suggestion should be an indication as to when settlement could be an issue for a pile foundation. Basically, Fellenius said that more evidence pointed towards smaller relative settlements being required (hence the "rule"), while larger relative settlements *could* be an exception.

Lambe and Baligh (1978) wrote a pamphlet which provided a method for predicting downdrag in piles. They state that the mechanism of shaft resistance is a function of effective horizontal stress which is in turn a function of effective vertical stress. Several methods of predicting negative skin resistance were presented. These methods included the Beta Method, the Terzaghi-Peck Method, De Beer Method, and more. At the time, the Beta Method was the recommended procedure for predicting downdrag. Lambe concluded the pamphlet with the greatest challenge of making accurate predictions: determination of the appropriate parameters. The appendix of the pamphlet included a manual for "Downdrag Prediction on End Bearing Piles." This manual elaborates on the beta method for downdrag prediction.

Lambe and Baligh also present the results of an interesting downdrag symposium. Several downdrag experts were provided with information needed to make downdrag predictions. These predictions were submitted to a referee (Prof. Peck) who locked them away in a safe. The research team then carried out the experiment and recorded the results. Prior to revealing the experimental results, the initial predictors presented their predictions. The results were then revealed, and each predictor evaluated their predictions. The purpose of the symposium was to demonstrate the difficulty of making accurate downdrag predictions.

Briaud and Tucker (1997) provided pile design and construction guidelines for both coated and uncoated piles. The presented method is based on static equilibrium of the vertical forces of the pile, as well as relative pile-soil movement compatibility. Piles bearing on hard, incompressible layers generate relatively small pile settlement when compared to the surrounding soil. This results in a neutral plane closer to the bottom of the compressible layer, and thus increased downdrag. Since the highest compressive forces experienced by the pile are at the neutral plane, they suggested that when

designing the pile for structural failure, one should consider the capacity at both the top of the pile and at the neutral plane. Additionally, since transient loads only temporarily reverse the downdrag forces, they are not typically considered at the neutral plane. Briaud and Tucker concluded that the ultimate plunging load for a pile is the same regardless of downdrag.

Davisson et al. (1983) presents various studies to establish allowable stresses in piles. Recommendations and changes to the AASHTO Specifications were proposed. They also discuss the importance of considering downdrag and negative skin friction when designing pile foundations. It was noted that load tests may not adequately demonstrate the structural capacity of a pile subjected to downdrag. During a load test, full positive skin friction is mobilized, resulting in the load transfer to be away from the pile tip. Under service conditions, however, downdrag can be a factor, resulting in the load transfer occurring towards the pile tip. Thus, caution was advised when designing piles for downdrag even with the aid of load tests.

Allen (2005) presented recommended downdrag load factors for piles based on calibration results of two general cases. The cases that were investigated involved concrete and steel piles with soil profiles of downdrag-inducing clay overlaying sand.

2.4 Field and Lab Measurements

Bozozuk (1972) monitored downdrag effects on a steel pipe friction pile in clay. The pile was part of a bridge abutment constructed over a soft embankment in Canada. Field measurements over a period of five years were plotted to observe the load distribution in the test pile. Bozozuk concluded that the skin friction forces acting on the pile were related to the effective horizontal stresses. Additionally, the in situ shear strength of the soil was concluded not to be related to the mobilized skin friction. The skin friction reduced to the remolded strength when there were excess pore pressures and large relative movements. On the other hand, the skin friction approached drained soil strength when there were small relative movements and pore pressures dissipated.

Koerner and Mukhopadhyay (1972) performed laboratory experiments to evaluate the behavior and effects of negative skin friction. The effects of pile group spacing, batter piles, and water content were also evaluated. The model tests involved a one-inch diameter pile placed within a three-foot diameter and three-foot high tank containing medium plastic silt. The pile was fixed in place to simulate an end bearing pile, and thick surcharge load plates were placed around the pile. Under low surcharge pressures, the upper portion of the pile carried the full downdrag force. Increasing the surcharge load resulted in higher relative settlement, in turn causing the downdrag force to descend towards the bottom of the pile as the negative skin friction was further mobilized (Figure 2.1). In other words, the higher the applied surface load, the more the downdrag accumulated and traveled farther down the pile before being transferred to the soil. The experiments demonstrated that smaller spacing to diameter ratios resulted in lower average negative skin friction values. Additionally, the study concluded that the average negative skin friction increased as water dissipated. This study did not show the classic neutral point or neutral plane typically associated with downdrag forces. In fact, a proving ring attached to the top of the pile is referenced but no values of force are presented in Figure 2.1. In short, the findings are somewhat inconclusive and vaguely presented.

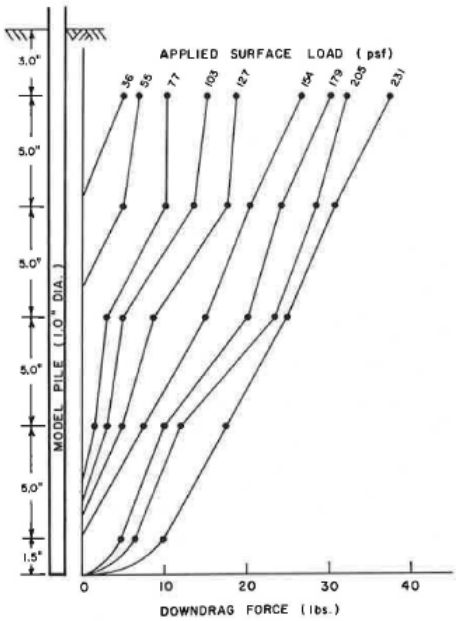

Figure 2.1 Distribution of downdrag force (Koerner and Mukhopadhyay 1972)

Fellenius (1972) presents the results of over three years of field measurements conducted on two driven piles through 130 feet of soft clay. Consolidation of the clay layer after driving resulted in relative settlement and the development of negative skin friction. The negative skin friction caused the forces in the piles to increase. It was observed that although applying load to the pile head eliminated negative skin friction, it began to return as relative settlements continued to take place. Recommendations for consideration of negative skin friction when designing pile foundations were also provided. The author has since then disregarded these recommendations (Fellenius 1997).

After conducting experiments consisting of medium sand underlain by a consolidating layer of peat, Bakholdin and Berman (1974) concluded that negative skin friction is only mobilized during the active settlement of the surrounding soil. The negative skin friction forces essentially disappear after consolidation of the compressible soil layers surrounding the piles stop. Additionally, the experiments demonstrated that for maximum mobilization of negative skin friction forces, soil-to-pile relative settlement should be on the order of nearly two inches (5 cm) or greater. Bakholdin and Berman also state that estimating negative skin friction solely from comparison of pile and surrounding soil settlement generally leads to incorrect computation and thus an unjustified reduction in pile capacity. Instead, it is suggested to estimate negative skin friction forces based on the rates of settlements of the piles and surrounding soil with respect to time. This suggested method considerably reduces the calculated negative skin friction forces when compared to previous methods and may even be negligible in some cases.

Indraratna et al. (1992) present the results of both long-term and short-term measurements on driven piles in soft clay in Bangkok. Both uncoated and bitumen-coated piles were instrumented and monitored. Negative skin friction was found to be fully mobilized three to six months after the embankment was surcharged. Compared to the uncoated piles, the coated piles experienced a significant reduction in negative skin friction. The full-scale measurements were compared to the data gathered from the short-term pullout tests. Based on the comparable results, it was concluded

that pullout test results can reasonably predict the negative skin friction of driven piles. Another way of predicting the negative skin friction involves the effective stress approach. A finite element method numerical analysis was also carried out to predict the skin friction. As downdrag is a function of relative settlement, it was stated that downdrag predictions are contingent on the accuracy of settlement computations. It was suggested to use residual values rather than peak values of the friction angle for the interface elements of the numerical models. The authors also proposed that maximum downdrag is reached as a critical value of normalized relative settlement is approached.

Fellenius (2006) presents a summary of several field studies performed in the 1960s through the 1990s. The studies were performed worldwide and involved driven steel and concrete piles. The field studies demonstrated that when piles are driven in soft, compressible soils, drag forces would be imposed on the piles. The results of static load pile testing performed by Bozozuk in 1981 illustrate that live load replaces drag load in a pile. All shaft resistance on the pile was positive after applying the static load on the pile; thus, the development of negative shaft resistance did not affect the geotechnical capacity of the pile. Fellenius concludes that for the temporary live load to effectively cancel out what he calls "the drag load," it must be twice the magnitude of the drag load at the neutral plane. Additionally, the maximum load seen by the pile is a sum of the dead load and drag load and occurs at the neutral plane. It is pointed out that the neutral plane represents both a location of force equilibrium within the pile and a location of zero relative pile-soil movement. Since locating the neutral plane through settlement computations is more likely to result in higher error, the location should be determined by either direct instrumentation or through resistance analysis.

Budge et al. (2015) synthesized the data of several monitored driven pile projects conducted by Minnesota Department of Transportation (MnDOT). These projects involved the instrumentation and monitoring of driven piles to investigate the effects of downdrag; a total of five projects were evaluated. It was evident from the results of these projects that the maximum forces the piles experienced occurred farther down the pile, rather than at the pile top. In some cases, the structural loads seen by the piles were greater than expected design loads. While the observed cases did not encounter deficiencies, it was noted that current practices underestimate downdrag. It was concluded that overall load increased over time, and that downdrag should be considered a permanent load when determining structural capacity.

2.5 Load Transfer

Coyle and Reese (1966) established a relationship between the pile movement, load transfer, and soil shear strength of steel friction piles in clay. The results of field studies illustrated that the percentage of shear strength developed is dependent on pile movement and lateral pressure. This relationship can be utilized to compute load-settlement curves.

Matyas and Santamarina (1994) evaluated and compared the rigid-plastic method of downdrag prediction to the elastic-plastic method. As the rigid-plastic method assumes full mobilization of toe resistance, positive and negative skin friction, it was concluded that the method overestimates both downdrag and the neutral plane depth. The authors presented the elastic-plastic model which implemented a closed-form solution to estimate negative skin friction. Some of the limitations and consequences of the presented model assumptions included relative stiffness, nonlinear settlement, nonuniform variation of shaft resistance, and construction history.

Poulos (2008) examined the effects that residual stresses may have on piles subjected to downdrag. It was concluded that piles with residual stresses experienced less downdrag than those which were initially stress-free. Thus, driven piles would likely have less downdrag effects than bored piles. Poulos also analyzed the effects of live load with respect to negative skin friction and suggested that the amount of live load required to cancel out the negative skin friction would be greater than allowable.

Kuhns (2008) states that as little as 0.15 inches of pile movement are needed to mobilize maximum skin friction resistance. The author discusses how the bearing capacity approach of pile design practice may not be reliable with respect to the effects of downdrag. Instead, a settlement-based approached should be utilized to properly account for the negative implications that downdrag may have on pile performance. This settlement-based analysis evaluates whether pile settlement is within tolerance and the structural integrity of the pile remains intact. The author also discussed the influence of live loads and residual loads. Interestingly, the residual load-transfer curve of a pile immediately after being driven had the same characteristics as the load-transfer curve from negative skin friction loads. The procedure for determining the depth of the neutral plane was presented because this is the first step in downdrag analysis. Finding the location of the neutral plane is an iterative process that involves calculating soil settlement, skin resistances in both directions, toe resistance, pile tip penetration, and pile settlement. The neutral plane depth is determined when the magnitudes of the soil settlement and pile settlement converge. A spreadsheet for this procedure, titled "SETTLE-DOWN," was developed to assist with concrete pile settlement calculations. The calculations in the spreadsheet are the same as those programmed into FDOT FB-Deep and FB-MultiPier. It was concluded that, prior to applying structural loads to a pile, settlement of the surrounding soil will compress the pile as well as the soil under the pile tip. After structural dead loads are applied, this pile and soil precompression limits pile settlement.

Stanton et al. (2015) provide an evaluation of semi-empirical *t-z* analysis methods for drilled shafts. The *t-z* relationships are discrete nonlinear springs used to model side friction and predict load-settlement response. It was concluded that the recently developed analysis approach is suitable for predicting axial loading response of drilled shafts. It was also stated that while the studied methods can be adapted for driven piles, more research is needed to provide an appropriate criterion for anything other than drilled shafts.

Dias and Bezuijen (2018) provide a framework for pile analysis under loading and unloading. A brief literature review on load-transfer analysis was performed, and it was concluded that there are still many discrepancies between various load-transfer methods. Despite these uncertainties, there are some common themes that are agreed upon. One of these being that the amount of displacement needed to fully mobilize shaft resistance is much smaller than the amount needed to fully mobilize toe resistance. A trilinear shaft mobilization model is proposed where shaft resistance is a function of relative displacement. An elastic-plastic behavior is adopted where once full mobilization of the shaft resistance has been reached, the shaft resistance remains constant while displacement continues to develop. The variation from the traditional load-transfer models is that a relationship for unloading is presented. Because pile loading is not perfectly elastic, it is reasonable to expect a response for the unloading stage. This is especially true because pile head settlements do not return to their original state upon removing the load. Thus, if unloading occurs after the plastic state has been reached, the

displacements follow an unloading slope. A toe mobilization model is also presented where toe resistance is a function of positive relative displacement. It was advised that any set of mobilization functions should be calibrated with field and/or centrifuge tests.

2.6 Neutral Plane Method

Fellenius (1989) presented a unified design approach for designing piles and pile groups. This approach, later known as the neutral plane method, involves the relationship between negative skin friction, compression, capacity, and settlement. Fellenius begins by presenting past cases of negative skin friction development along piles in clay, and he concluded that all piles experience this phenomenon. This conclusion was made on the basis that since a pile is much more rigid than soil, and since there will always be soil settlement over time (even without surcharge loads), relative settlements are inevitable. Additionally, small relative settlements will be enough to induce shear forces on the piles.

The iterative method starts out by determining the location of the neutral plane, then checking the structural strength of the pile. The structural strength at the pile top, considers dead load and live load. Only dead load and dragload are considered at the neutral plane for structural strength—no live load. If the strength is adequate, the settlement of the piles is calculated by placing an equivalent footing at the neutral plane. The final step is to verify the bearing capacity of the pile where all portions of the pile contribute in the bearing resistance and downdrag is not considered. The bearing capacity thereby supports dead and live loads but excludes dragload.

Interestingly, Wang and Brandenberg (2013) suggest the assumption that pile settlement is equivalent to soil settlement at the depth of the neutral plane is false. Instead, it is proposed that pile settlement velocity is equal to soil settlement velocity at that depth. The traditional neutral plane solution is valid only if the neutral plane depth is constant. Since the location of the neutral plane changes over time, it is proposed to calculate pile displacement as an integral of soil settlement velocity. A neutral plane method was proposed with the assumption that relative velocity at the neutral plane is zero.

2.7 Pile Groups

Depending on the geometry of the pile group, the effects of negative skin friction on a single pile may differ from the effects on piles in a group configuration. Briaud and Tucker (1997) further state that the interior piles within a pile group can experience as little as 15% of the downdrag force experienced by the corner piles. It was then suggested to place a curtain of sacrificial or “dummy” piles surrounding the pile group to experience most of the downdrag effects, and thus the inner piles can be designed with lighter consideration to downdrag.

Kuwabara and Poulos (1989) analyzed the effects of downdrag forces on symmetrical pile groups by extending the simplified boundary element procedure previously used for single pile evaluation. It was concluded that a large movement of soil is required for the magnitude of the loads experienced by the single and group piles to be similar. Furthermore, as pile spacing decreases, the maximum downdrag forces seen by the piles significantly reduce. Additionally, the tops of outer piles within a rigid cap may experience tensile forces.

2.8 Bituminous Coatings

Lambe and Baligh (1978) further presented several methods of reducing negative skin friction when the induced loads are expected to be large. These methods included electric-osmosis to release soil-pile friction, pre-loading to eliminate post-pile-installation settlement, casing to prevent soil-pile contact, and application of a friction reducer. Emphasis was placed on the friction reducer application, specifically bitumen, as this was the basis of their research, and the other methods were costly or impractical. The bitumen was selected as it is an adequate viscoelastic substance which can both behave elastically under rapid pile-driving conditions and offer little resistance to negative shearing under slower loading.

Tawfiq (1994) investigated and compared the effectiveness of bitumen coating and polyethylene sheeting as a means of reducing downdrag in piles. The studies were conducted using both well-graded sand and well-graded gravel. Various parameters need to be considered when using a bitumen coating on piles. These parameters including temperature, soil type, bitumen type, shearing rate, and normal stress affected the bitumen ability to mitigate downdrag. On the contrast, factors such as particle size, deformation rate, and temperature did not affect the polyethylene sheeting's shearing characteristics. It is stated that the development of downdrag on short piles of approximately 26 feet (8 m) or less is negligible.

In their design and construction guidelines, Briaud and Tucker (1997) concluded that the proper application of bitumen on driven piles would be sufficient to reduce negative shaft resistance.

2.9 Finite Element Modeling

Jeong et al. (1997) utilized the program ABAQUS to conduct 3D nonlinear finite element models. The modeled elastic pile was surrounded by initially linear elastic soil, followed by elastic-plastic material. These models were validated by comparing results with previous theoretical and field studies. Parametric analysis was performed to evaluate the influence of pile group spacing, end bearing and friction piles, and soil type. It was concluded that linear analysis of downdrag calculation is largely conservative when compared to nonlinear analysis. Additionally, the interior piles within a cap experience substantially less downdrag force than the exterior piles.

Jeong et al. (2014) analyzed the behavior of piles embedded in soft soils through both long-term field monitoring and 3D finite element (FE) numerical modeling. Two conventional negative skin friction analysis methods were presented: the shear strength method (α-method) and the effective stress method (β-method). The α-method is a function of clay strength and pile material, while the β-method is a function of pile material, pile installation method, and soil type. The field monitoring involved 16 test piles in various soil conditions in three different locations in Korea. Each site had fill placed two weeks to one month after pile installation. The hyperbolic fitting method was applied to evaluate final settlement. The α and β values were calculated from the field measurements to examine and interpret the negative skin friction behavior. The numerical analysis was conducted with PLAXIS 3D and was compared to the field results. A single pile under soil consolidation was modeled. The pile was characterized as linear-elastic, the sand layers as linearly elastic-perfectly plastic, and the clay layers as soft soil creep materials. Parametric analysis was performed to observe the influence of

interface property, uncoated versus coated pile, and pile tip location. It was concluded that an extensive 3D FE analysis can be utilized to approximate dragload distribution.

Tan and Fellenius (2016) validated the unified pile design concept through finite-element method (FEM) models with PLAXIS 2D and PLAXIS 3D. The soil profile included a fill and thick, soft clay layer overlying a stiff soil layer. A Mohr-Coulomb model was utilized for the pile-soil interface. The 2D model involved a single pile, while the 3D model involved a symmetrical pile group. Analysis of the single pile model led to the conclusion that the downdrag is a function of relative settlement. The pile group behavior followed that of previously observed field cases, where the inner piles had significantly less drag force than the outer piles. For a more economical structural loading approach, the lower drag forces experienced by the inner piles can be computed by the 3D FEM models and used in design. It was emphasized that negative skin friction is a serviceability issue, rather than a geotechnical capacity issue.

2.10 Chapter Summary

Regardless of the soil type, density, or consistency, all soils settle under the weight of newly constructed embankments. A summary of 36 sources was presented that dealt with both steel and concrete piles in clay, silt, and sand. Some sources note downdrag to be insignificant or unimportant while others note failures. Discrepancies most likely stem from variations in soil type, layer thicknesses, embedment length in the bearing layer, etc. These inconsistencies lead to uncertainty and confusion, both of which are undesirable in engineering practice.

Much of the published literature on the topic of downdrag has focused on soft clays. The long-term effects and nature of the clays likely attracted the attention of numerous researchers to deal with maintenance and service issues with settling approach embankments. Despite all the research that has been performed, it is still not clear whether all piles develop problematic downdrag forces particularly when embedded in compressible sands. Sands, which experience immediate settlement, may also be considered problematic and cause just as much or even more downdrag related issues. It was the intent of this study to address these points for sand applications in Florida soils by way of field measurements and selected numerical models.

Chapter Three: Instrumentation and Monitoring of Embankment Piles

3.1 Introduction

As noted earlier, downdrag occurs when the downward movement of soil settling around a pile (or pile group) is greater than the movement of the pile(s). In many cases, only a fraction of an inch of relative downward movement of the soil is required to fully develop the maximum side shear force on a pile in the form of upward or downward resistance. Numerous methods exist to predict soil settlement; two widely accepted methods were used is this study to assess the suitability of potential project sites: the FHWA Method (modified Hough Method) and Schmertmann Method. It should be noted that experience of many engineers has shown that settlement predictions in sands are often conservative by a factor of two to three.

The driving force for settlement of the soils around the piles stems from embankments constructed around piles already driven through native compressible soils. Thus, identifying bridge construction projects involving end bents and MSE walls, located on or near compressible sandy soils, wase essential for this study. Potential sites were assessed by analyzing the soil profiles and the pile driving logs to estimate relative settlement. Recall, this project focused on conditions where compressible cohesionless soils undergo immediate settlement and the bridge-supporting piles may be unwittingly loaded to levels above that anticipated by the designer at the onset of the bridge service life.

Three sites were selected for this study. Two sites were in FDOT District 2, the third site was in FDOT District 7. New vibrating wire technology capable of measuring dynamic events as well as static events was selected to streamline strain gauge installation requirements. The capabilities of the advanced system components, as well as the details of the sites under investigation are described in this chapter.

3.2 Settlement Prediction Methods

Downdrag is a pile shaft resistance force that develops alongside the piles. This force is mobilized by relative movement between the piles and the soil surrounding them. There are various ways to estimate immediate settlements. A discussion of the two methods used to estimate soil settlement under embankments at potential sites for this study is presented.

3.2.1 Modified Hough Method

The original Hough method provided a relationship between soil compressibility expressed as the Bearing Capacity Index (C') and SPT donut hammer blow counts. This original relationship was reported by the FHWA *Design and Construction of Driven Pile Foundations Volume I* to have the potential to overestimate settlements by a factor of two. The Modified Hough Method provides a correlation between C' and SPT blow counts from donut, safety, and automatic hammers (Figure 3.1); this modification was noted to improve settlement estimation accuracy (Hannigan et al. 2016). The equation to determine the settlement of each subdivided layer is provided in Eqn 3.1.

$$S = H\left(\frac{1}{C'}\right)\log\left(\frac{p_o+\Delta p}{p_o}\right) \qquad \text{Equation 3.1}$$

Where:

S = total layer settlement
H = initial soil layer thickness
C' = Bearing Capacity Index from Figure 3.1
p_o = vertical effective stress at midpoint of layer prior to stress increase
Δp = distributed embankment pressure at the center of the layer

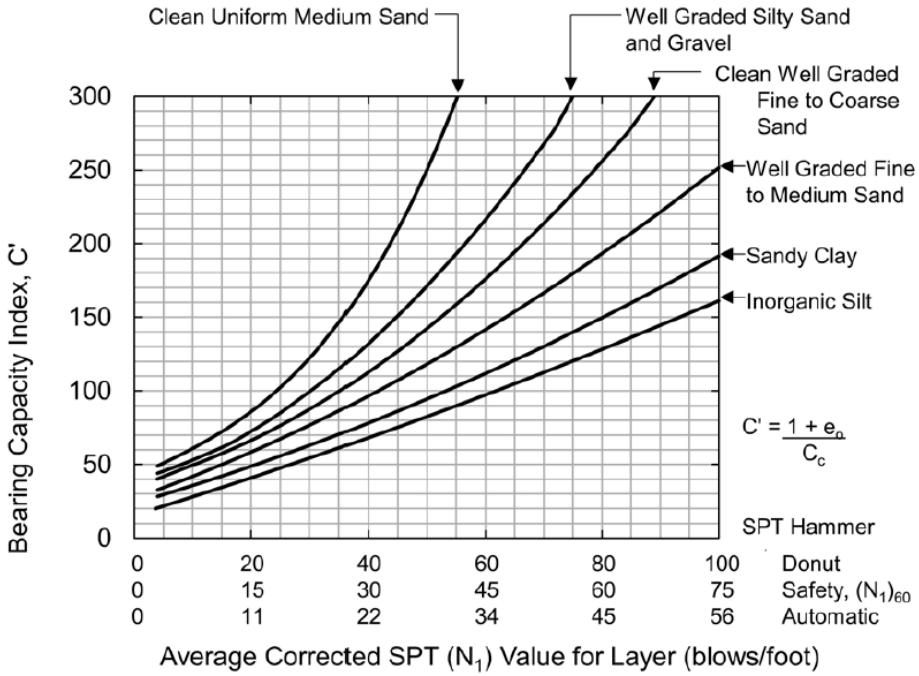

Figure 3.1 Bearing capacity Index (C') values for granular soil (Hannigan et al. 2016)

The first step is to divide the soil profile based on the boring log depths and blow counts. The SPT blow counts (N) are then adjusted according to their hammer type to N_{60}. The unit weight of each soil layer is estimated based on uncorrected blow counts (N_{60}) as well as the water table depth. The overburden pressure is then calculated to the center of each layer as defined by the boring log depths. From this, corrected blow counts (N_1) are determined. The corrected blow counts are in turn used to determine the C' term (defined as $(1+e_o)/C_c$) from six equations generated from the FHWA Publication (HI-88-009) *Soils and Foundations Workshop Manual-Second Edition* (Cheney and Chassie 1982) by selecting one of six sandy soil types. The change in pressure distribution beneath the footing imposed by the new load is determined at the center of each layer and used to calculate the displacement from each layer using the previously determine compression indices. The settlement for each layer is calculated per Equation 3.1 and summed to determine the total settlement.

3.2.2 Schmertmann Modified Method

The Modified Hough method as presented in FHWA NHI-06-088 *Soils and Foundations Reference Manual Vol 1* (Samtani and Nowatzki 2006) is stated as being conservative. Thus, a second method of predicting immediate settlement was also employed, the Schmertmann modified method (Schmertmann et al. 1978). The equation for estimating immediate settlement is given in Eqn 3.2.

$$S = C_1 C_2 \Delta p \sum_{i=1}^{n} \Delta H_i \qquad \text{Equation 3.2}$$

where:

$$\Delta H_i = H_c \left(\frac{I_z}{XE}\right)$$

and

S = immediate settlement
H_c = soil layer thickness
I_z = strain Influence Factor
n = number of soil layers within zone of strain influence
E = elastic modulus of i^{th} layer (Table 3.1)
X = factor used to determine elastic modulus
Δp = net foundation pressure
C_1 = strain relief correction factor due to embedment

$$C_1 = 1 - 0.5(p_o/\Delta p) \geq 0.5$$

p_o = effective in situ overburden stress at the foundation depth
C_2 = creep correction factor

$$C_2 = 1 + 0.2\log(t/0.1)$$

t = time in years

The Schmertmann Modified Method of calculating immediate settlement was implemented by idealizing the embankment as a shallow footing. This method considers the strain distribution as a function of depth expressed in multiples of the minimum footing width, B (Figure 3.2). The first step is to divide the soil profile based on the boring log depths and blow counts. The SPT blow counts (N) are then adjusted according to their hammer type to N_{60}. The unit weight of each soil layer is estimated based on uncorrected blow counts (N_{60}) as well as the water table depth. The overburden pressure is then calculated to the center of each layer as defined by the boring log depths. From this, corrected blow counts (N'_{60}) are determined. The elastic modulus of each layer is then estimated as a function of the corrected blow count from that layer as reported in Table 3.1 obtained from FHWA NHI-06-088 (Samtani and Nowatzki 2006). The strain influence factor at each depth is then determined from vertical strain influence factor distributions proposed by Schmertmann et al. (1978) and shown in Figure 3.2. Finally, the total immediate settlement is calculated per Equation 3.2 as a sum of all layer settlement values.

Table 3.1 Estimating E_s from SPT N-value (Samtani and Nowatzki 2006)

	E_s (tsf)
Silts, sandy silts, slightly cohesive mixtures	$4\ N'_{60}$
Clean fine to medium sands and slightly silty sands	$7\ N'_{60}$
Coarse sands and sands with little gravel	$10\ N'_{60}$
Sandy gravel and gravels	$12\ N'_{60}$

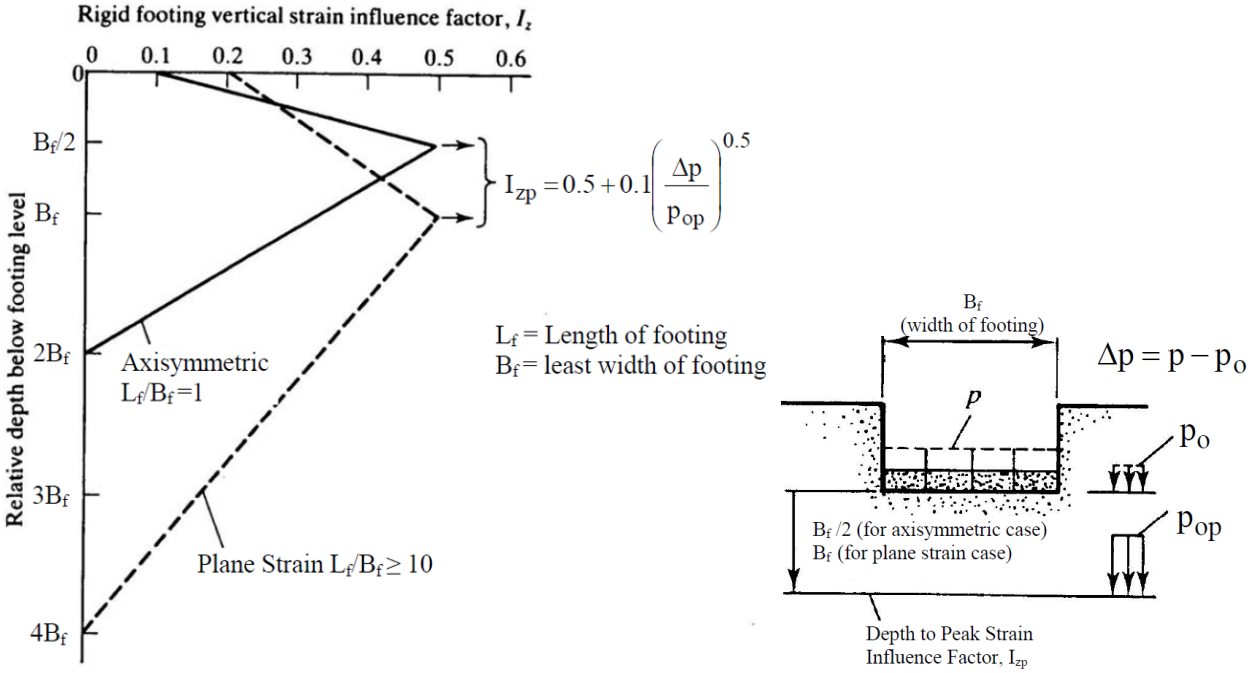

Figure 3.2 Vertical strain influence factor diagram (left) and illustration of pressure terms in I_{zp} equation (Samtani and Nowatzki 2006)

3.3 Site Evaluation and Pile Instrumentation

Multiple sites were scrutinized for applicability to this study. Required parameters included: an appreciable amount of anticipated settlement, settlement was to be caused by compressible cohesionless soil layers, and the construction timeline aligned with the research project contract timeframe. Preliminary screening for suitability of the three selected sites is discussed along with initial instrumentation procedures. Only sites that met project criteria are presented.

3.3.1 SR-23 Southbound over CR-739 (Henley Road) Bridge No. 710120

Financial Project ID: 422938-6-52-01

Bridge No. 710120 is part of SR 23 Southbound alignment over CR-739 in Clay County, Florida. The bridge was designed with two spans supported by three piers with a total of nineteen 24-inch

square prestressed concrete piles with nominal bearing resistance between 257 tons (end bents) and 380 tons (center pier). Once an evaluation was performed where the settlement and soil types met the project needs, pile instrumentation was a critical path issue in some cases being performed long before the onset of embankment construction. The pier under investigation for this site was in End Bent 1 where Pile 3 near the center of the bent was instrumented with sister bar type strain gauges. Figure 3.3 shows the plan layout showing End Bent 1.

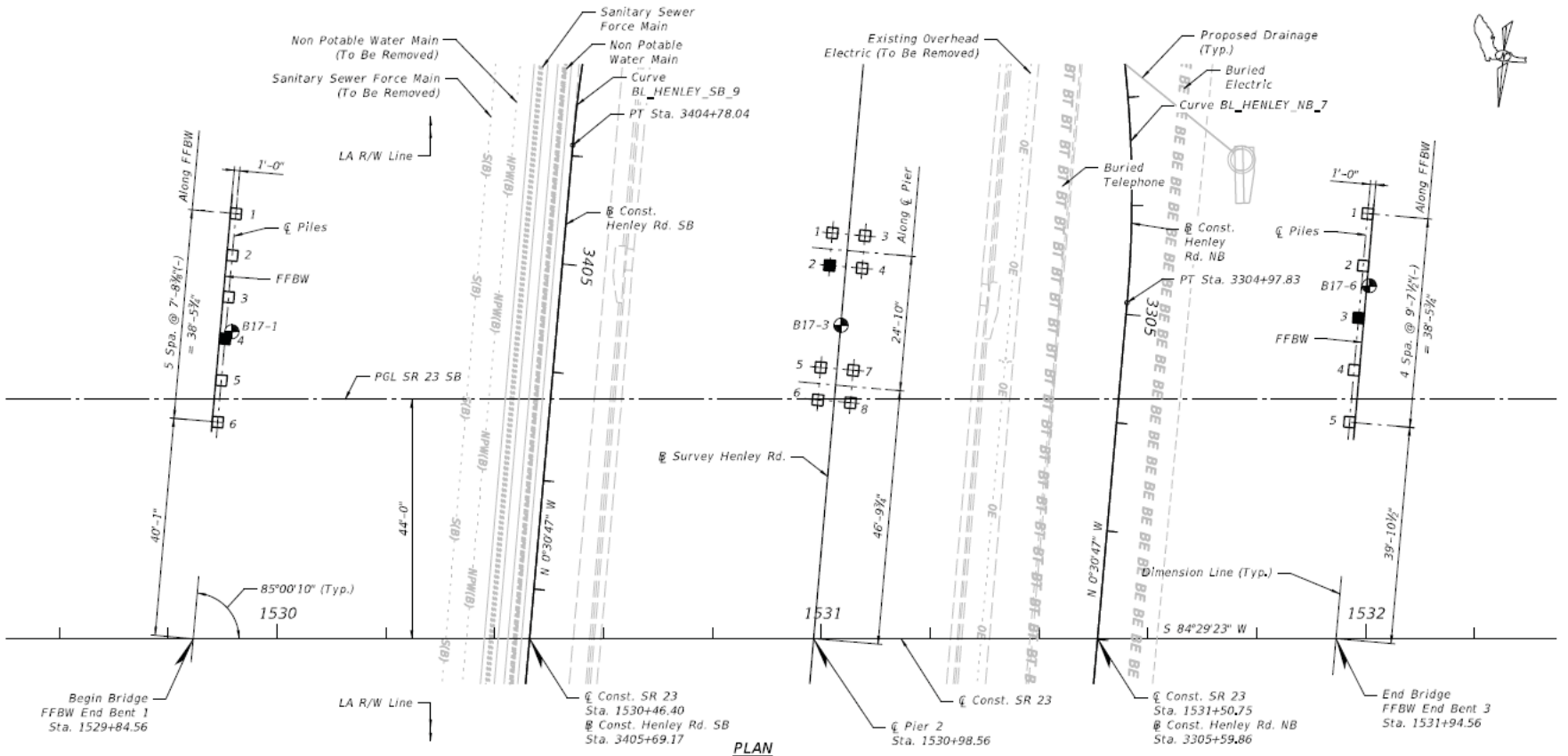

PLAN

Direction of Stationing

LEGEND:

- Denotes Proposed 24" Square Prestressed Concrete Pile
- Denotes Proposed 24" Square Prestressed Concrete Test Pile
- Soil Boring Location

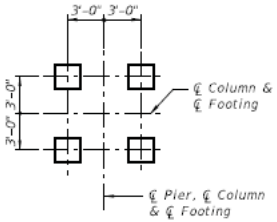

PILE LAYOUT

NOTES:

1. All proposed piles are 24" square prestressed concrete piles and shall be driven plumb. See Index Nos. 455-001, 455-002 & 455-024.
2. Work this sheet with PILE DATA TABLE sheet.
3. For additional utility information, see ROADWAY PLANS.
4. See PLAN AND ELEVATION sheet for horizontal curve data.

Bridge No. 710120

REVISIONS					
DATE	BY	DESCRIPTION	DATE	BY	DESCRIPTION

STEVEN T. STARNES, P.E.
P.E. LICENSE NUMBER 58183
RS&H, INC.
10748 DEERWOOD PARK BLVD. SOUTH
JACKSONVILLE, FL 32256
CERTIFICATE OF AUTHORIZATION 5620

DRAWN BY: JTC 02-17
CHECKED BY: AWP 05-17
DESIGNED BY: STS 02-17
CHECKED BY: AWP 05-17

STATE OF FLORIDA
DEPARTMENT OF TRANSPORTATION

ROAD NO.	COUNTY	FINANCIAL PROJECT ID
SR 23	CLAY	422938-6-52-01

SHEET TITLE: FOUNDATION LAYOUT
REF. DWG. NO.
PROJECT NAME: SR 23 SOUTHBOUND OVER CR-739 (HENLEY ROAD)
SHEET NO. B13-8

VelasquA 5/15/2018 4:47:31 PM c:\pw_work\rsh_pw\velasqua\d0125691\B13FoundLay.dgn

THE OFFICIAL RECORD OF THIS SHEET IS THE ELECTRONIC FILE DIGITALLY SIGNED AND SEALED UNDER RULE 61G15-23.004, F.A.C.

The location for End Bent 1 in Bridge No. 710120 (referenced as Henley Road throughout the rest of this report) corresponds to boring log B17-1 (shown in Figure 3.6). This boring log showed mostly fine sands in the upper soils and some limestone and sandy silt where the piles were tipped. The Modified Hough Method settlement was calculated to be 4.7 inches, while the Schmertmann Modified Method settlement was calculated to be 2.4 inches. The calculated settlements from each soil layer cumulated from bottom up for Henley Road are shown in Figure 3.4.

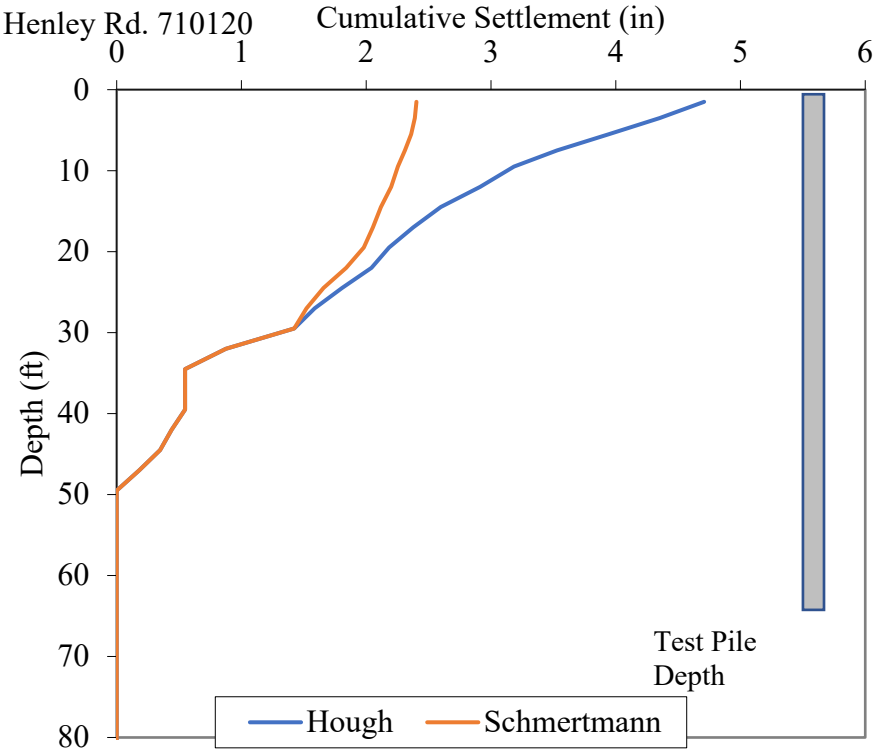

Figure 3.3 Henley Road soil settlement (boring log B17-1)

Pile 3 within FDOT Bridge No. 710120 End Bent 1 was instrumented on January 8, 2021 at the CDS Manufacturing casting yard in Gretna, Florida (Figure 3.5). Coordination with state engineers facilitated the instrumentation layout and scheduling. Eight Geokon vibrating wire strainmeters (sister bars) were tied to the rebar cage per the layout illustrated in Figure 3.6. Each strainmeter was color coded with electrical tape, and the wires were stubbed out of the pile with varying lengths to further enhance identification in case the tape was inadvertently removed. The End Bent 1 piles were driven January 14th, 2021. Soil instrumentation behind the end bent, near Pile 3, and underneath the future embankment was to be installed later, pending the contractor's schedule. A point of zero or near zero settlement was anticipated at a depth of 50 ft from the ground surface. Four extensometer assemblies (also shown in Figure 3.6) were slated for installation in a 65ft deep, four- to six-inch diameter borehole (discussed later).

Figure 3.4 Instrumentation of Pile 3 (24 in) for End Bent 1 at Henley Road (Bridge 710120).

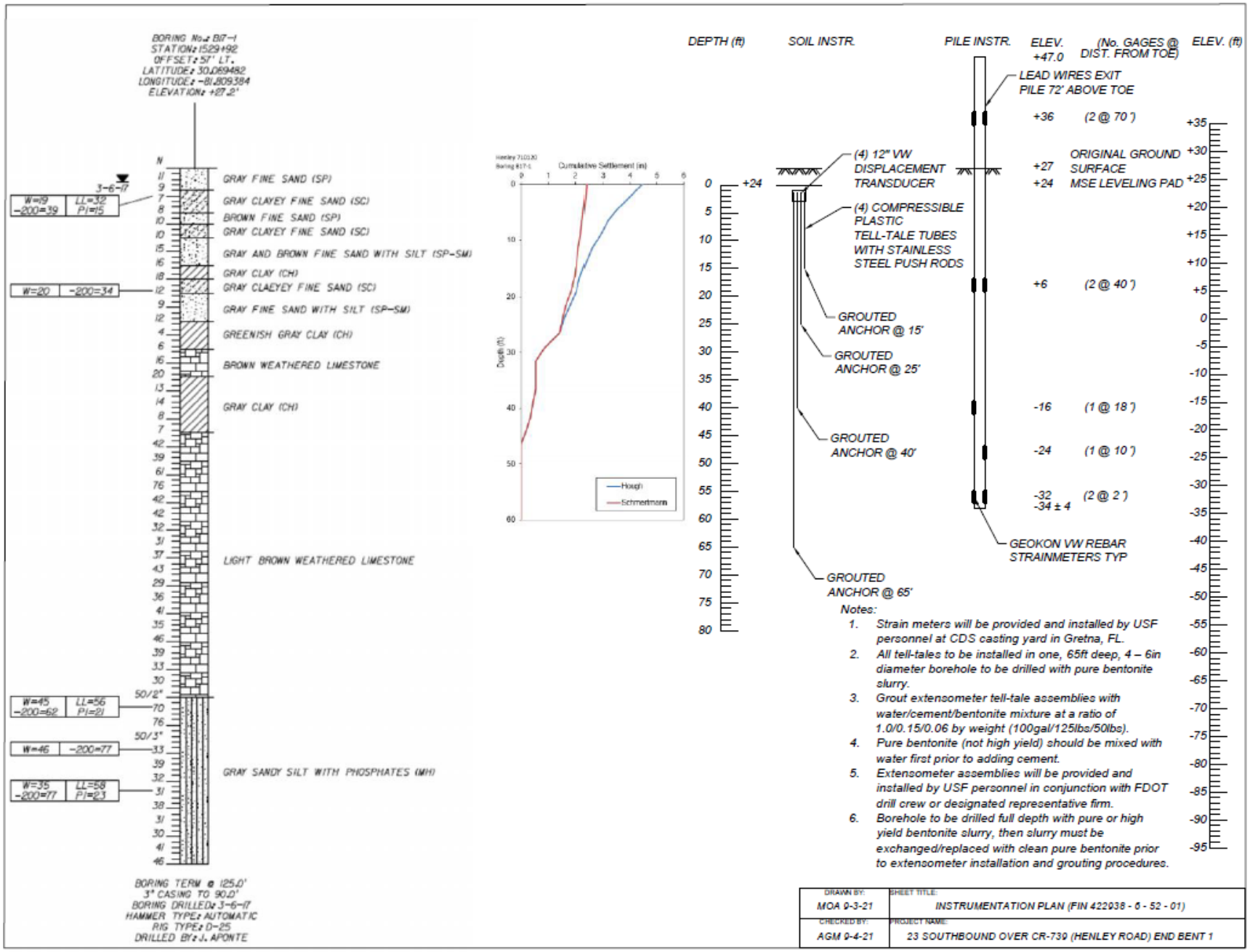

Figure 3.5 As-built Henley Road pile and soil instrumentation scheme.

Lead wires from the strainmeters in the pile would later be joined with wires from the four extensometers and routed via conduits to a location outside the MSE wall where a standalone, solar-powered, data collection system would be mounted for the duration of the bridge construction. This method was planned for all three sites. Figures 3.7 and 3.8 show the piles after driving and the anticipated location of the data collection system.

Figure 3.6 End Bent 1 looking south; Pile 3 has duct tape holding lead wires used to protect them during driving (Pile 1 farthest to the south; used with permission from J. Bosnoian, HTNB)

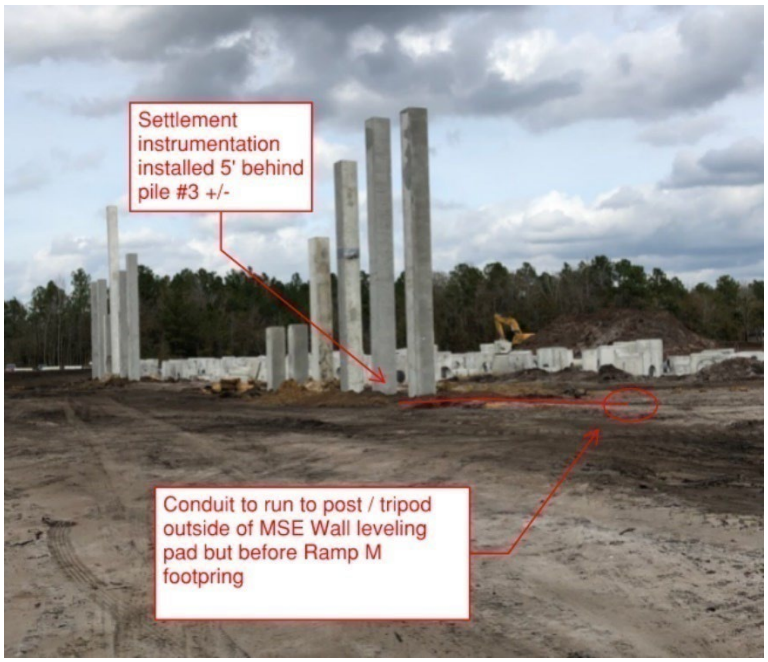

Figure 3.7 End Bent 1 looking north; approximate location of the data collection system outside the embankment footprint (used with permission from J. Bosnoian, HTNB).

3.3.2 SR-23 Northbound over CR-739B (Sandridge Road) Bridge No. 710113

Financial Project ID: 422938-6-52-01

FDOT Bridge No. 710113, like the Henley Rd crossing, was also a part of the new SR 23 alignment. In this case the bridge provided the northbound crossing over CR-739B also in Clay County, Florida. The bridge plans (Figure 3.10) showed a single span and was designed to be supported by two End Bents, each consisting of six 18-inch square prestressed concrete piles with 267 tons of nominal bearing resistance. The pier under investigation for this study was End Bent 1. Pile 4 was selected for instrumentation. Figure 3.10 shows the plan layout of End Bent 1.

The soil profile for the location of End Bent 1 in Bridge No. 710113 (referenced as Sandridge Road throughout the rest of the report) is characterized by boring B24-1 (Figure 3.11). It was concluded from the literature review and preliminary modeling that sites with dense bearing layers characterizing an end-bearing pile condition have the most potential for significant downdrag effects where pile movement from structural loads would be minimal. Therefore, the very dense sands located towards the lower end of Boring 24-1 were expected to result in an end-bearing pile type condition that would satisfy one of the conditions sought by this study. The soil profile consisted of mostly loose light gray sands in the upper strata over dense light gray sands. The Modified Hough Method settlement was calculated to be 4.6 inches, while the Schmertmann Modified Method settlement was calculated to be 3.6 inches. The calculated cumulative settlements for Sandridge Road End Bent 1 are shown in Figure 3.9.

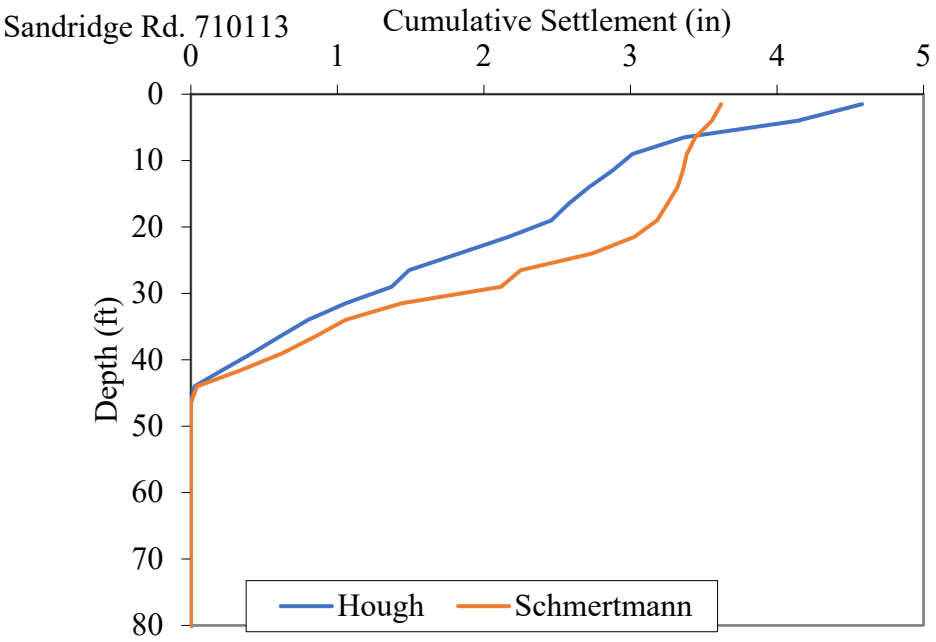

Figure 3.8 Sandridge Road soil settlement (boring log B24-1)

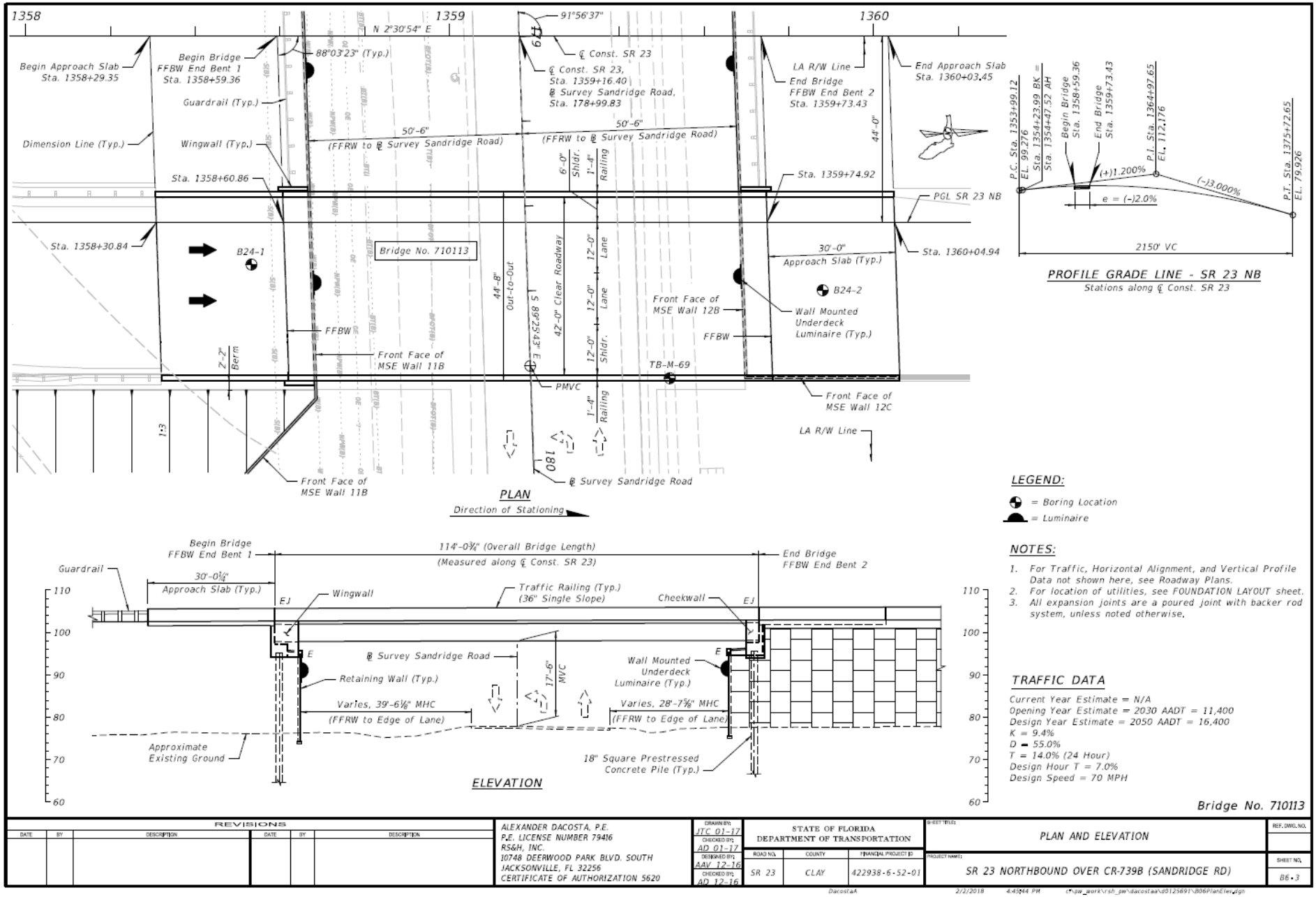

Figure 3.9 Foundation layout for Bridge No. 710113 (Sandridge Rd)

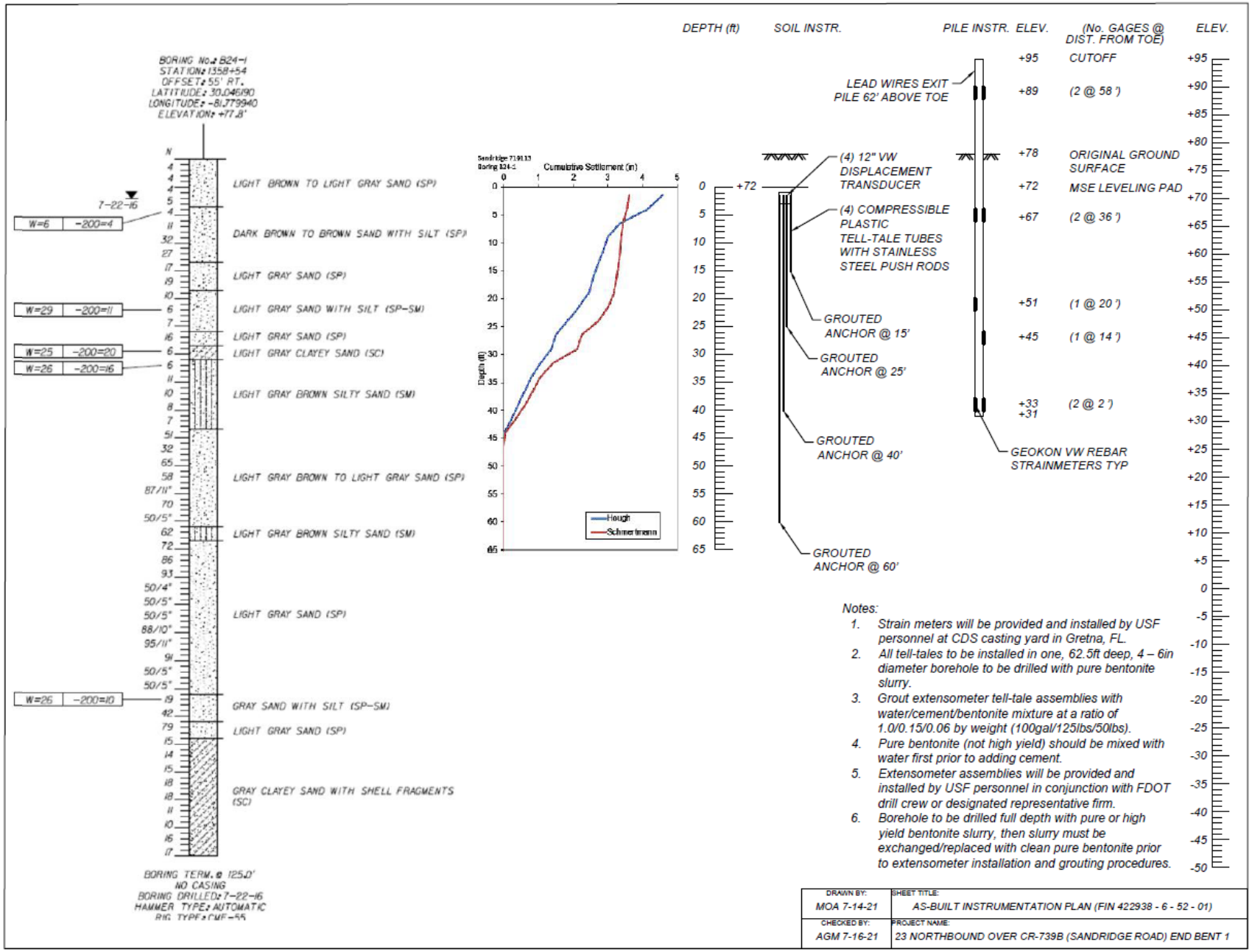

Figure 3.10 As-built Sandridge Road pile and soil instrumentation scheme

Pile instrumentation was similarly performed to coordinate with the casting and anticipated driving schedules. Figure 3.12 shows the same pile instrumentation process used for the Henley Rd pile but for the 18 in pile used at the Sandridge Rd site.

Figure 3.11 Instrumentation of Pile 4 (18 in) for End Bent 1 (Sandridge Road).

3.3.3 Paseo al Mar Boulevard I-75 Flyover Bridge No. 104495

Financial Project ID: 438752-1-54-01

The Paseo al Mar Boulevard I-75 Flyover (Bridge No. 104495) is part of a project that connected US-41 in Apollo Beach to US-301 in Wimauma in Hillsborough County, Florida. The bridge was designed to be supported by three piers with a total of fifty-seven 24-inch square prestressed concrete piles with nominal bearing resistance between 277 (end bents) and 324 tons (center pier). The pier under investigation for this study was End Bent 3 where pile 12 near the center of the bent was instrumented with sister bar type strain gauges. Figure 3.13 shows the foundation plan layout of the bridge.

The location for End Bent 3 in Bridge No. 104495 (referenced as Paseo al Mar Boulevard throughout the rest of this report) corresponds to boring BB-131 (Figure 3.14). This boring log showed sand and silty sand in the upper strata underlain by weathered limestone and calcareous clay where the piles were tipped. The Modified Hough Method settlement was calculated to be 4.4 inches, while the Schmertmann Modified Method settlement was calculated to be 4.0 inches as shown in Figure 3.15.

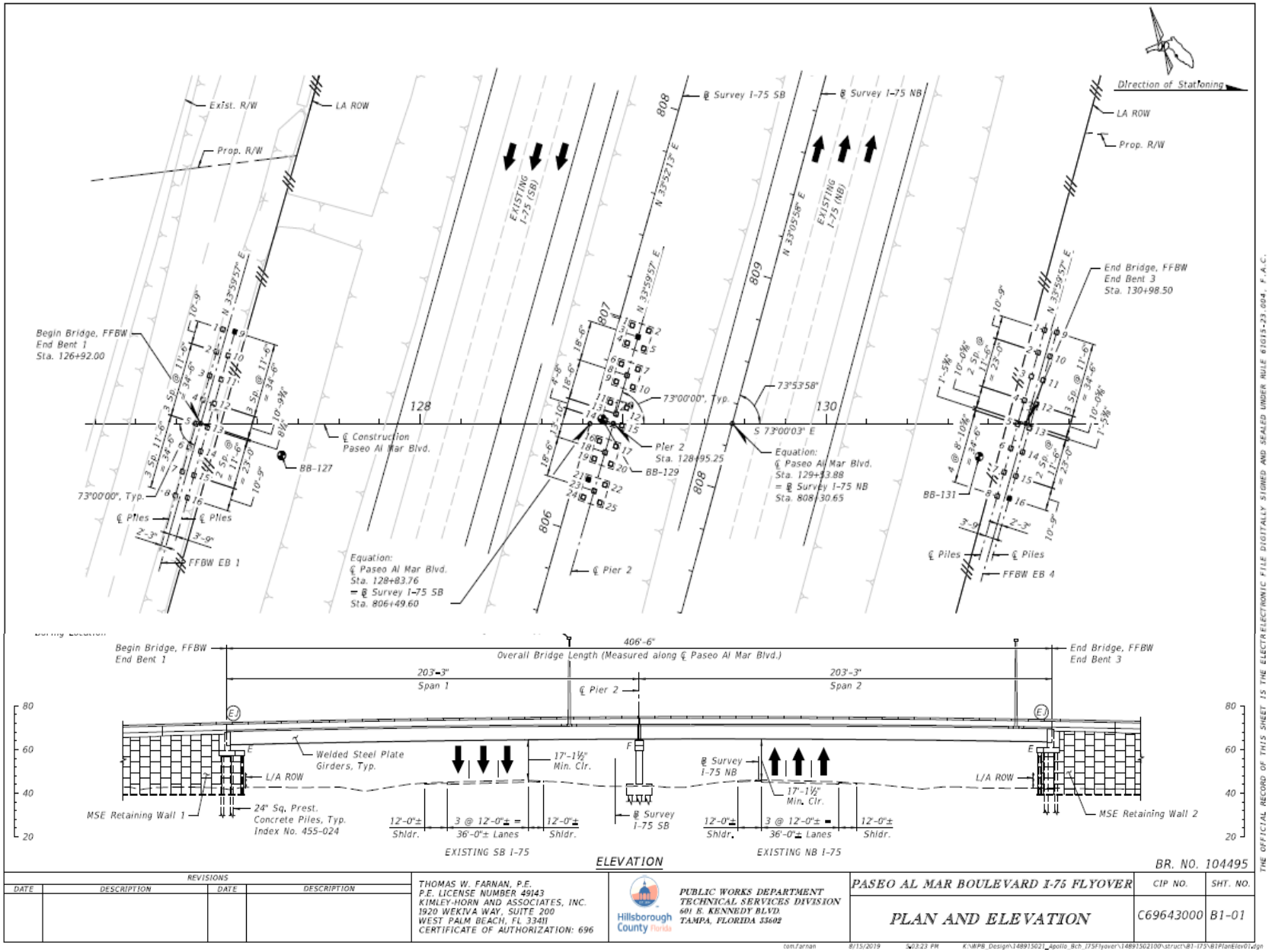

Figure 3.12 Foundation layout for Bridge No.104495 (Paseo Al Mar Blvd)

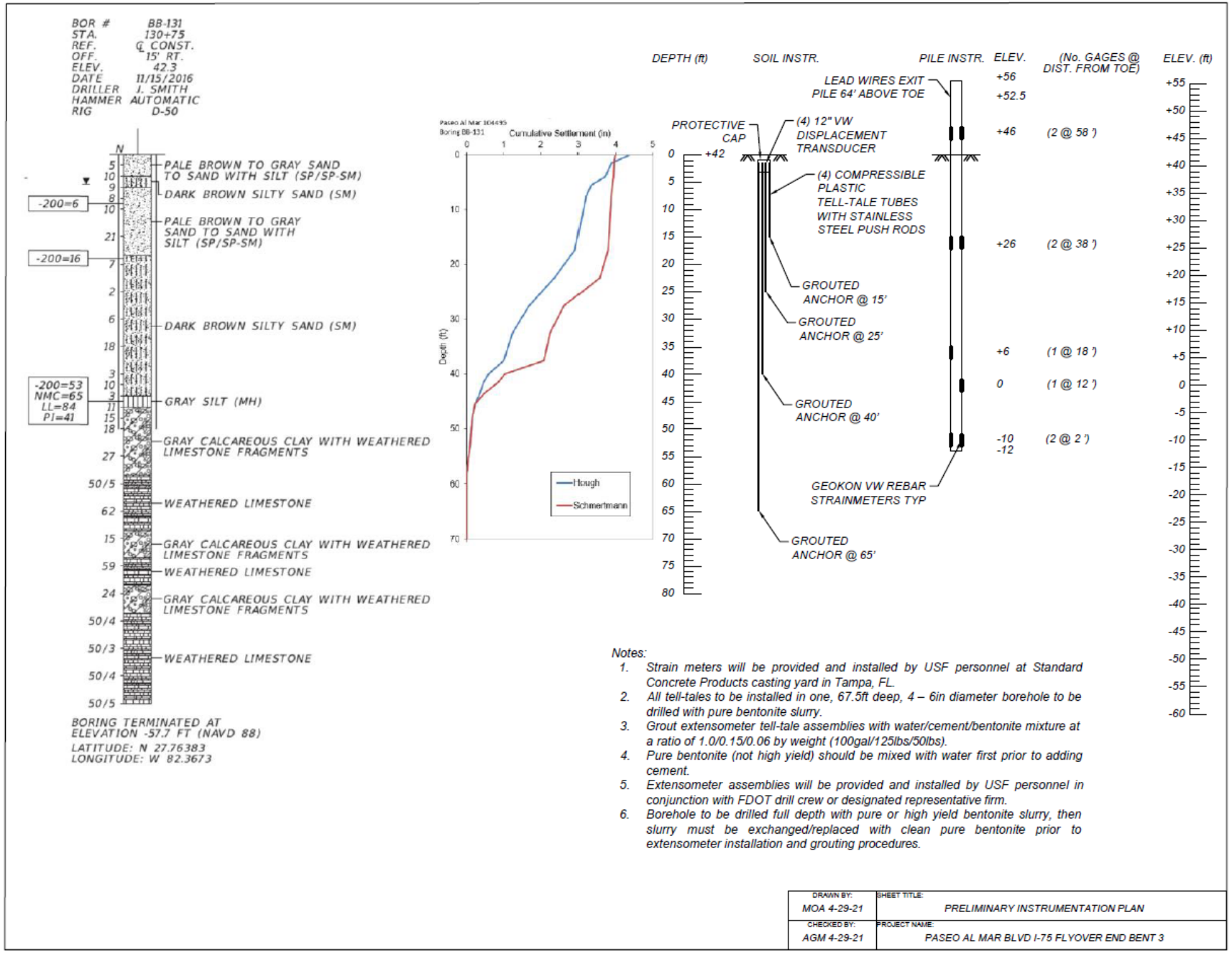

Figure 3.13 As-built Paseo Al Mar Blvd instrumentation plan

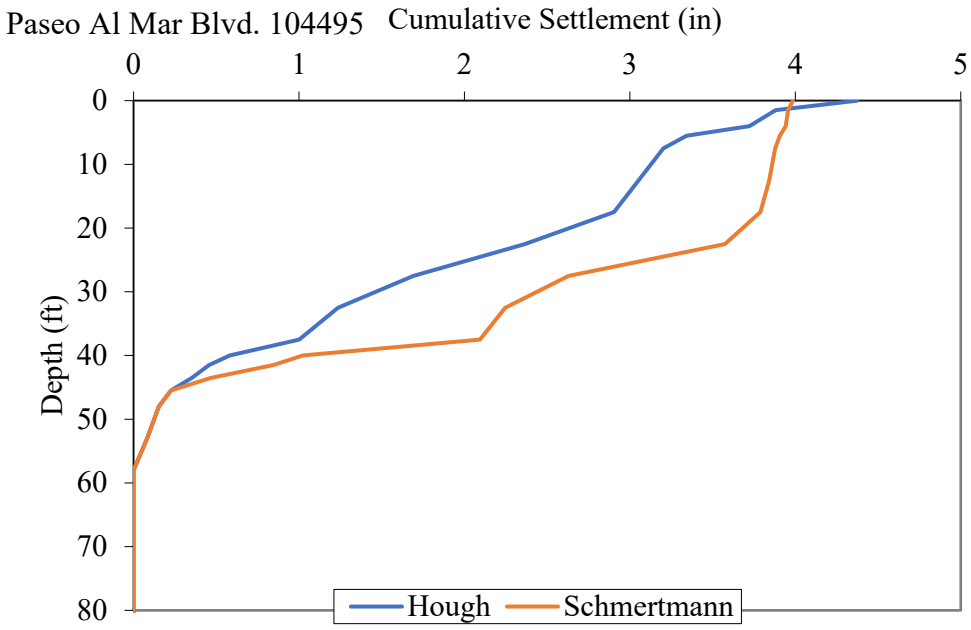

Figure 3.14 Paseo Al Mar Blvd soil settlement (boring log BB-131)

Pile 12 of End Bent 3 was instrumented on April 15th, 2021 at Standard Concrete Products casting yard in Tampa, Florida (Figure 3.16). Eight Geokon vibrating wire strainmeters were tied to the reinforcement cage per the layout illustrated in Figure 3.14. The pile was driven eight days later April 23rd, 2021.

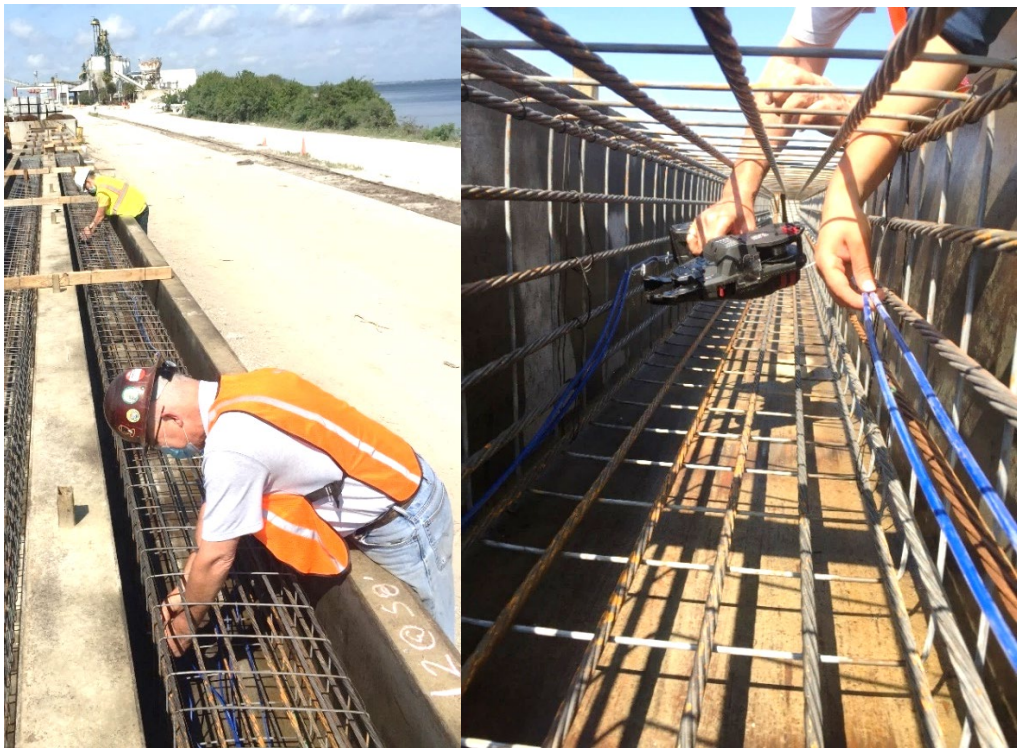

Figure 3.15 Instrumentation of Pile 12 (24 in) for End Bent 3 (Paseo Al Mar Blvd)

3.4 Settlement Instrumentation and Data Collector Installation

Like the pile instrumentation information presented above, installation of settlement sensors, data collectors, and connections with the pile gauges are presented in chronological order based on contractor readiness.

3.4.1 Paseo Al Mar Blvd.

On May 1st, 2021, conduit was placed in a trench, one foot below the leveling pad elevation, approximately 80 ft long, stretching from the instrumented pile to the data acquisition system located 20 ft south of the planned MSE wall (Figure 3.17). The wires on the piles were spliced to extension leads by stripping the wire insulation, sliding adhesive-lined heat shrink tubing onto one of the wires, twisting the wires together, soldering the twisted wires, sliding the heat shrink over the soldered connection, and heating the adhesive-lined shrink tube with a heat gun until sealed tight. This process was repeated for each of the four conductors for each strainmeter-thermistor assembly. Each bundle of four conductors was then bundled together by sliding a larger adhesive-lined heat shrink tube over the spliced connections and again sealing with a heat gun (Figure 3.17). The eight strainmeter wires as well as the wires leading from the extensometer assembly were then routed through the conduit. The wires were connected to a Campbell Scientific CR1000 data acquisition unit housed inside a weather enclosure mounted on a pole (Figure 3.17). The batteries powering the CR1000 were charged via solar panel facing south with an angle from horizontal roughly matching the latitude of the site.

Soil instrumentation near Pile 12 and underneath the embankment was installed on May 3rd, 2021. A Geokon A-3 extensometer assembly with four vibrating wire displacement transducers was installed within a 65.5-ft deep borehole that was drilled by the FDOT SMO drill crew. The settlement sensor depths correspond to the as-built instrumentation plan in Figure 3.14. The borehole was drilled 15 ft east of Pile 12 (behind the row of piles) at the elevation of the MSE wall leveling pad (Figure 3.18). Bentonite slurry was pumped through the borehole to stabilize the hole and bring up the cuttings from the drilling. Cuttings-laden drill slurry was exchanged with clean slurry prior to instrumentation installation. The extensometer assembly was inserted into the borehole, and grout was then placed by tremie with a ¾” grout tube (Figure 4.10).

Figure 3.16 Trenching for conduit placement (left), wire splicing (center), and datalogger enclosure (right)


Figure 3.17 Extensometer assembly installation (Paseo Al Mar Blvd).

3.4.2 SR-23 Northbound over CR-739B (Sandridge Road) Bridge No. 710113

Soil instrumentation near Pile 4 and underneath the embankment was installed on May 4th, 2021. The Geokon A-3 extensometer assembly with four vibrating wire displacement transducers was installed within a 62-ft deep borehole that was drilled by the FDOT SMO drill crew. The settlement sensor depths correspond to the as-built instrumentation plan in Figure 3.11. The top of the borehole matched the elevation of MSE wall leveling pad and was drilled 15 ft south, behind the row of piles closest to the instrumented pile (Figure 3.19). Pure bentonite slurry was used as the drilling fluid to stabilize the borehole and bring up the cuttings from the drilling. Once the target depth was achieved, the borehole was flushed with clean bentonite slurry, the extensometer assembly was inserted, and grout was pumped to the bottom of the borehole using a ¾" grout tube expelling all slurry.

Figure 3.18 Borehole drilling location (left) and extensometer assembly (right) at Sandridge Rd

A trench was dug from the predetermined data acquisition system location east of the MSE wall to the instrumented pile. A 1.5in ID PVC conduit was then buried in the trench to house the lead wires from both the extensometer assembly and the strainmeters within the pile (Figure 3.20). On May 5th, the wires leading from the pile and the extensometer head assembly were spliced and routed through the conduit to the solar powered data collector location. The wires were then connected to a Campbell Scientific CR6 or Granite VWIRE 305 for data collection (Figure 3.21).

Figure 3.19 Trenching and conduit installation for lead wires (Sandridge Rd).

Figure 3.20 Lead wires connected to data acquisition system (Sandridge Rd).

3.4.3 SR-23 Southbound over CR-739 (Henley Road) Bridge No. 710120

Soil instrumentation near Pile 4 and underneath the embankment was installed on September 7th, 2021. The Geokon A-3 extensometer assembly with four vibrating wire displacement transducers (Figures 3.22 and 3.23) was installed within a 65ft deep borehole drilled by the FDOT SMO drill crew. The settlement sensor depths correspond to the as-built instrumentation plan in Figure 3.6. The top of the borehole matched the elevation of MSE wall leveling pad and was drilled 15 ft east, behind the row of piles closest to the instrumented pile (Figure 3.19). Bentonite slurry was used during drilling to stabilize the hole and bring up the cuttings from the drilling. Once the target depth was achieved, the borehole was flushed with clean bentonite slurry, the extensometer assembly was inserted, and grout was pumped to the bottom of the borehole using a ¾" grout tube expelling all slurry.

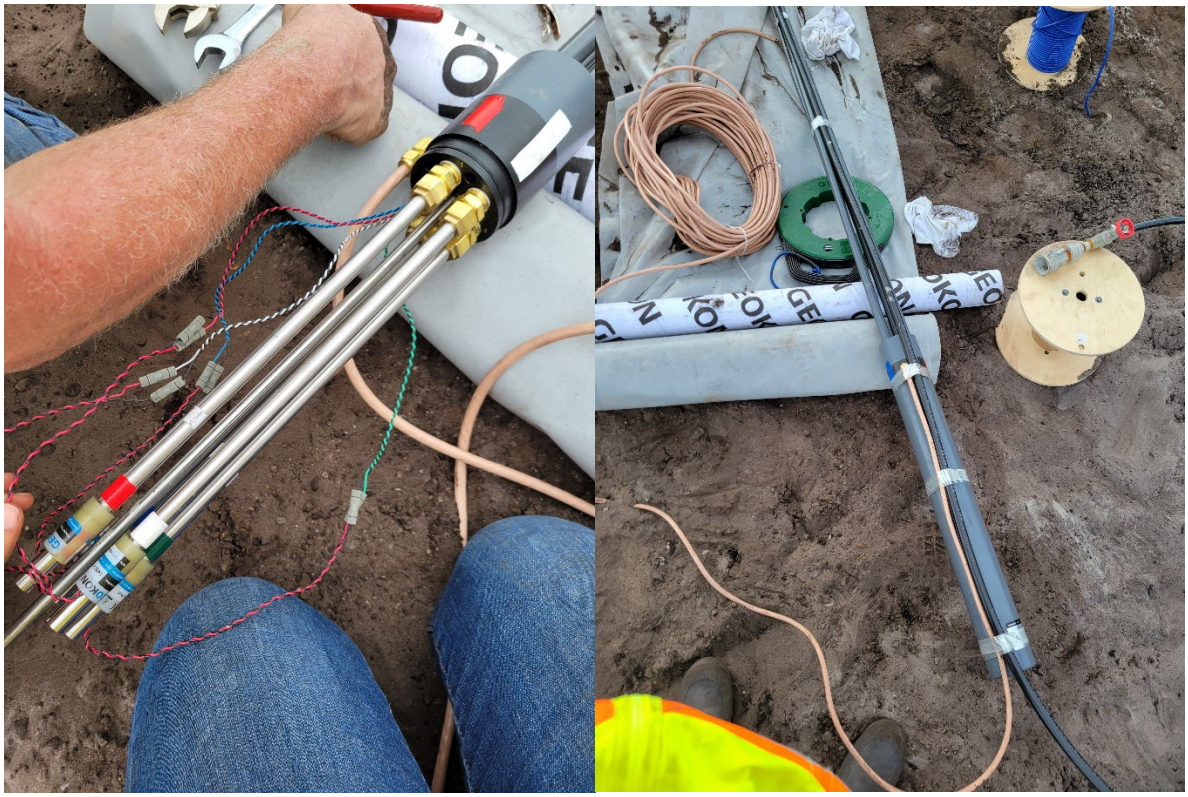

Figure 3.21 Four extensometers connected to settlement head unit before and after installing water-tight protective shroud.

Figure 3.22 Settlement assembly supported and negotiated into borehole by multiple installers.

Splicing, trenching, and routing the lead wires to the data acquisition system was performed like the other two sites. The data acquisition system used the same dual purpose (high speed / low speed) unit as the Sandridge Road Bridge site, but additional sensors were added to provide weather information (temperature and rain gauge) and a digital camera to document construction events. Figure 3.25 shows the updated data collector station.

Figure 3.23 Solar-powered data collector complete with rain gauge, camera, cellular communications, and lightning rod.

3.5 Instrumentation Equipment and Sensor Summary

For completeness, all sensor and data acquisition system information are described in this section. These include Campbell Scientific data acquisition systems, Geokon strainmeters, and ground settlement sensors.

3.5.1 Campbell Scientific Component:

CR6 Measurement and Control Datalogger
GRANITE VWIRE 305 8-Channel Dynamic Vibrating-Wire Analyzer
RV50X Industrial 4G LTE Cellular Gateway
32262 4G/3G Omni 2dBd Antenna with Type N
31315 Bulkhead Surge Protection Installed in Enclosure
COAXNTN-L10 Antenna Cable RG8 with 2 Type N Male Connectors
ENC14/16-DC-MM Weather-Resistant Enclosure
PS84-SC-CR-NM 84 Ah Power Supply with 14 x 16 in. Enclosure
SP50-L25-PT 50 W Solar Panel
CM106B 10-ft Tripod

3.5.2 Geokon Components

4911-4 VW Rebar Strainmeter, "Sister Bar", #4 rebar with 02-250V6-E cable
02-250V6-E Blue PVC Cable, 0.250", 2 twisted pairs with extra cable for splicing
1150-1-2-3 Head assembly for Model A-3 MPBX
1150-10A PVC Standpipe
1150-14 Groutable Anchor
ROD-101-E Flush coupled 1/4" stainless steel rod
TUB-101-E 1/4" Schedule 40 PVC Tube
TUB-104-E 3/4" Grout Tube
1150-30 Installation Tools for extensometers
1150-31 Installation Tools for extensometers with vibrating wire transducers
1150-35 Grouting accessories
4450-1-300 mm VW Displacement Transducer, 300 mm (12") range
04-375V9-E Violet PVC Cable, 0.375", 4 twisted pairs

3.5.3 Campbell Scientific Equipment

Older measurement systems for dynamic and long-term static monitoring were typically composed of two separate systems: one with high-speed foil resistive-type gauges and another with low-speed vibrating wire gauges. Additionally, data acquisition systems that measure the voltage of gauges have a propensity to pick up ambient noise. Campbell Scientific's GRANITE VWIRE 305 is an eight-channel analyzer that measures the frequencies of vibrating-wire gauges at both static and dynamic sampling rates (Campbell Scientific 2021). The dynamic measurement rates range from 20 to 333 Hz, while the static measurement rates are no faster than 1 Hz. Older vibrating systems required measurement of each individual channel before moving on to the next one using multiplexers. A bystander could hear the clicks as each channel was scanned individually. The

new state-of-the-art interface can simultaneously measure each channel. There are two terminals on each channel for vibrating-wire gauge connection. The VWIRE 305 maintains the connected wire in a vibrating state by applying a sinusoidal excitation. A general wiring schematic for the VWIRE305 is shown in Figure 3.25.

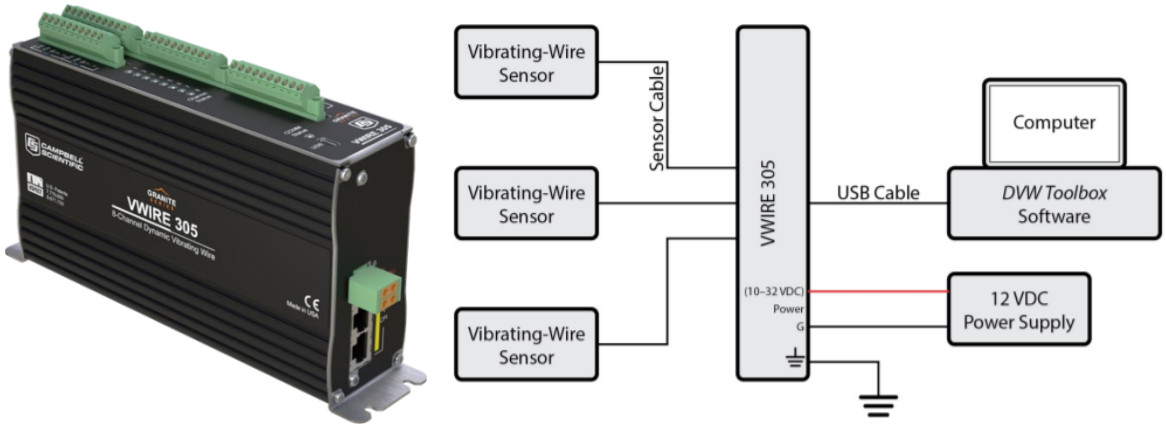

Figure 3.24 Campbell Scientific GRANITE VWIRE 305 (left) and General Schematic (right) (Campbell Scientific 2021a)

The CR6 Measurement and Control Datalogger (Figure 3.26) can measure virtually any sensor, perform calculations, control external devices, and can store data in statistical form. With a maximum scan rate of 1000 Hz, the CR6 contains 12 universal inputs for either digital or analog functions along with 16 pulse counters. This datalogger can perform static vibrating-wire measurements and can easily connect to other devices for integrated measurements via RS-232 serial port (Campbell Scientific 2021).

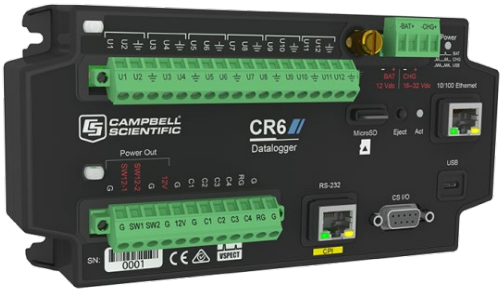

Figure 3.25 Campbell Scientific CR6 Datalogger (Campbell Scientific 2021b)

The RV50X industrial Sierra Wireless Airlink 4G LTE cellular gateway (Figure 3.27) is the link to monitoring data remotely (Campbell Scientific 2021). The Konect Router Service provided by Campbell Scientific was acquired to establish a secure connection with the data acquisition system. The RV50X is directly connected to the CR6 via Ethernet.

Figure 3.26 Campbell Scientific RV50X Sierra wireless (left) and Omni 2dBd antenna (right) (Campbell Scientific 2021c and 2021d)

The 32262 4G/3G Omni 2dBd Antenna (Figure 3.27, right) is an omnidirectional, multiband antenna suited for the 4G RV50X cellular gateway (Campbell Scientific 2021). The antenna is connected to a bulkhead surge protection (31315) installed in the enclosure (Campbell Scientific 2021) via COAXNTN-L10—a 10 ft long coaxial cable with type N male connectors (Campbell Scientific 2021). The surge protector is then connected to the cellular gateway via an 18-inch type N to SMA coaxial jumper within the enclosure.

Shown in Figure 3.28 is Campbell Scientific ENC14/16 white fiberglass-reinforced polyester weather-resistant enclosure that is 14 by 16 by 5.5 inches complete with pre-punched backplate for data acquisition mounting and two conduits for cables (Campbell Scientific 2021). The white color is meant to reflect solar radiation and thus reduce the temperature within the enclosure. The "MM" designation at the end of the product name signifies that the enclosure be mounted to the tripod's mast via three-piece brackets.

Figure 3.27 Campbell Scientific ENC14/16 Enclosure (left) and PS84 enclosure (right) (Campbell Scientific 2021e and 2021f)

The PS84 is a system consisting of a 14 by 16 weather resistant enclosure, 84 Ah battery, and a mounting bracket (Campbell Scientific 2021). The PS84 system (Figure 3.28) also includes a CH200 Regulator (Figure 3.29) that connects and manages the charging source, in this case an unregulated solar panel, to the battery. The system can deliver 12 volts from the rechargeable

battery to the units housed in the neighboring enclosure via two-foot SDI-12 interface cable (20769).

Shown in Figure 3.29 is Campbell Scientific CM106B, which is an adjustable seven- to ten-foot tripod assembled with galvanized steel tubing (Campbell Scientific 2021). Each leg can be individually adjusted, allowing for easy setup on uneven surfaces. The respective enclosures can then be mounted on the mast or on the tripod leg.

The SP50-L tripod-mounted solar panel will convert energy from the sun into direct current to power the PS84 system via the CH200 regulator. The panel has a maximum peak power of 50 watts (P_p), 17.5 volts at peak power (V_{pp}), 2.9 amps of current at peak power (I_{pp}), and a temperature coefficient of –0.45% per degree Celsius (Campbell Scientific 2021). The ordered SP50-L25-PT includes 25 feet of cable and an extended mounting kit for tripod attachment. The panels are to be installed at a specified tilt by adjusting the brackets of the extended mounting kit. The potential sites in FDOT District 2 are located at approximately 30 degrees latitude. The recommended solar panel tilt angle for a site located at 30 degrees latitude is 40 degrees (site latitude plus 10°) (Campbell Scientific 2020).

Figure 3.28 Campbell Scientific tripod (left), SP50-L solar panel mounted on tripod (center), and CH200 regulator (right) (Campbell Scientific 2021g and 2021h)

3.5.4 Geokon Equipment

Geokon vibrating wire rebar strainmeters (Model 4911) consist of a #4 rebar with 1/4” 02-250V6-E blue PVC cable. Each strainmeter has an encapsulated thermistor to enable temperature measurement, as well as a strain gauge coated with protective epoxy (Geokon 2021). Number four rebar is welded to each end of the gauge section to allow for easy pile installation. These sensors are installed and embedded within a concrete pile to measure concrete strains (Figure 3.30). The strainmeters have a standard range of 3000 microstrain, a resolution of 0.4 microstrain, 0.25% full-scale accuracy, less than 0.5% full-scale nonlinearity, and a temperature range of –20 °C to 80 °C (Geokon 2021a). Eight gauges have been allocated to each instrumented pile to be installed in pairs: one level near the top; two near the neutral plane; and one at the toe of the pile. Each strainmeter will be connected to the VWIRE 305 for data collection.

Figure 3.29 Geokon VW rebar strainmeters tied to pile rebar cage (Henley Rd project)

Geokon Model 1150 (A-3) Rod-Type Borehole Extensometers are designed to measure movement within soil (Figure 3.31). Up to eight anchors can be installed within the same borehole with each anchor having measurement rods extending to the surface (Geokon 2021b); four anchors per borehole were used in this study. The flush coupled 1/4” stainless steel measurement rods (ROD-101-E) come in five-foot lengths for easy manipulation in the field. The rods are assembled with the groutable anchors (1150-14). and pipes outside the borehole, and the assembly is then anchored in place with grout. Geokon TUB-101-E 1/4" Schedule 40 PVC Tubing with couplings house the stainless-steel rods to both protect them from the grout and allow them to move freely. 1150-10A PVC Standpipe coupled in five-foot increments encase the entire assembly. Geokon TUB-104-E is a 3/4" (outside diameter) grout tube that is typically ten feet longer than the deepest anchored extensometer.

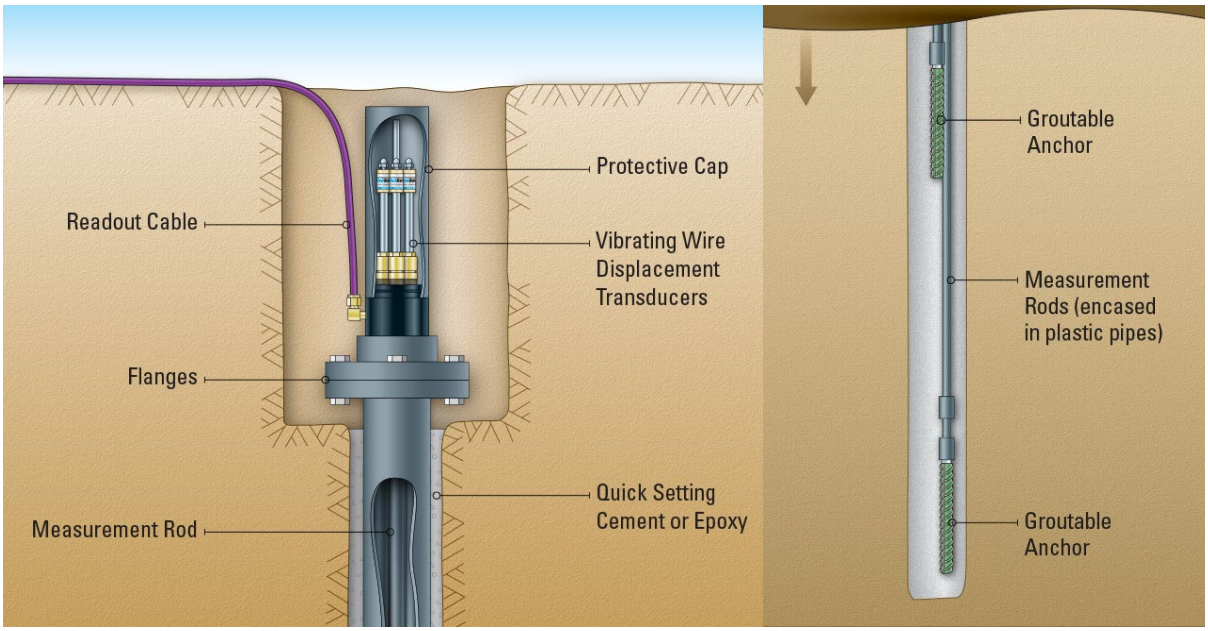

Figure 3.30 Geokon 4450 extensometer head assembly (left) and Geokon multiple point rod extensometer installed in sandy soils (right). (Geokon 2021b)

A set of installation tools for the extensometer (1150-30), a set of additional installation tools for extensometers with electrical transducer heads (1150-31), as well as grouting accessories for inclined downward installations (1150-35) was used to facilitate assembly installation. The extensometer assemblies were grouted with water/cement/bentonite mixture at a ratio of 1.0/0.15/0.06 by weight (100gal/125lbs/50lbs). Pure bentonite (not high yield) was mixed with water first prior to adding cement. The borehole was drilled full depth with pure or high yield bentonite slurry, then slurry was exchanged/replaced with clean pure bentonite free from cuttings prior to extensometer installation and grouting procedures.

The vibrating wire transducers shown in Figure 3.32 provide remote readout for the attached extensometer assemblies. Geokon 4450-1-300 mm VW Displacement Transducers are 12-inch range (300 mm) sensors with 0.02% full scale resolution, ±0.1% full scale accuracy, less than 0.5% full scale nonlinearity, and a standard temperature range of –20°C to 80°C (Geokon 2021c). The transducers and subsequent extensometers were configured to the CR6 Datalogger safely housed in the nearby weather enclosure for remote monitoring. An extra 150 feet of 0.375-inch 04-375V9-E Violet PVC Cable for extensometers with four sensors was used for the connection between the assembly head and datalogger.


Figure 3.31 Geokon vibrating wire displacement transducers (Geokon 2021c)

Each complete system was initially programmed to record and store data from the strainmeters and displacement transducers at 15-minute intervals. A sample datalogger program is listed in the Appendix.

To capture dynamic vehicular traffic loads, the high-speed capabilities of the VWIRE 305 module was employed where the sampling rate was increased to 20 Hz and data was captured when triggered by a loading event. Dynamic data collection and storage is always a balance between obtaining the data and storing the data. Trigger levels must be set such that data is not missed nor unintentionally triggered/gathered/stored. Hence, once the data loggers were in place and the dead load of the structure was in place data was monitored long enough to establish a baseline and a reasonable trigger threshold.

3.6 Chapter Summary

Two methods were employed to determine embankment settlement: Modified Hough Method and Schmertmann Modified Method. The former correlates soil compressibility and SPT blow count to determine settlement for each subdivided soil layer, while the latter considers the strain influence beneath the idealized footing. The two methods produced comparable embankment settlement values for each of the investigated sites. The estimated pile settlement was minimal, and the relative pile-soil settlement was well above AASHTO and FDOT downdrag thresholds of 0.4 inches and 0.5 inches, respectively.

A total of three sites were chosen: two in Clay County, Florida (FDOT District 2) and one in Hillsborough County, Florida (FDOT District 7). Other sites were rejected for the study either due to soil type or atypical construction sequencing where a surcharge program was instituted to remove the anticipated excessive settlement prior to pile driving. The compressible soils at the selected sites consisted predominantly of sandy soils, which met the requirements for this study. At each site, one pile was installed with instrumentation that could monitor both long-term and short-term loading events. Additionally, an extensometer / soil settlement assembly was installed near the instrumented pile to monitor embankment surcharge effects. For all sites the settlement gauges were installed outside the zone of influence usually associated with driven piles approximately 5-10 pile diameters behind the row of end bent piles.

Chapter Four: Data Analysis

4.1 Introduction

The previous chapter discussed site evaluation of potential bridge construction projects for the field instrumentation and monitoring component of this study. Of the three sites, only one has concluded construction, the other two are nearing completion. Analyses of data available at the time of this report are discussed. The data are presented in the order of project completion: Sandridge Rd was built to substantial completion first; Paseo Al Mar Blvd was fully completed with traffic load second; and the Henley Rd site was still under construction.

4.2 Data Monitoring and Analysis

Static loading responses from each site were monitored continuously and stored every fifteen minutes for all three sites. Raw frequency from vibrating wire sensors was measured from strainmeters within the pile and extensometers beneath the embankment. The temperature determined from thermistors associated with each vibrating wire sensor strainmeter was used to determine the local temperature and correct for frequency changes associated with the expansion or contraction of the vibrating wire. Calibration constants specific to each strainmeter and extensometer were used to convert the frequency into strain or displacement, respectively. Temperature-corrected strain was converted to pile force by multiplying it with the area of the pile and its modulus of elasticity (5700 ksi used for all piles).

The forces in the test pile at each site were observed as backfill height increased over time, structural load was applied, and for live load events where possible. Displacements beneath the embankments were similarly determined as a function of time and construction loading events.

4.2.1 SR 23 Northbound over CR-739B (Sandridge Road) Bridge No. 710113

The MSE wall leveling pad was poured shortly after the site was instrumented. Soon thereafter, backfill was placed in six-inch lifts over a period of three weeks as illustrated in Figures 4.1 and 4.2. The piles were cut off on June 1st, 2021 (Figure 4.1). Table 4.1 shows the timeline for significant construction/loading events.

Table 4.1 Construction events demarcated in later graphs.

No.	Date	Event
1	5/7/2021	First of fill placement
2	5/26/2021	Last of fill placement
3	6/1/2021	Pile cutoff
4	6/25/2021	Cap and pedestals poured
5	7/1/2021	Backwall and cheek walls poured
6	8/6/2021	Girder Placement
7	9/30/2021	Bridge Deck Pour

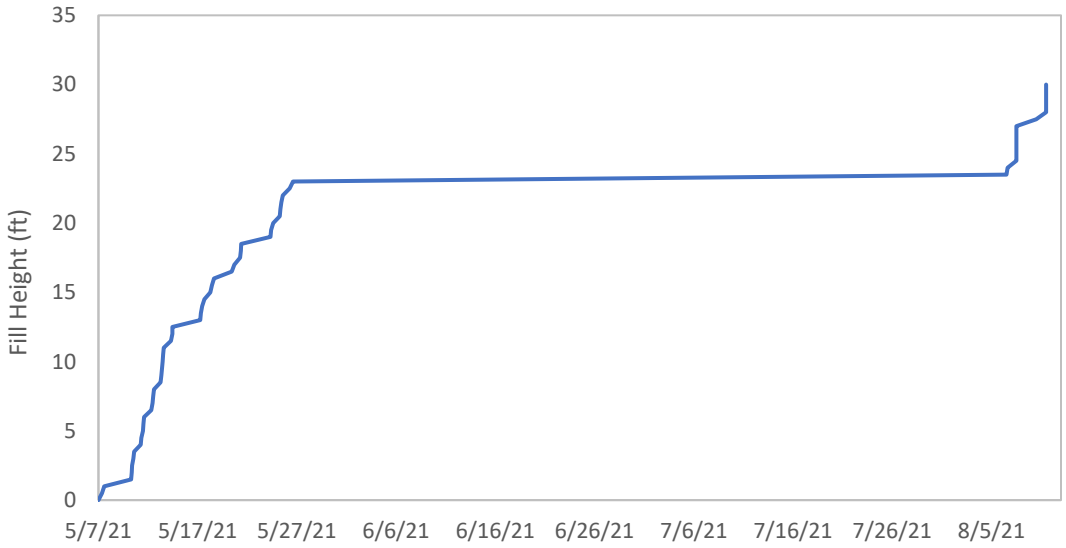

Figure 4.1 Embankment height progression (Sandridge Rd)

Figure 4.2 Sandridge Road fill height progression.

Strainmeter designations within the pile are illustrated in Figure 4.3. Figure 4.4 shows the computed pile forces for each gauge. The vertical dashed lines indicate points of interest, such as the slight decrease in force at time of pile cutoff, increase from pier cap, girders, deck, etc. Additionally, thermal effects of the cap and pedestal are visible after events 4 and 5. Figure 4.5 is a close-up of these effects and shows that as ambient temperature increased, the pile force

decreased from cap expansion and vice versa. Figure 4.6 shows the evolution of pile force distribution as a function of fill height. As the backfill height increased, the downdrag forces within the pile notably increased. Figure 4.7 shows the displacement from each extensometer.

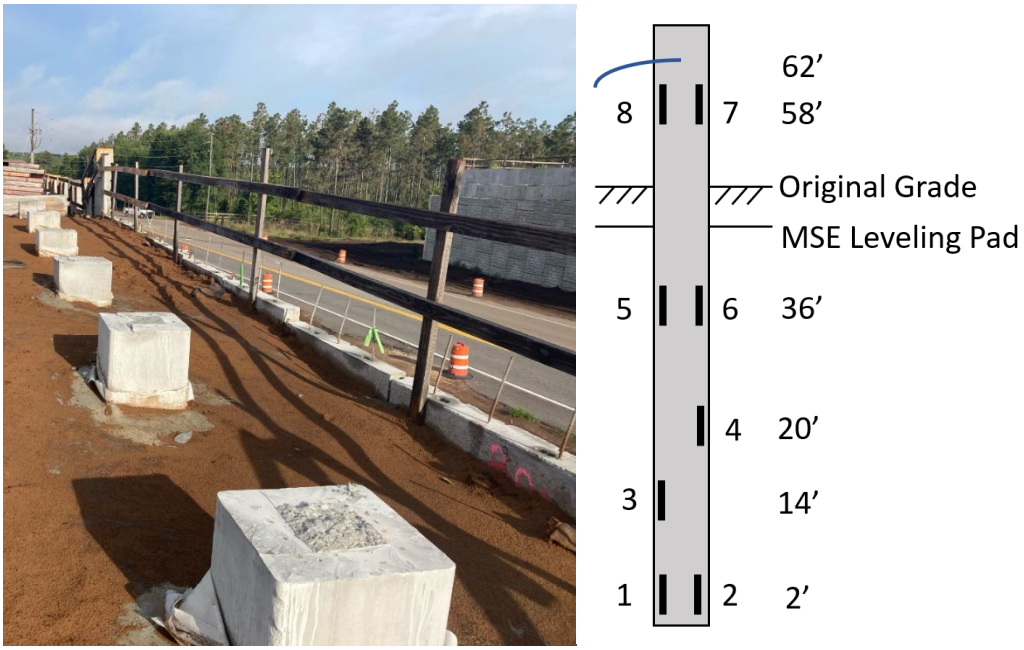

Figure 4.3 Sandridge Road pile cutoff (left) and gauge designation and elevations (right)

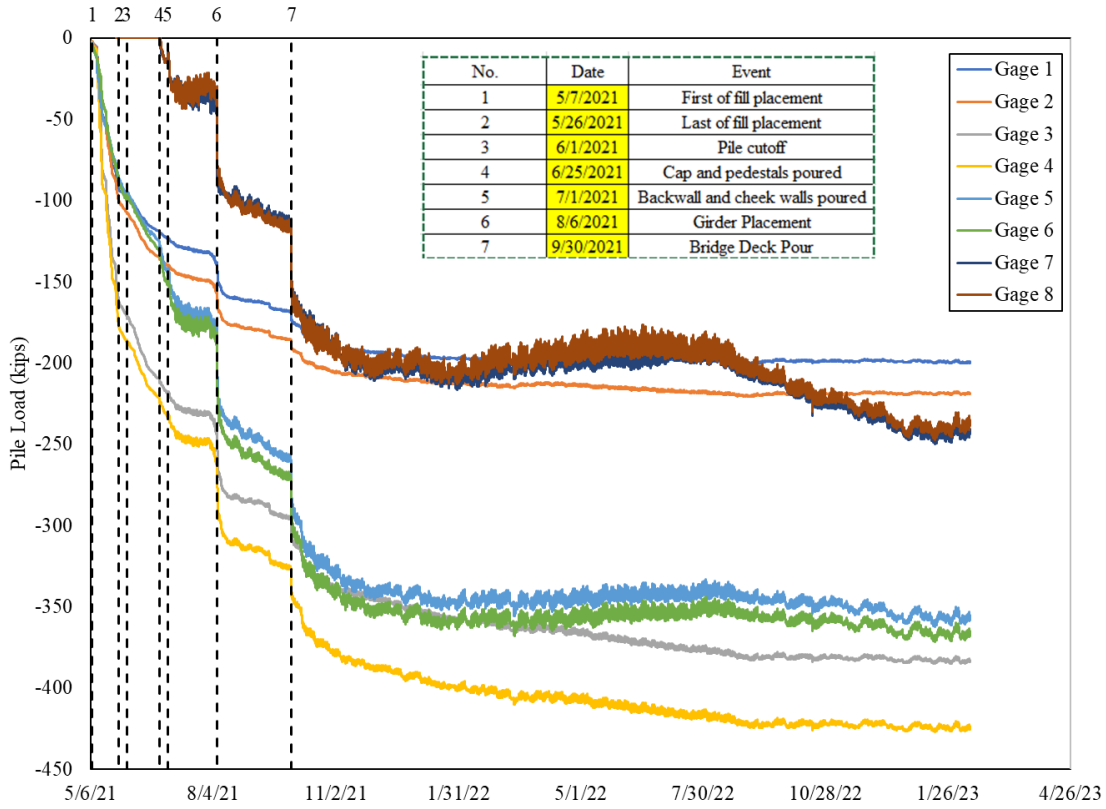

Figure 4.4 Sandridge Road pile force (creep corrected discussed later)

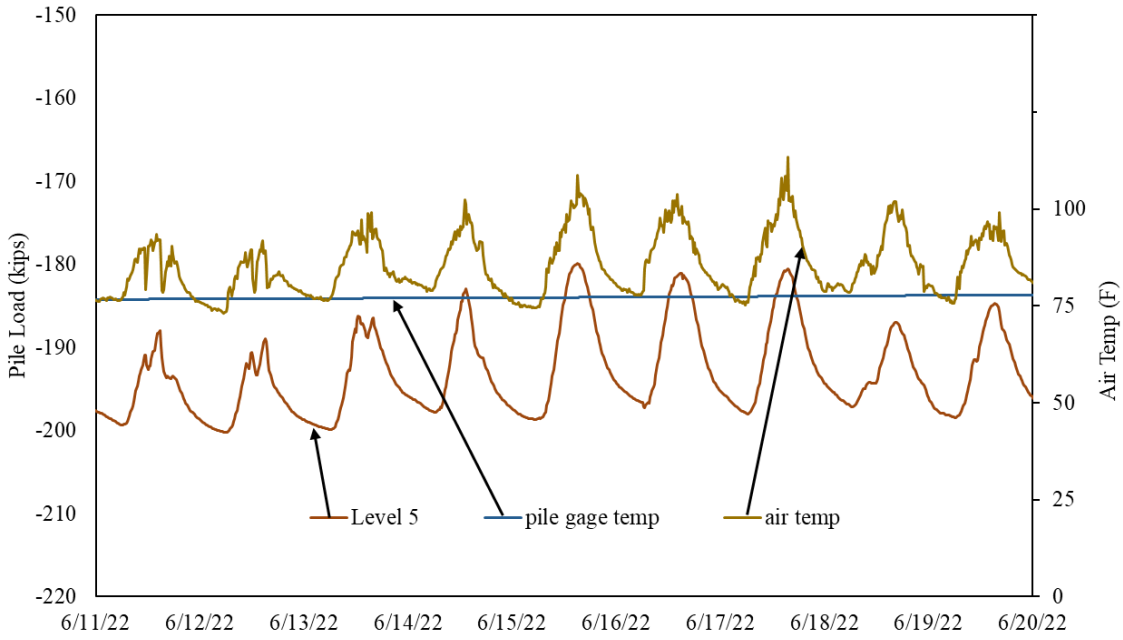

Figure 4.5 Sandridge Road pile force and air temperature (level 5 is top of pile)

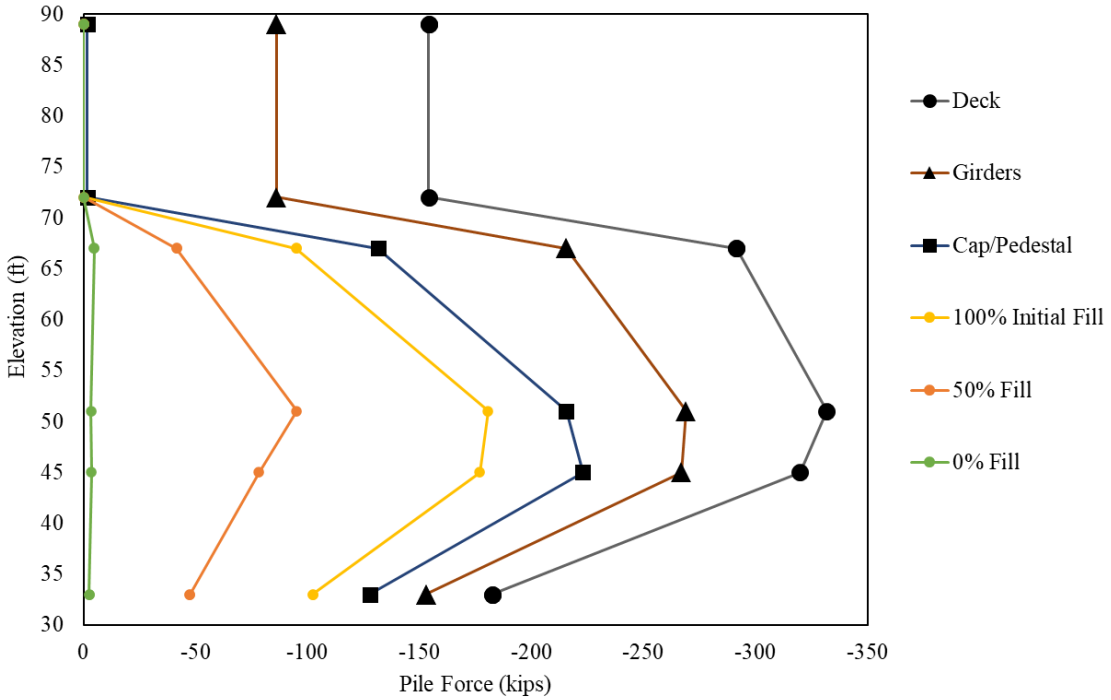

Figure 4.6 Sandridge Road pile force evolution (creep corrected discussed later).

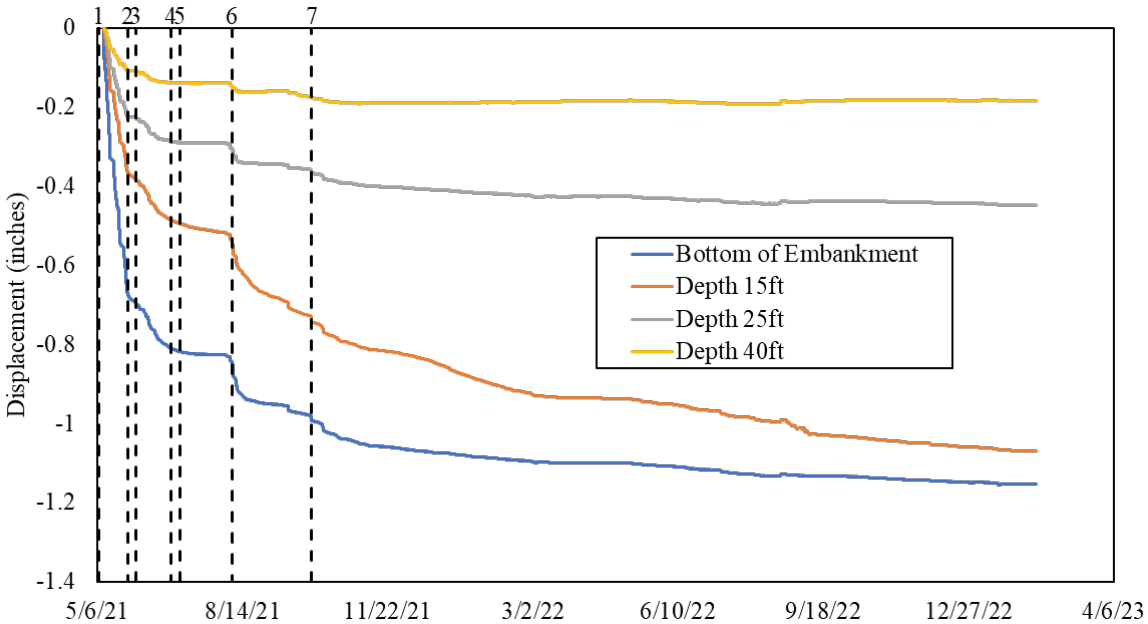

Figure 4.7 Settlement records for all four extensometer locations.

Temperature induced strains can cause force when an element is restrained or an element may simply expand or contract with no associated force when unrestrained. Figure 4.5 shows the force in the upper most level of the pile (Level 5) where the changes in force are mimicked by the change in temperature. However, the temperature at the location of the strain gauge did not change

meaning the force in the pile is due to external restraints. The mechanism of temperature effects on the pile bent system is discussed later.

4.2.2 Paseo Al Mar Boulevard I-75 Flyover Bridge No. 104495

The MSE wall construction for Paseo Al Mar Blvd progressed at a similar rate to that of the Sandridge Rd site. The leveling pad was poured soon after site instrumentation, and fill placement immediately followed. Figures 4.8 and 4.9 show the backfill height progression. Pile cutoff occurred on June 8th (Figure 4.10). Table 4.1 shows the chronology of construction events.

Table 4.2 Paseo Al Mar construction events

1	5/12/21	Begin fill placement
2	6/2/21	Fill completed to pile cutoff elevation
3	6/8/21	Pile cutoff
4	6/21/21	Cap poured
5	6/23/21	Pedestal poured
6	6/26/21	Diurnal temperature induced forces begin
7	7/2/21	Stem/back wall poured
8	10/19/21	Girder Placement
9	12/8/21	Bridge Deck Poured
10	1/13/22	Barriers
11	2/7/22	Approach Slab

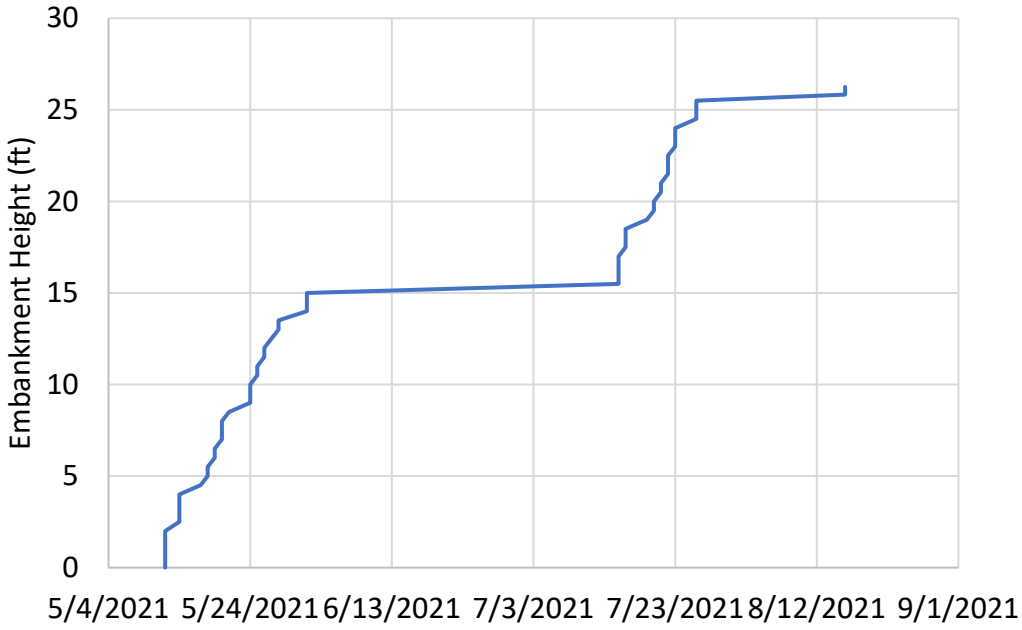

Figure 4.8 Paseo Al Mar Blvd fill height vs. time

Figure 4.9 Paseo Al Mar Blvd fill height progression.

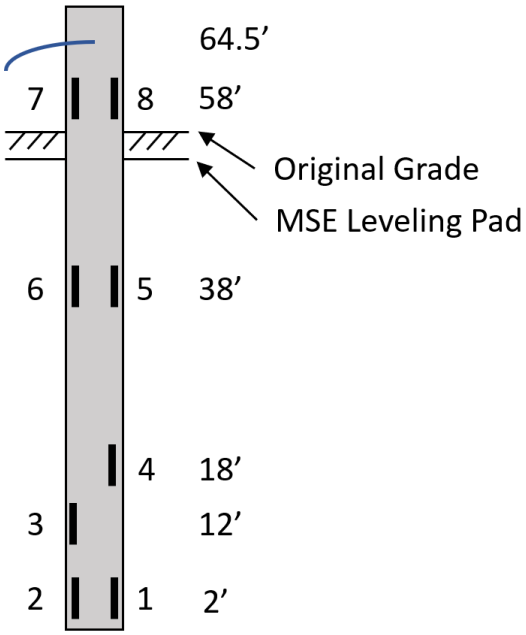

Figure 4.10 Paseo Al Mar Blvd pile cutoff (left) and gauge designation (right).

Figure 4.10 also shows the strainmeter designations within the pile. The pile force as a function of time is shown in Figure 4.11. Like the Sandridge Rd site, diurnal fluctuations in pile load began after the cap was poured. The evolution of pile force distribution as a function of fill height is shown in Figure 4.12. As expected, the forces at depth within the pile notably increased as backfill height increased.

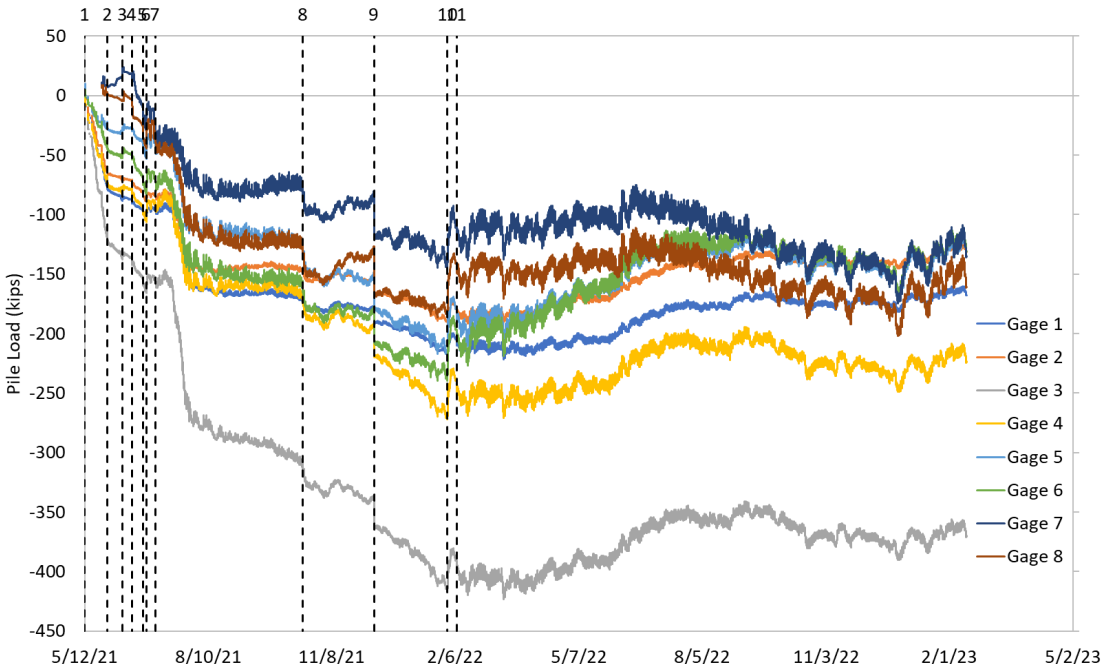

Figure 4.11 Force from each gauge throughout the timeframe of the study.

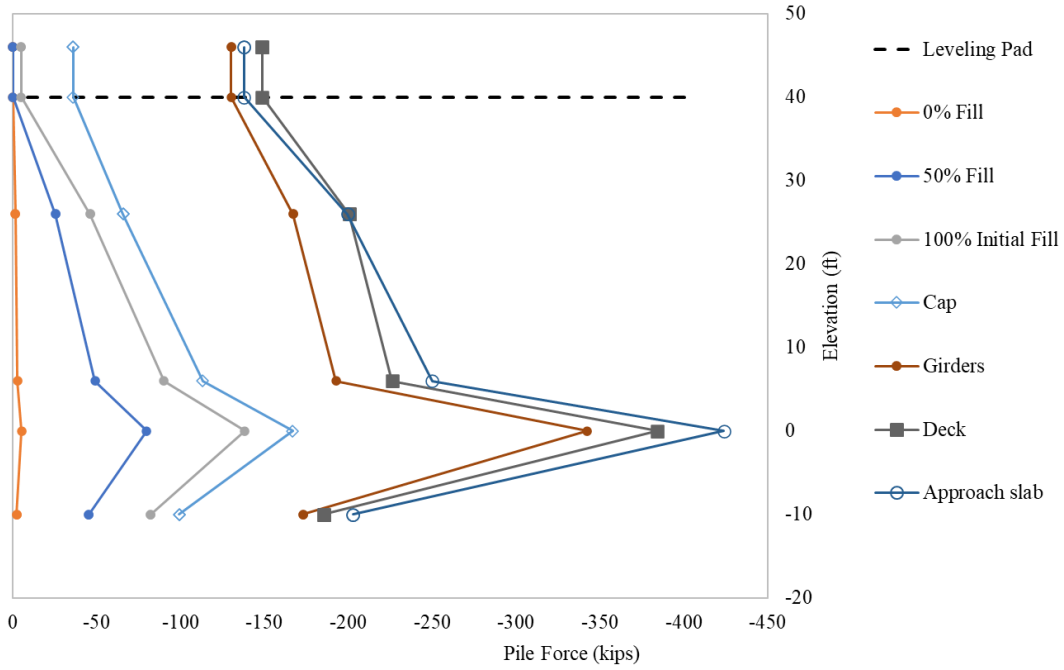

Figure 4.12 Paseo Al Mar Blvd pile force evolution (creep corrected discussed later).

The amount of settlement experienced by each grouted anchor locations are shown in Figure 4.13 throughout the timeframe of the study. The extensometer head and the first anchor location showed near identical displacement traces indicating no appreciable compression in the upper, higher blow count layer.

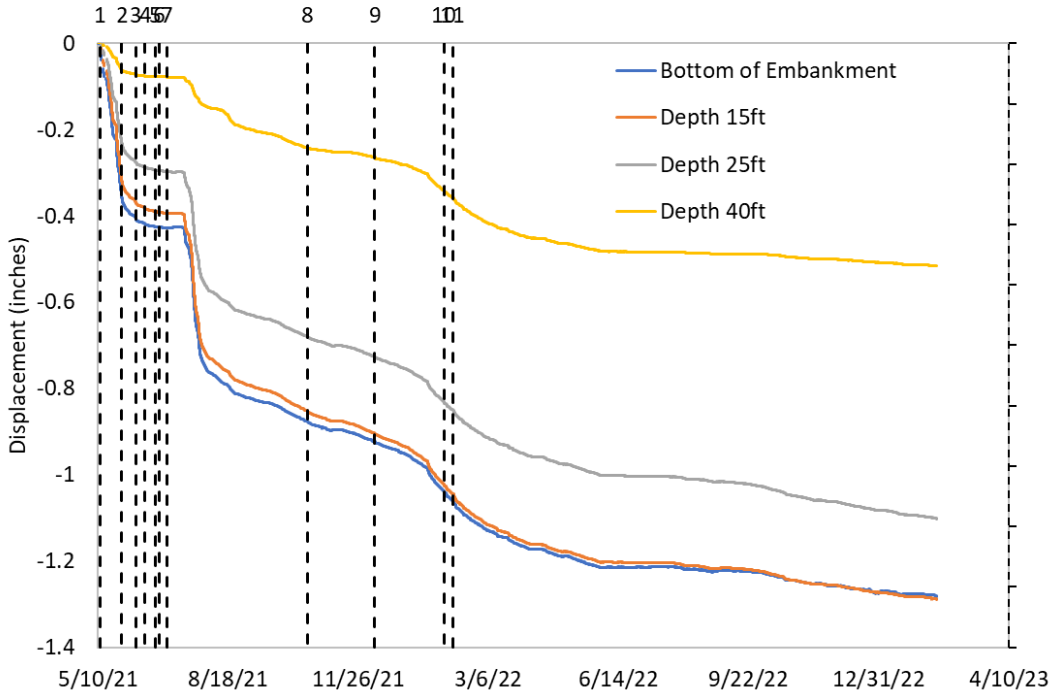

Figure 4.13 Paseo Al Mar settlement data over the timeframe of the study.

4.2.3 SR 23 Southbound over CR-739 (Henley Road) Bridge No. 710120

The MSE wall construction for the Henley Rd site began 20 months after the pile was instrumented and driven. The leveling pad was poured soon after site instrumentation, and fill placement immediately followed. After an 8-month pause pile cut off elevation was achieved where two of the piles required splicing. Figures 4.14 and 4.15 show the backfill height progression. Pile cutoff occurred on May 6th, 2022 (Figure 4.16). Table 4.3 shows the chronology of construction events.

Table 4.3 Henley Rd Construction Events

1	9/22/2021	First of fill placement
2	4/4/2022	Fill completed to pile cutoff elevation
3	5/6/2022	Pile cutoff
4	10/26/2022	Cap and pedestals poured
5	10/31/2022	Backwall / Wingwall / Cheekwall poured
6	11/15/2022	Beams Placed
7	12/6/2022	Backwall fill commenced
8	1/6/2023	Backwall fill almost complete
9	2/2/2023	Diaphragm Walls

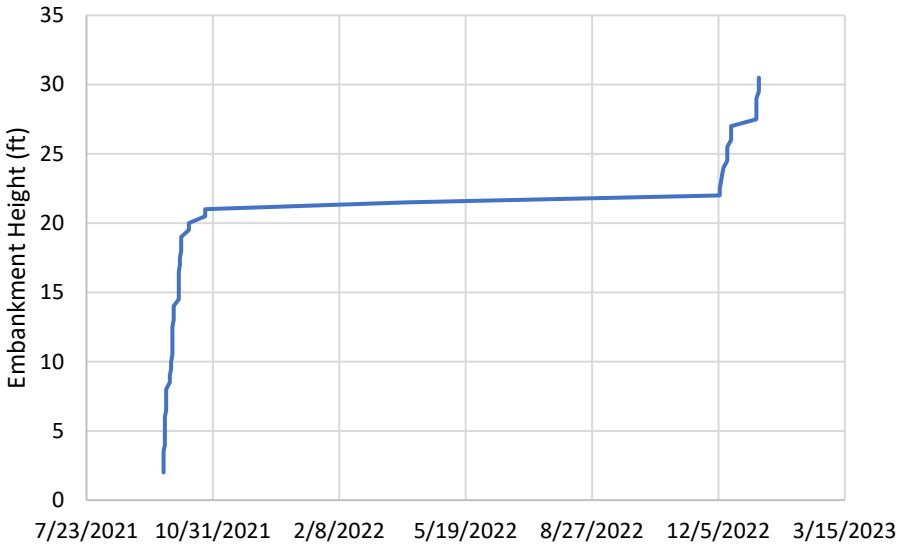

Figure 4.14 Daily embankment heights vs. time (Henley Rd)

Figure 4.15 Henley Rd fill height progression.

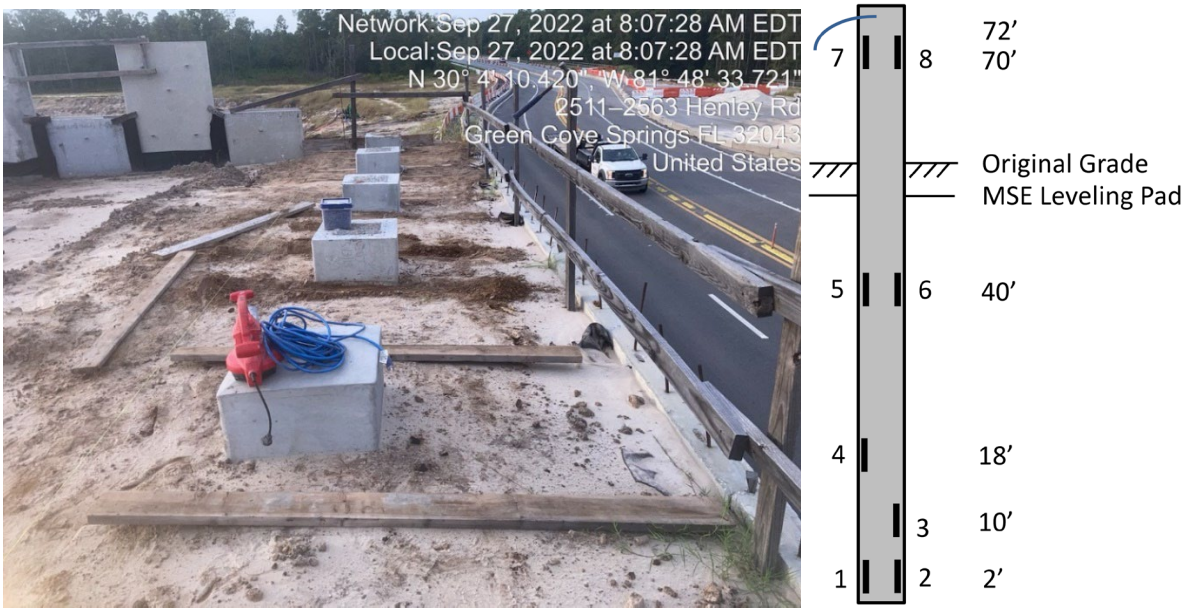

Figure 4.16 Henley Rd backfill at cutoff elevation (left); gauge designation (right)

Figure 4.16 also shows the strainmeter designations within the pile. The pile force as a function of time is shown in Figure 4.17. Like the other two sites, diurnal fluctuations in pile load began after the cap was poured. At the time of this report only the girder weight had been applied.

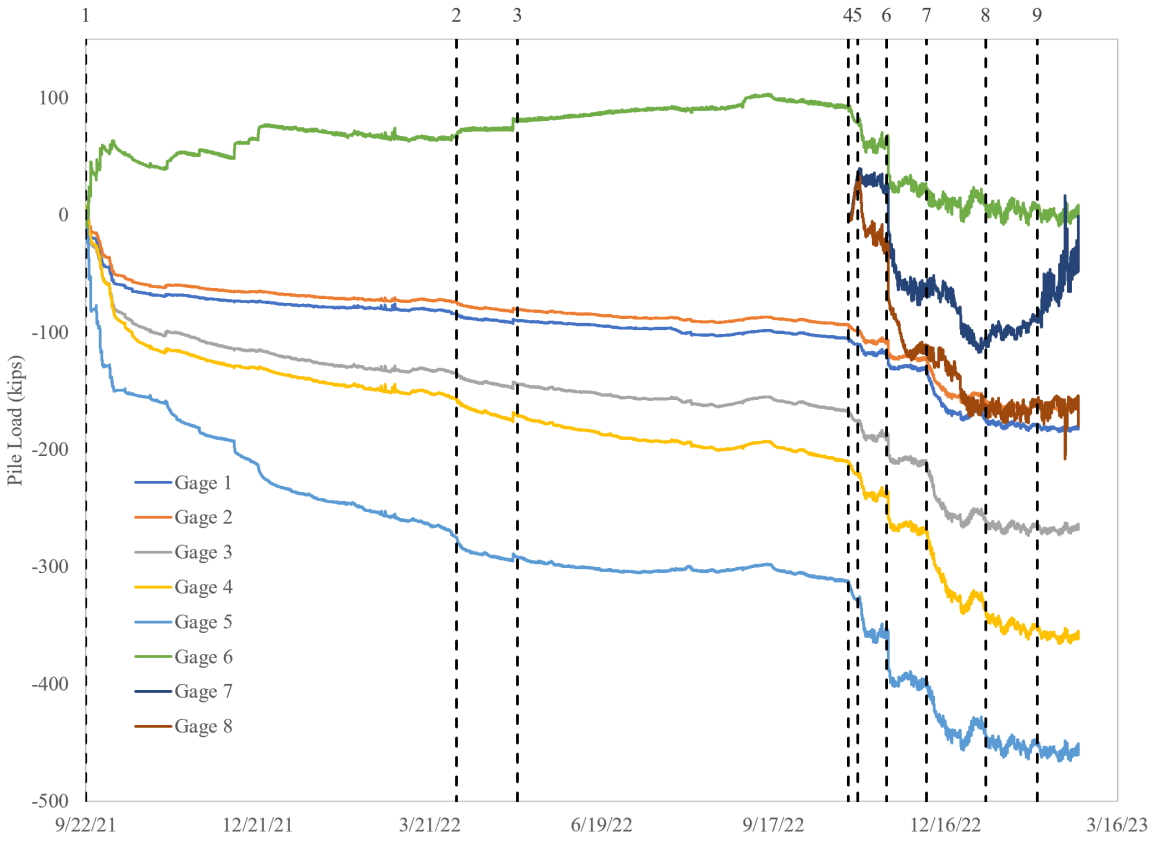

Figure 4.17 Henley Road pile force (creep corrected)

Strains were converted to load assuming uniform strain but Gauge 6 did not experience a 100k tension load. Rather the average of gauges 5 and 6 strain values (Level 4) translates into a 49k axial compression force. The orientation of the piles as they were placed into the templates and driven were not dictated by the research team and in the cases of the previous two sites the strain gauges located on opposite sides of the piles at the neutral axis of the pile were aligned with the line of piles in the bents. In this case, at Henley Rd, the gauges were aligned orthogonal to the pile bent orientation. Of particular interest in Figure 4.17 is the large bending stresses detected by gauges 5 and 6 located 20 ft below the original ground surface. Figure 4.18 shows the same data along with the pile gauge location per the instrumentation plan. The compaction of the embankment fill is shown to promote an outward force on the piles toward the wall causing a 50k-ft bending moment at that depth. The effects of solar radiation and diurnal temperature effects on the unrestrained exposed piles can also be seen in gauges 7 and 8 prior to being covered (omitted from Figure 4.17 for clarity).

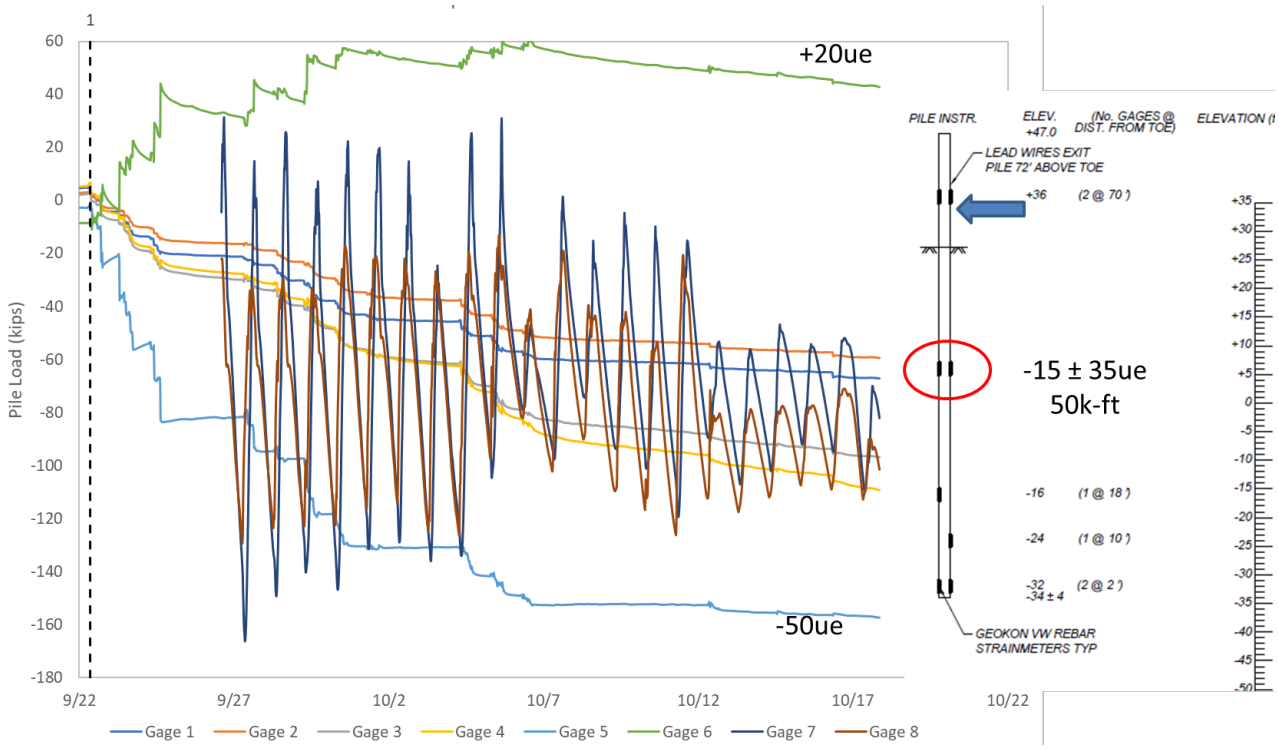

Figure 4.18 Non-uniform compaction around the test pile induced bending simultaneous to downdrag.

The evolution of pile force distribution as a function of fill height is shown in Figure 4.19. Again, the forces at depth within the pile increased noticeably as backfill height increased. The settlement from each extensometer is shown in Figure 4.20.

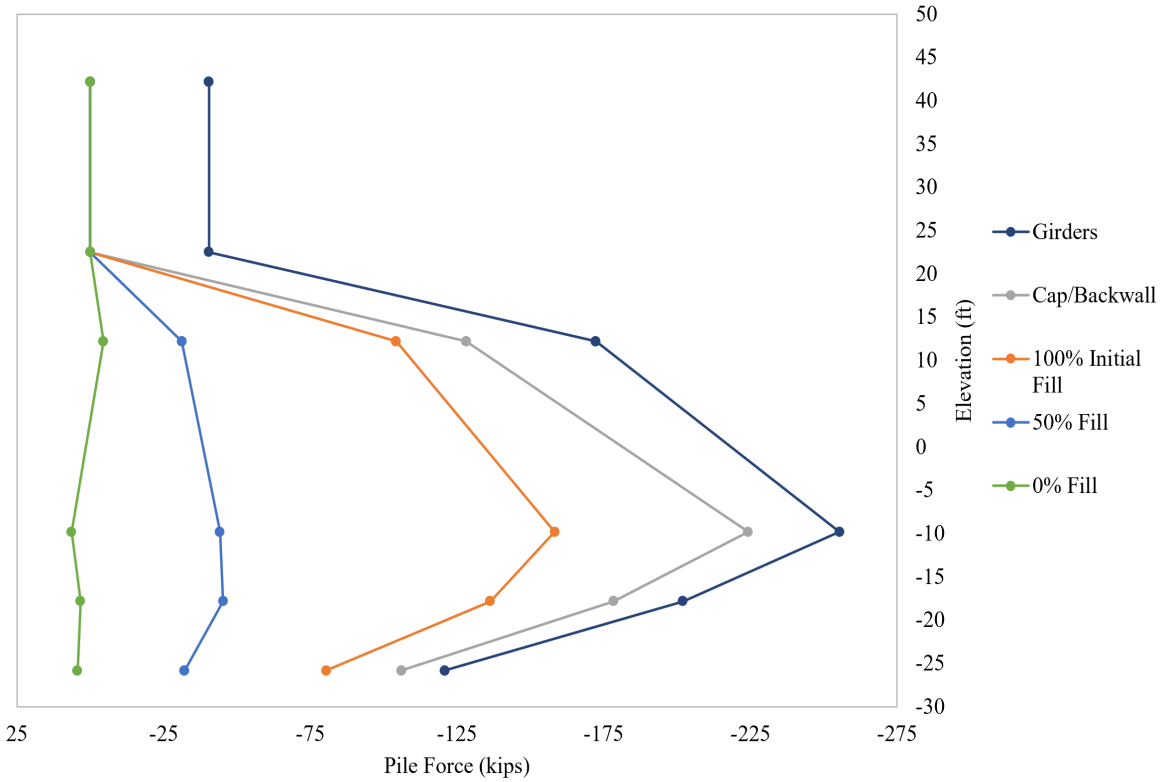

Figure 4.19 Henley Road pile force evolution (creep corrected discussed later).

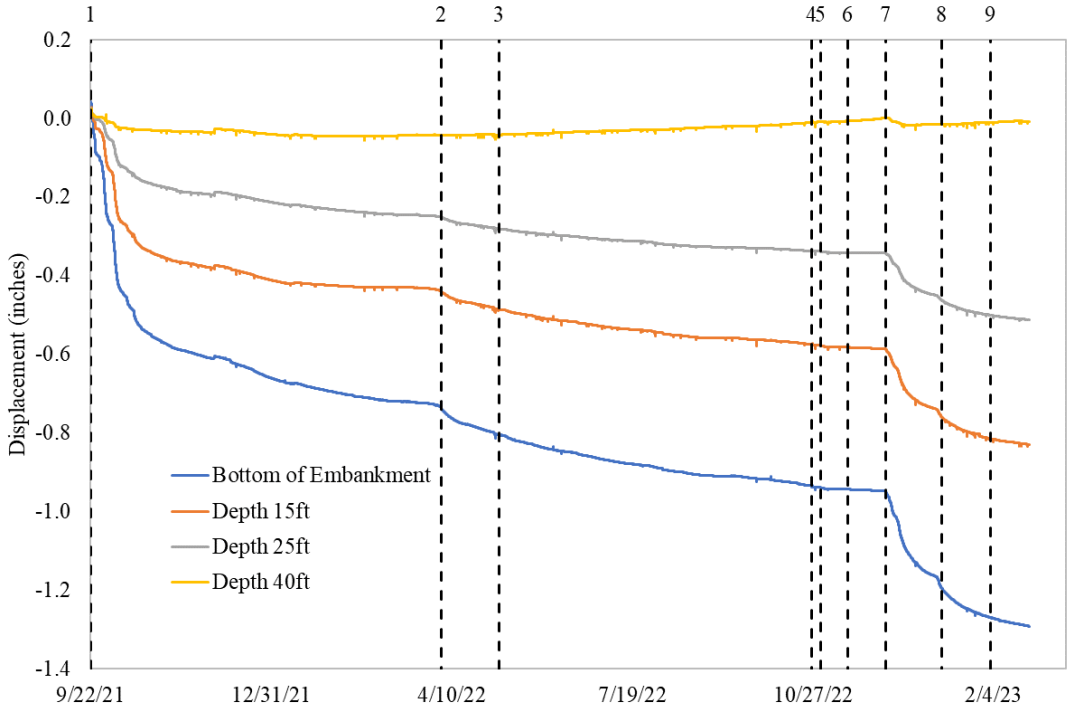

Figure 4.20 Henley Road settlement data over the timeframe of the study.

4.3 Creep Correction Considerations

The pile force versus time graphs shown earlier (Figures 4.17 and 4.23) were all corrected for progressively increasing strain (creep) during times when no external loads were applied. Strains can increase with time due to time-dependent soil settlement or from creep which is most pronounced immediately after a new load is applied. Creep strain can be computed using equation 4-1 where the magnitude of the initial strain (from loading) has the most effect.

$$c_p = e_0 v_u \frac{t^{\varphi}}{d+t^{\varphi}} \tag{4-1}$$

where,

c_p is creep strain
e_0 is initial strain from new load
t is time in days after the load is applied
φ is the time exponent ranging from 0.4-0.8 (0.5 typical)
d is a time constant which can range from 6 to 30 days (30 typical)
v_u is an empirical constant ranging from 1.30 to 4.15 (1.818 typical)

Daily creep strain rates were estimated by taking the average rate of change in the overnight strains. Those rates were then discretely integrated (rate multiplied by net change in time) to obtain creep strain at any given time. The accumulated creep strain was then subtracted from the temperature-corrected strain to compute the creep-corrected pile forces (Figures 4.26 and 4.27). The creep measurements were commensurate with literature values from Equation (4-1) so this equation was used for all sites to remove the effects of creep strain which can artificially increase the computed load on the piles.

The largest initial strain the pile would have experienced was the detensioning strains (~ -200ue) which was induced by the initial prestress in the piles (~1 ksi). The onset of pile strain monitoring occurred 21, 33, and 178 days after casting for Paseo Al Mar, Sandridge, and Henley sites, respectively. Hence, creep effects from prestressing were dependent on the age of pile for a given strain measurement and corrections were different for each site. Other significant increases in load caused by casting the concrete pier cap, girder placement, or the bridge deck pour each started a new time dependent creep correction. These corrections were superimposed. Figure 4.21 shows the time dependent total shortening of the pile at the Sandridge Rd site which includes strain from creep and new loads. The total embankment settlement is also shown. Where settlement ceases so should pile shortening in the absence of creep effects. However, progressive strain during dormant loading phases and with no progressively increasing settlement can be seen and were necessarily removed using Equation 4-1. Figures 4.22 and 4.23 show an example of the effects of creep on pile load from the Paseo Al Mar bridge site before and after correction, respectively. This type of correction was applied to all force data presented in this study.

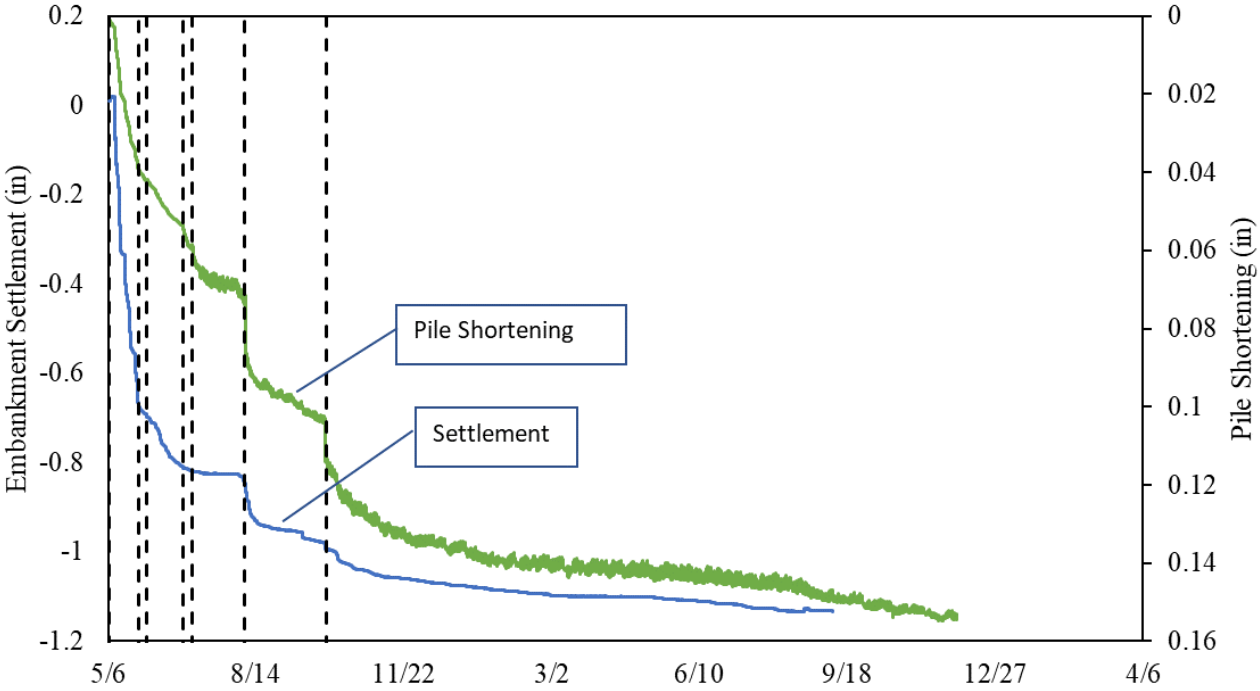

Figure 4.21 Creep-induced pile shortening vs actual embankment settlement.

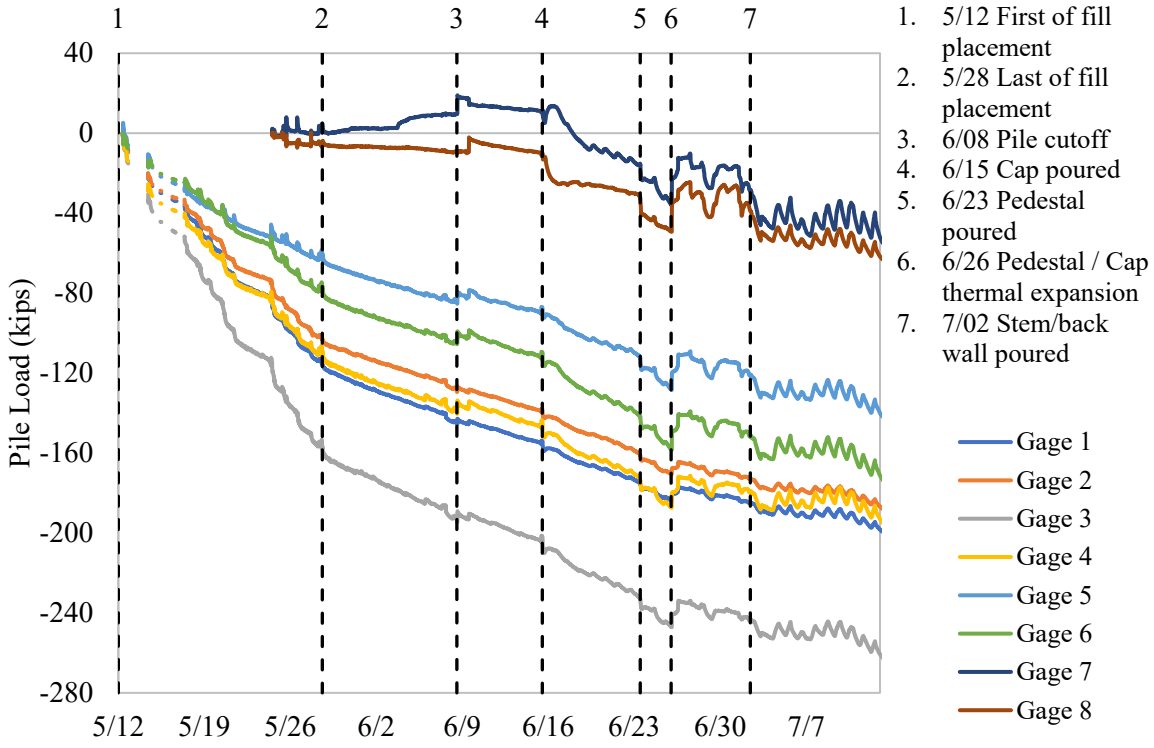

Figure 4.22 Paseo Al Mar Blvd raw pile force

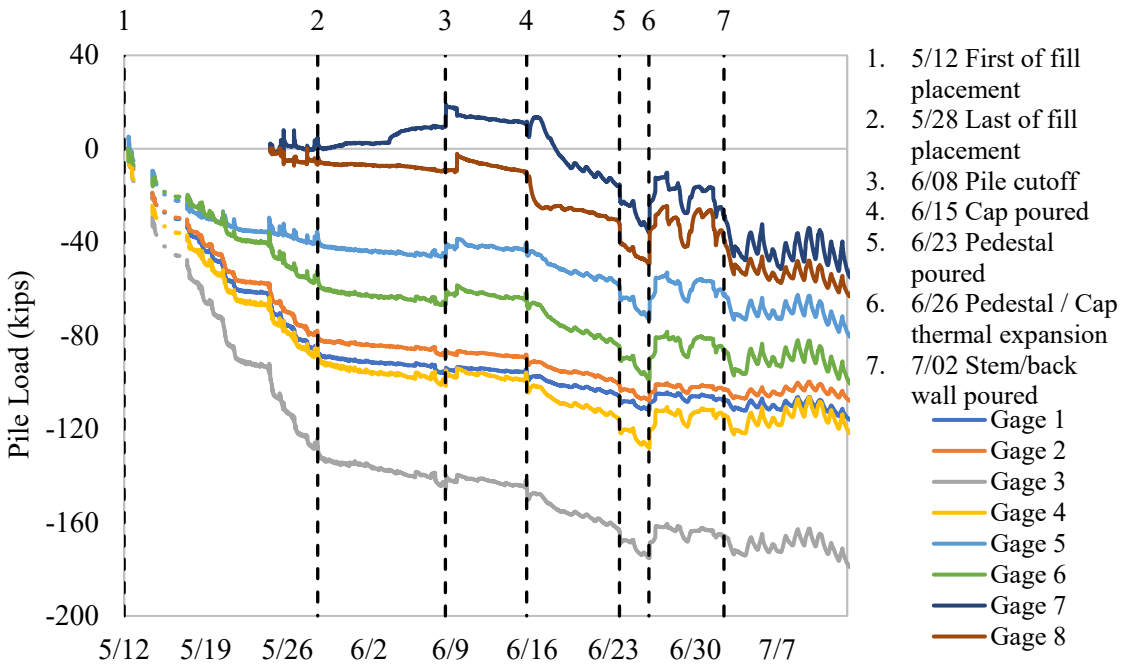

Figure 4.23 Paseo Al Mar Blvd corrected pile force

Note the corrections shown in Figures 4.22 and 4.23 from Paseo Al Mar cover a two-month timeframe and do not completely eliminate progressive increase in strain and force from time 2 to 3. When comparing the force and settlement traces for almost two years in Figures 4.10 and 4.12 force increases mimic settlement trends which are the result of a clayey sand layer that did not settle immediately.

4.4 Effects of Diurnal and Seasonal Temperature Change on Pile Force

Temperature changes are known sources of error when computing internal forces in structures. When considering the vibrating wire type sensors for instance, the measurement is based on changes in frequency due to shortening or lengthening the fixed restraints holding the wire. However, if the restraints do not move but the wire temperature changes the force and vibrating frequency of the wire will change disproportionately to the strain of the wire restraints. These types of corrections have already been discussed and are routinely applied based on the incorporated thermistors providing vibrating wire temperature changes. On a larger scale, bridge decks expand/lengthen or contract/shorten due to changes in ambient temperature which in turn can impose severe forces on the bearing pads or pier caps. If unrestrained with expansion joints or similar, no force is induced throughout the bridge deck.

In the cases of the end bent piles in this study, various types of temperature fluctuation were observed. Pile temperature changes below ground were modest and remained constant below the depth of no seasonal soil temperature fluctuation (typically 15 ft). Some conductive heat transfer within the piles to a deeper depth was observed although minimal. Figure 4.24 shows the temperature traces from Sandridge Rd where ambient air temperature was measured along with the temperature from each vibrating wire sensor. No appreciable change is noted below a depth of 20 ft; the other levels show a phase lag in the season temperature changes increasing with depth.

Figure 4.25 shows the maximum and minimum temperature ranges for all gauges with respect to elevation.

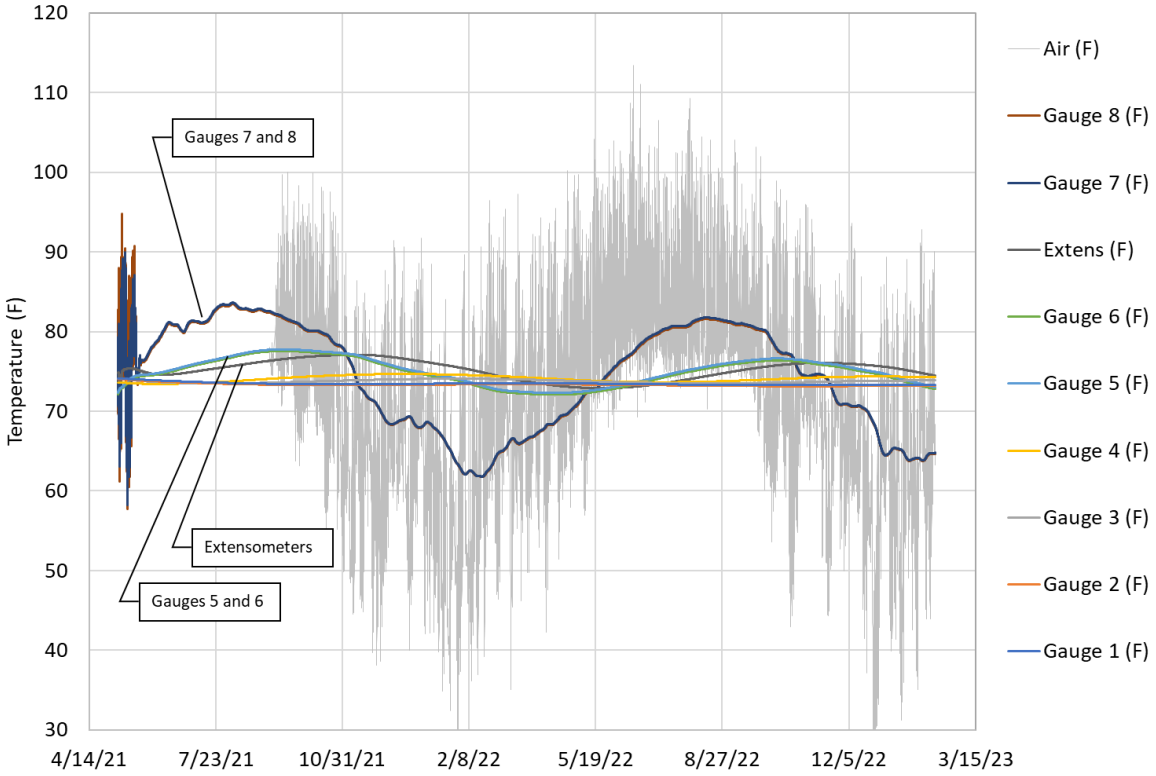

Figure 4.24 Seasonal temperature variations.

The at-depth soil temperature is the average annual air temperature for a given site which takes multiple seasonal cycles to achieve. Hence for a given year, the annual air temperature may vary slightly from previous or a larger number of years. In this case the at depth gauge temperatures are 0.5 degrees warmer than the one-year average.

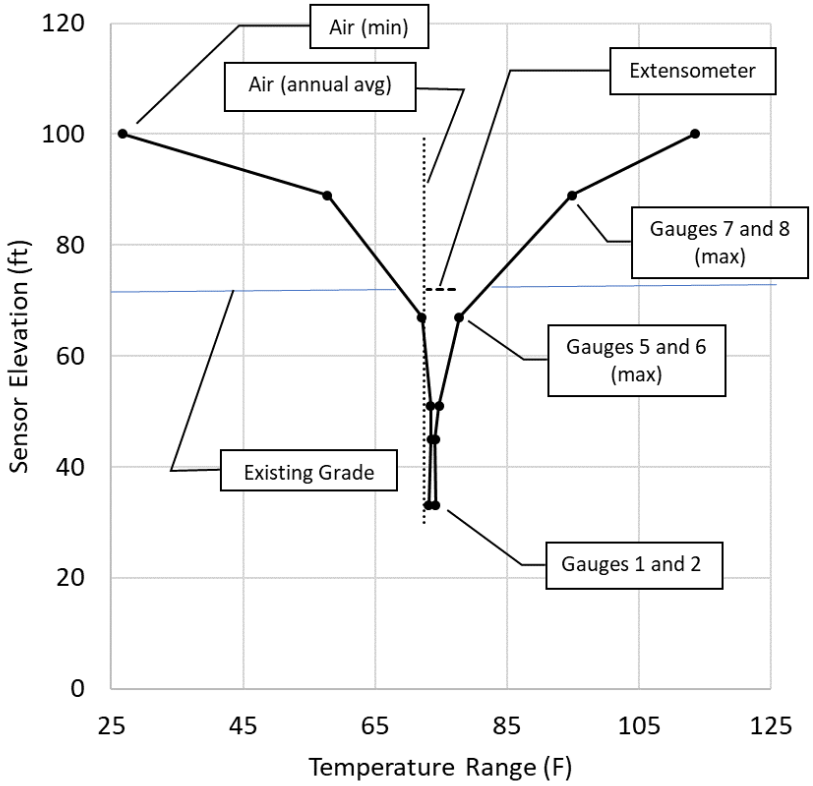

Figure 4.25 Temperature range for all sensors and elevations (Sandridge Rd).

Not reported in Figure 4.24 is the early air temperature where gauges 7 and 8 experienced large temperature fluctuations. This was shown to be true thermal expansion and contraction from solar radiation which if converted to pile force would be artificial or an apparent pile load (Figure 4.26). A closer look at the data reveals the effect of morning sun on the east side (Gauge 7) and afternoon sun on the west side (Gauge 8) shown in Figure 4.27. Gauges 7 and 8 remained unburied until 5/24/21 when the gauges were zeroed as the baseline no-load condition. Some bending can be seen as the ground level raised and was compacted, and then residual stresses were unlocked when the pile was cutoff and load above the gauges was reduced by approximately 1.6 kips.

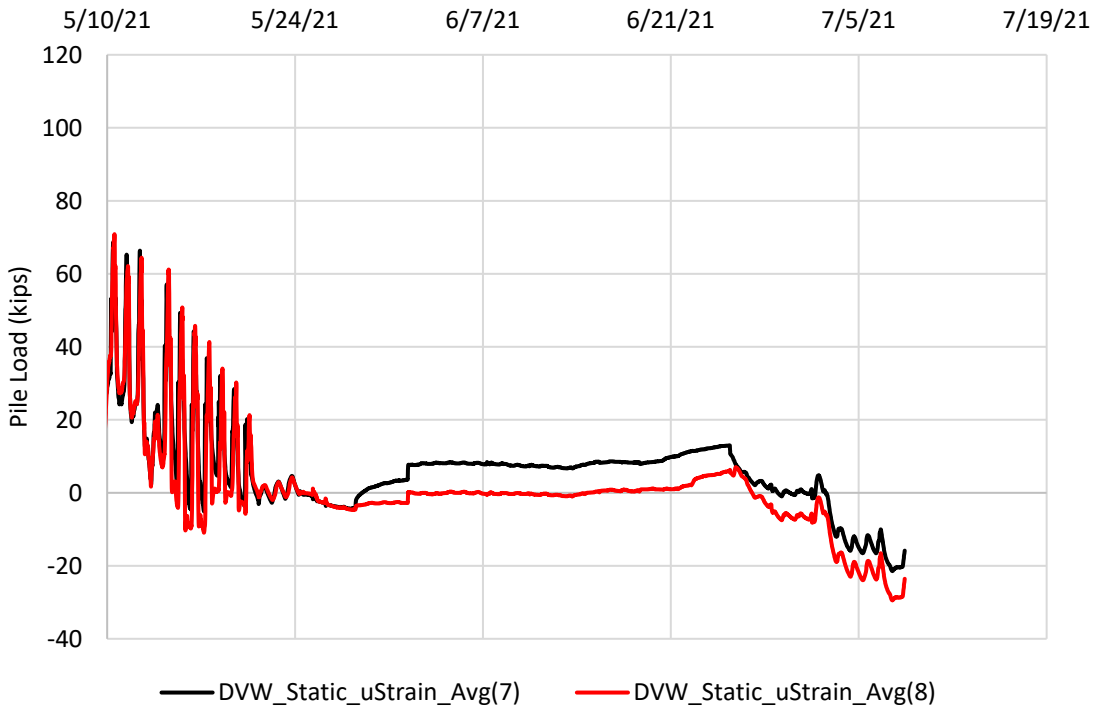

Figure 4.26 Load registered by strain gauges that does not reflect true load on pile.

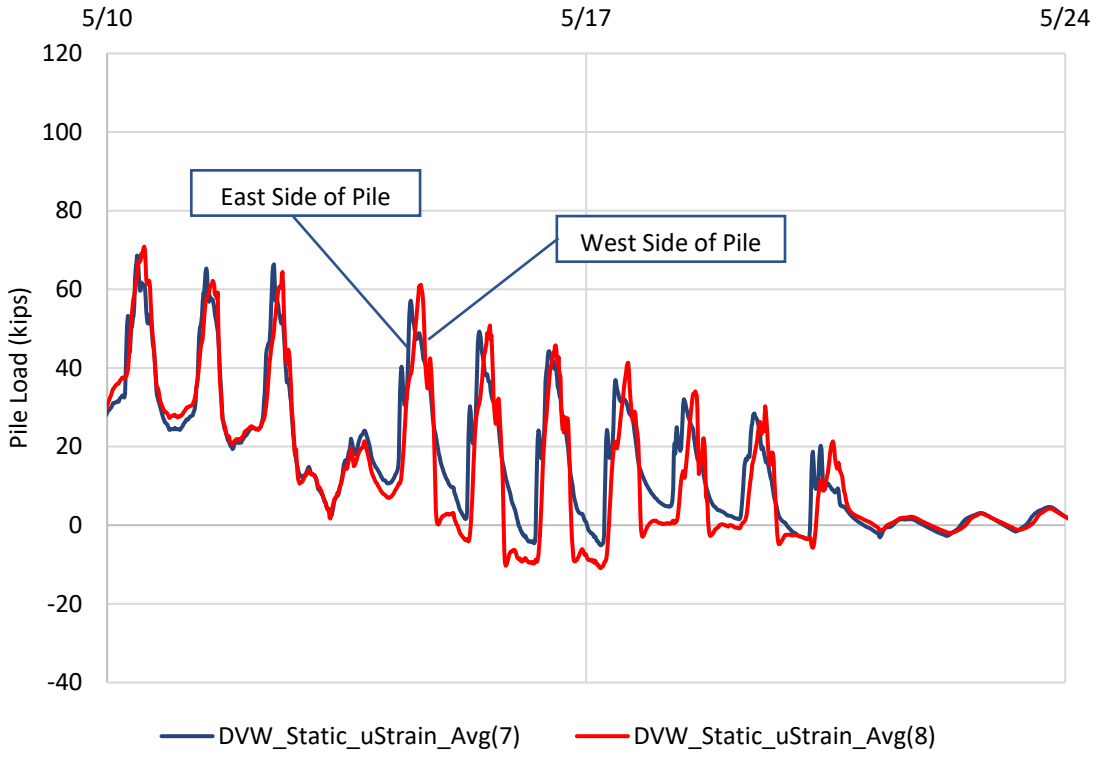

Figure 4.27 Solar heating of east and west sides of the test pile above ground.

After the upper level gauges were buried and solar and daily temperature changes ceased, force in the pile began to change again coinciding with the fluctuations in air temperature (Figure 4.27). But this occurred after the pile cap and backwall were cast. The weight of the pile cap was detected along with subtle diurnal variations. After the back wall was cast, an increase in self-weight was again noted but diurnal load changes were more apparent. All three sites showed the same trends. Figure 4.28 shows a slight lag of approximately one hour where the load reduces in the pile after a rise in air temperature. This rate of heat transfer is reasonable with the direct access of air temperature changes on the pile cap, beam seats, and back wall between the girders under the deck.

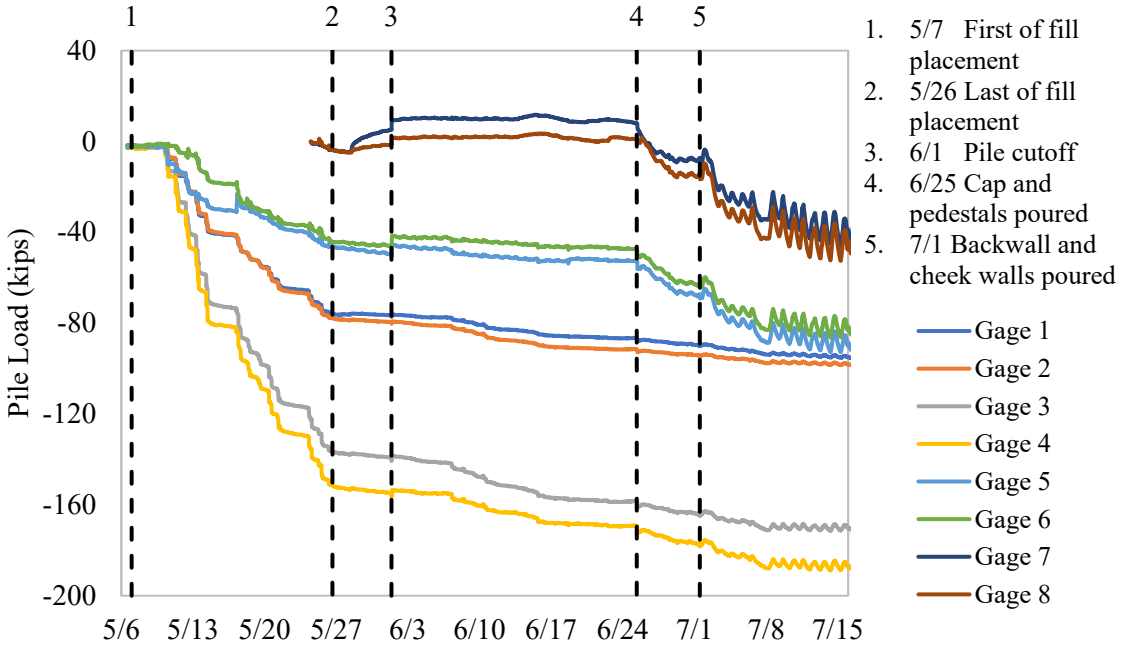

Figure 4.28 Diurnal changes in force commenced after casting cap and backwall.

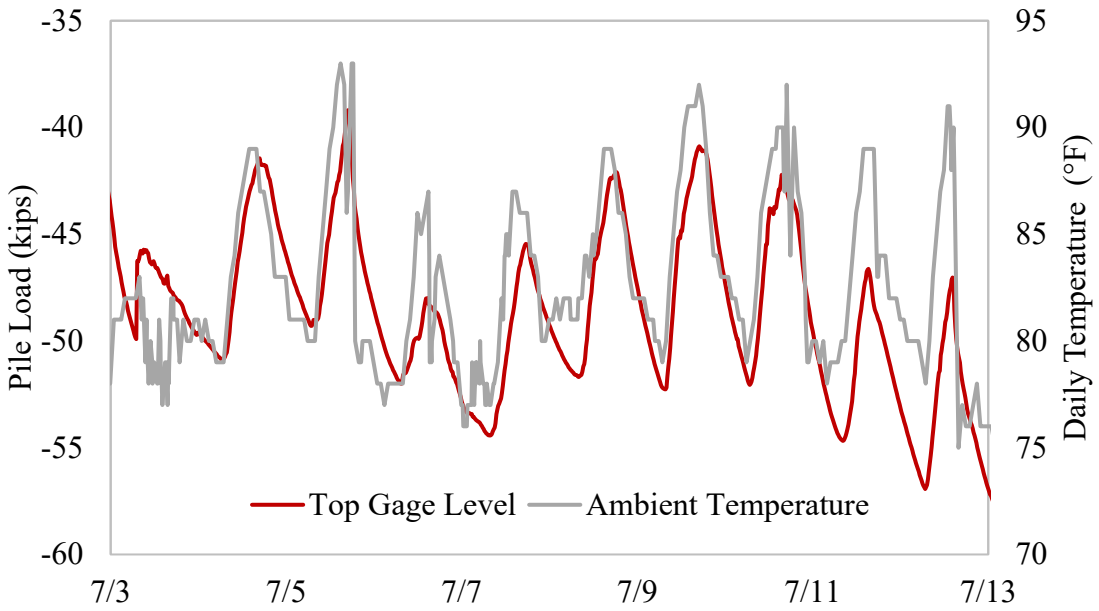

Figure 4.29 Paseo Al Mar Blvd pile force and air temperature

Figure 4.30 shows the same trend at the Sandridge Rd site where a 10 kip change in pile load is experienced each day. But the load is not the by-product of strain gauge thermal effects; the gauge location temperature does not show the same diurnal fluctuation.

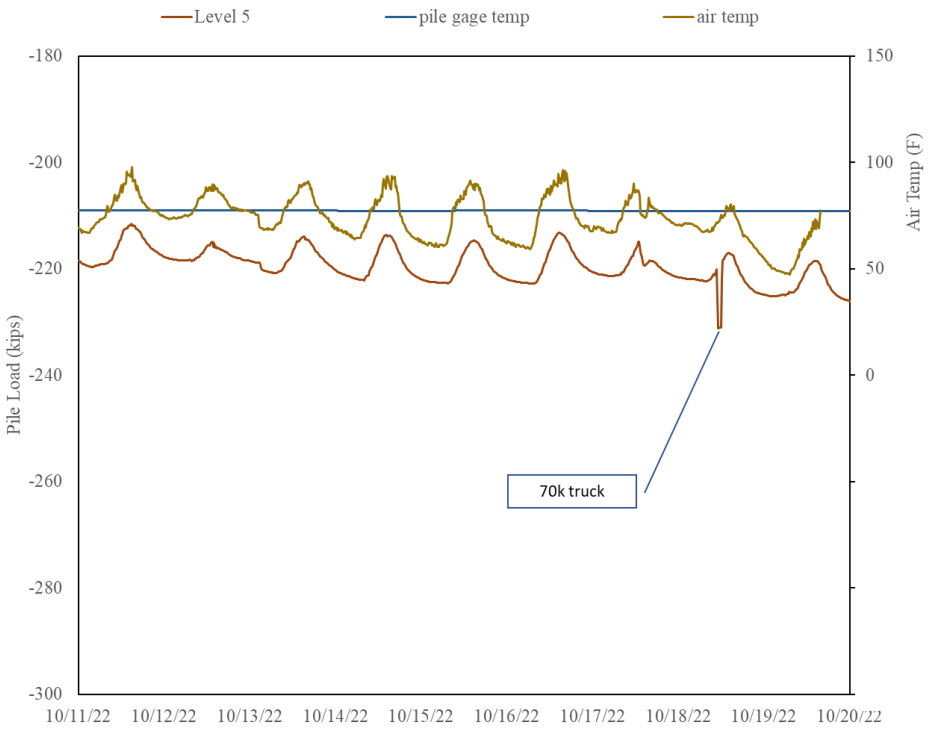

Figure 4.30 Diurnal variations in load magnitude similar to truck loading event.

Figure 4.30 also shows the effect of a truck loaded to 70 kips parked on the span closest to Sandridge Rd End Bent 1 (study bent) for one hour. Figure 4.31 shows the placement of the truck. Although the full weight of the truck is not directly over the end bent, an 11 kip change in pile force was registered, very close to the 11.7-kip load obtained by dividing the load equally into the six piles in the bent. Some load is lost to position in the span (not parked directly on end bent) yet some is regained from pile cap flexure and the load being closely centered over the test pile position within the cap. Also note the effect of the truck load is similar in magnitude to daily changes in load from ambient temperature variation.

Figure 4.31 Seventy-kip loaded truck parked over test pile in end bent (Sandridge Rd).

The mechanism of diurnal force fluctuations is thought to have been caused by pile cap and back wall warming and cooling and from being so close to the changing air temperature. Reviewing the construction sequencing, the cap was poured on compacted fill and bonded to the exposed piles. Minimum pile embedment into the cap is 12 inches which is considered a “pin” connection. Studies have shown significant bond is developed even with such small embedment lengths. Figure 4.3 shows more than 12 inches, closer to 24 inches, in that case. The estimated bond capacity for an 18-inch pile with 18 inches of embedment would produce near 260 kips of pullout resistance. Recall, the force fluctuations did not occur until after the cap and backwall were poured. Warming the pile cap (and near surface soil) causes the cap to expand and push down on the soil thus supporting the bridge in part by shallow bearing on the MSE wall-stabilized soils and reducing the deadload on the pile.

The magnitude of daily temperature fluctuations remains similar regardless of season (20°F on average winter or summer) yet the magnitude in pile force change appears to be less in the cooler winter months suggesting a net reduction in pile cap footing pressure against the compacted soil

(Figure 4.32). However, the total seasonal pile force again remains in phase with seasonal air temperature changes and not changes in the concrete pile temperature. Delays in pile temperature change relative to force changes remove the possibility of artificially registered pile force (Figure 4.33). The changes in seasonal pile force (50 kips) far exceed the 70-kip truck loading event (11 kips). The fluctuations in pile force are shown to reduce with depth but can be seen (Figure 4.32).

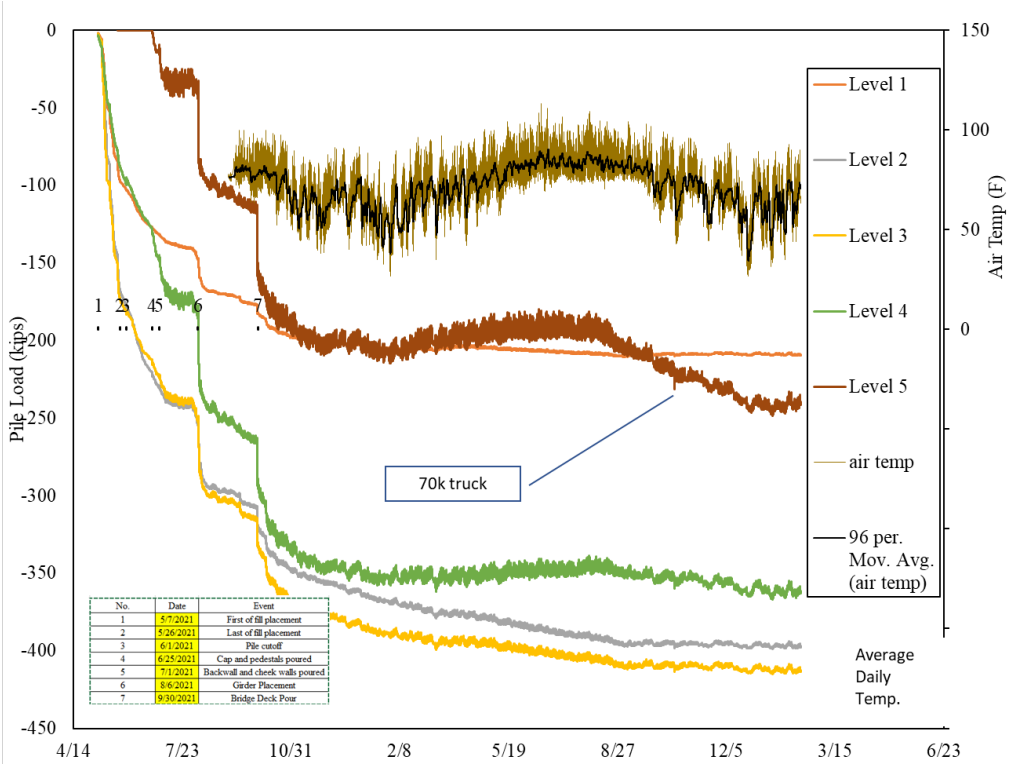

Figure 4.32 Seasonal temperature changes induce large changes in pile force.

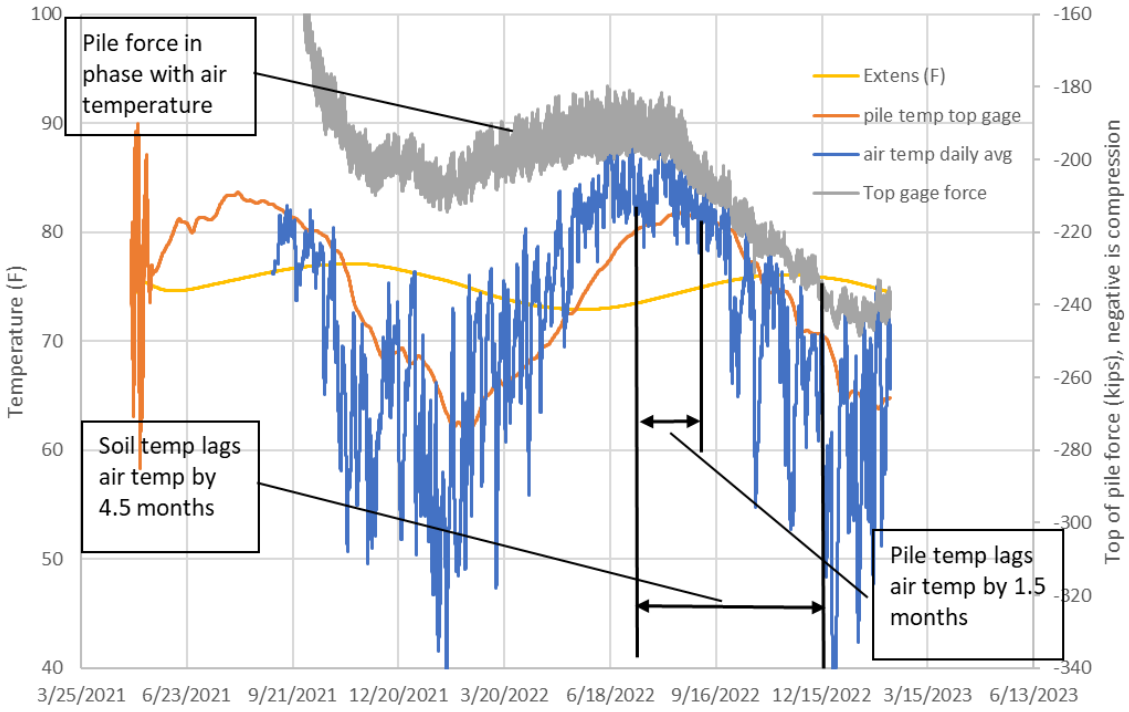

Figure 4.33 Pile force and air temperature changes in phase.

4.5 Chapter Summary

This chapter presented the raw data collected from pile strainmeters and ground settlement gauges from three sites where settlement around the piles in end bents was expected to exceed downdrag criteria. Results showed the force in the piles experienced significant levels of downdrag forces in conjunction with the ground settlement. Temperature variations were shown to induce forces where the pile cap was restrained from freely expanding due to contact with the ground surface.

Chapter Five: Numerical Modeling

5.1 Introduction

When investigating engineering problems, it is helpful to combine field testing and monitoring with numerical analysis and laboratory experiments. The combination of the three (field testing, lab testing, and numerical modeling) can provide answers to puzzling questions and the development of new theories. This chapter describes two phases of numerical modeling carried out to better isolate the parameters affecting downdrag forces. Preliminary finite element models were first carried out with the program PLAXIS 3D on single pile configurations. The motivation for these models was to identify soil strata characteristics that will be most beneficial to the field instrumentation and monitoring component of this study. Models were then conducted using COMSOL where the field conditions (multi-pile configurations) noted in Chapter 3 and field measurements from Chapter 4 were used to confirm model output and then evaluate conditions not encountered in the field.

5.2 Preliminary Numerical Modeling using PLAXIS 3D

Generic sandy soil parameters were considered to identify the types of output possible using PLAXIS 3D, a soil-specific finite element software.

5.2.1 Geotechnical Profile

Two simple soil profiles of strictly sands were considered. The soil profile of the first model consisted of 10 ft of fill, 20 ft of loose compressible sand, 30 ft of medium dense, and 20 ft of very dense sand (Table 5.1). The soil profile of the second model consisted of 100 feet of medium sand (Table 5.2). The soils were modeled as Mohr-Coulomb (MC) model type with drained behavior. The MC model assumes linear-elastic perfectly plastic model with Mohr-Coulomb failure. The inputs include stiffness, strength, and interface parameters.

5.2.2 Structural Elements

Individual concrete piles were modeled as linear elastic with nonporous behavior. The input parameters for the material included elastic modulus, density, and Poisson's ratio. A positive interface was created around the pile to simulate soil-pile interaction. The interface reduction factor is proportional to the skin friction and axial loads; thus, it is critical to choose appropriate interface parameters to simulate soil-pile interactions. A value of 0.70 was used for the interface reduction factor because it is common engineering practice to assume the soil-pile friction angle to be approximately 2/3 of the soil friction angle.

Table 5.1 Model 1 soil profile parameters

Parameter	Name	Unit	Fill	Loose Sand	Med. Dense Sand	Dense Sand	Concrete
Elevation	Top	ft	10	0	-20	-50	10
Elevation	Bottom	ft	0	-20	-50	-70	-56
Material Model	Model	-	Mohr-Coulomb	Mohr-Coulomb	Mohr-Coulomb	Mohr-Coulomb	Linear-Elastic
Material Behavior	Type	-	Drained	Drained	Drained	Drained	Nonporous
Unsaturated Soil Weight	Υ_{unsat}	pcf	120	97	114	138	150
Saturated Soil Weight	Υ_{sat}	pcf	120	99	116	140	-
Cohesion	c	psf	0.1	0.1	0.1	0.1	-
Friction Angle	φ	deg	34	25	33	41	-
Young's Modulus	E	psf	432,000	80,664	372,298	2,001,600	6.35 x 10+8
Poisson's Ratio	ν	-	0.3	0.2	0.3	0.4	0.2
Interface Reduction Factor	R_{inter}	-	0.3	0.7	0.7	0.7	1

Table 5.2 Model 2 soil profile parameters

Parameter	Name	Unit	Med. Dense Sand	Concrete
Elevation	Top	ft	0	0
Elevation	Bottom	ft	-100	-50
Material Model	Model	-	Mohr-Coulomb	Linear-Elastic
Material Behavior	Type	-	Drained	Nonporous
Unsaturated Soil Weight	Υ_{unsat}	pcf	115	150
Saturated Soil Weight	Υ_{sat}	pcf	117	-
Cohesion	c	psf	0.1	-
Friction Angle	φ	deg	32	-
Young's Modulus	E	psf	648,000	6.35 x 10+8
Poisson's Ratio	ν	-	0.3	0.2
Interface Reduction Factor	R_{inter}	-	0.7	1

5.2.3 Mesh

The mesh was finer directly around the pile with a coarser mesh farther from the pile to minimize computation time. Too coarse of a mesh resulted in asymmetrical outputs (i.e., bending in the pile even though a centric load was applied). The mesh was then refined until subsequent refinements produced symmetrical results. The mesh tested to ensure increased refinements were not necessary to increase accuracy.

5.2.4 Loads and Boundary Conditions

The domain consisted of a 200 ft by 200 ft plane. The boundary conditions of the models were the standard fixities set by PLAXIS 3D. The bottom boundary was fully fixed, the side boundaries were normally fixed (rollers), and the top boundary was free. For Model 1, a 55-ft pile was in placed prior to the application of the 10ft layer of surcharge. After the fill was activated to induce surcharge pressures, the pile was axially loaded. For Model 2, a surface surcharge load was applied around the pile to simulate the placement of the embankment fill. Concentrated loads were then applied on the pile to simulate structural loads.

5.2.5 Staged Construction

PLAXIS 3D has a "Staged Construction" mode where geometry and load configuration can be activated or deactivated. The model can then be calculated in the desired loading sequence. The initial phase generated horizontal K_0 stresses (calculated from user input friction angles and the corresponding lateral earth pressure coefficient K_0). The first phase activated pile installation by replacing the initial soil material with pile material within a specified volume and activating the interface. For Model 1, the second phase activated the fill layer of soil around the pile. The second phase of Model 2 involved application of surcharge pressure around the pile to simulate the filling of an embankment. The final phase for both profiles introduced axial load on the pile to simulate structural loads. The final phase for Model 2 also has the same surcharge pressure applied as in phase two. Because once the fill is placed representing the permanent approach embankment, it will apply a continuous surcharge pressure.

5.2.6 Results

Total and relative settlement, mobilized shaft resistance (skin friction), and axial loads in piles were evaluated. Each model was run several times with the concentrated load acting on the pile increasing each time. It was observed that as the applied load at the pile top increased, the depth of the neutral plane shifted upwards towards the pile top with increasing load (Figure 5.1, Figure 5.2). Similarly, with additional structural load, the slope of the negative side shear vs depth progressively changed to positive side shear as expected. Figures 5.1 and 5.2 also show some convergence errors near the bottom and top, respectively which will be addressed in future models to remove the aberrant trends. Figures 5.3 through 5.8 are cross sections of the models illustrating scaled up total vertical displacement of the soil for each phase. The surcharge in Figure 5.8 is hidden so the point load can be seen more clearly.

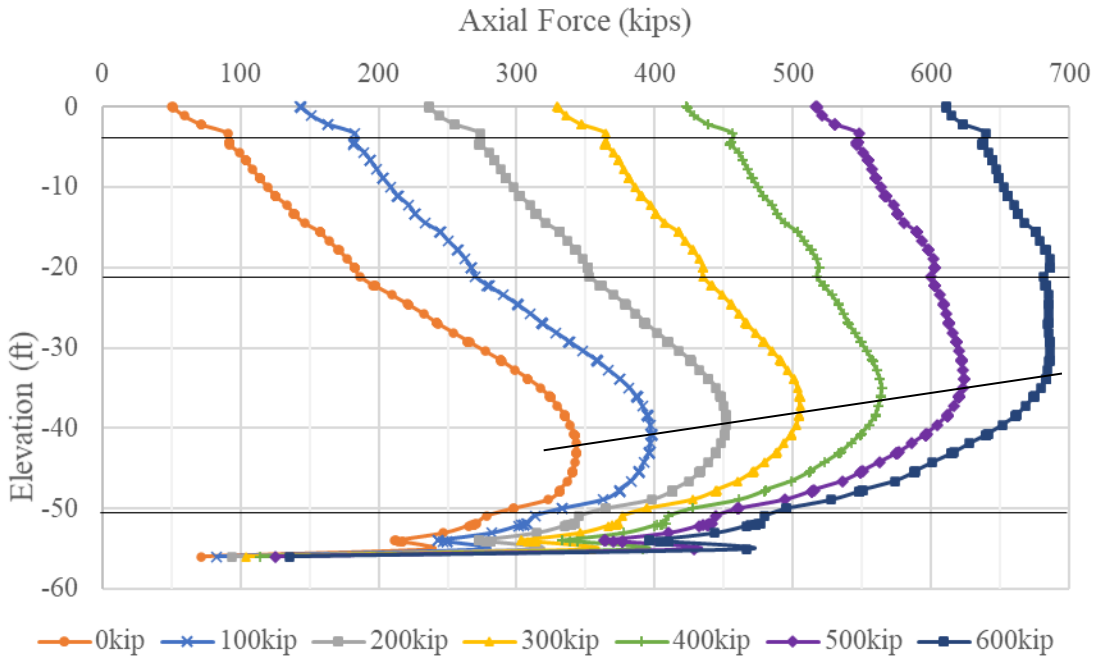

Figure 5.1 Model 1 axial force in the pile versus elevation

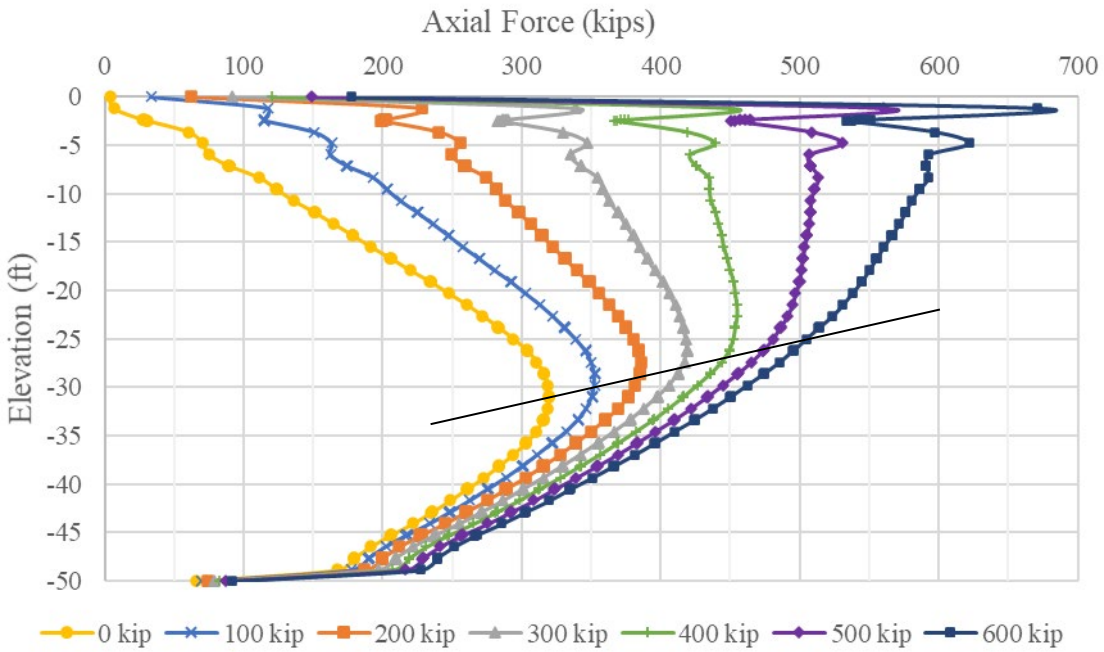

Figure 5.2 Model 2 axial force in the pile versus elevation

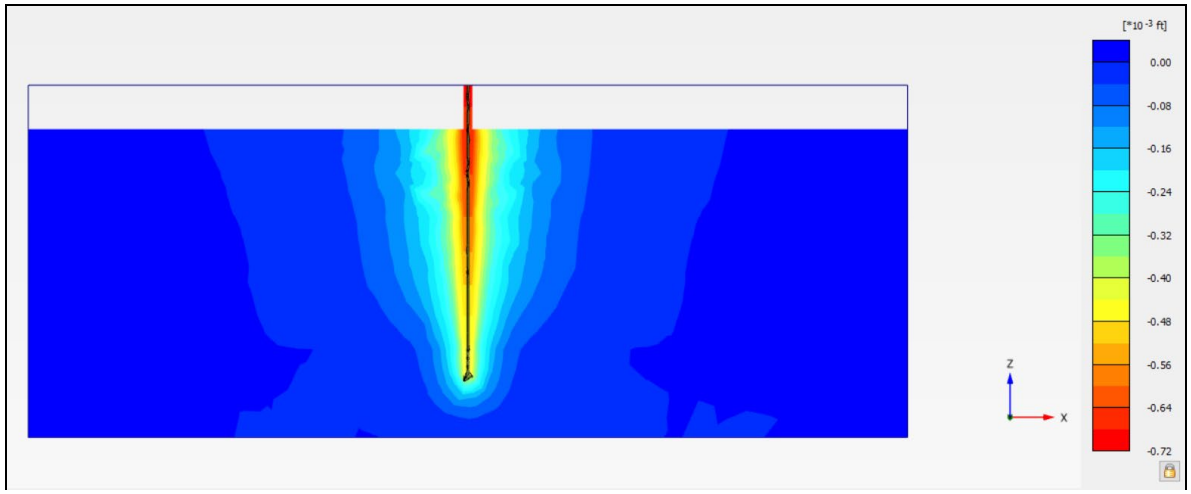

Figure 5.3 Model 1 Phase 1 (pile installation) vertical displacement

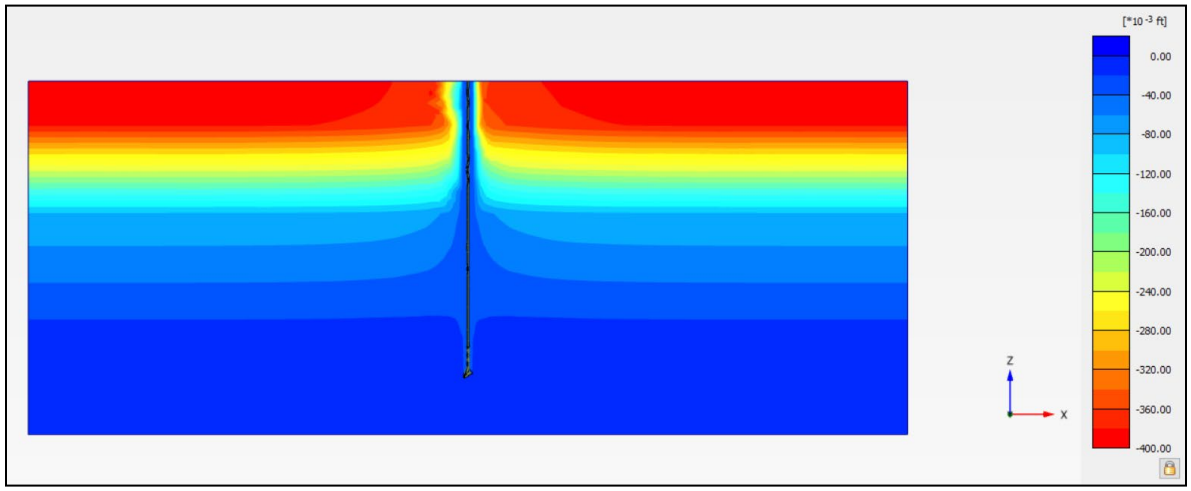

Figure 5.4 Model 1 Phase 2 (fill placement) vertical displacement

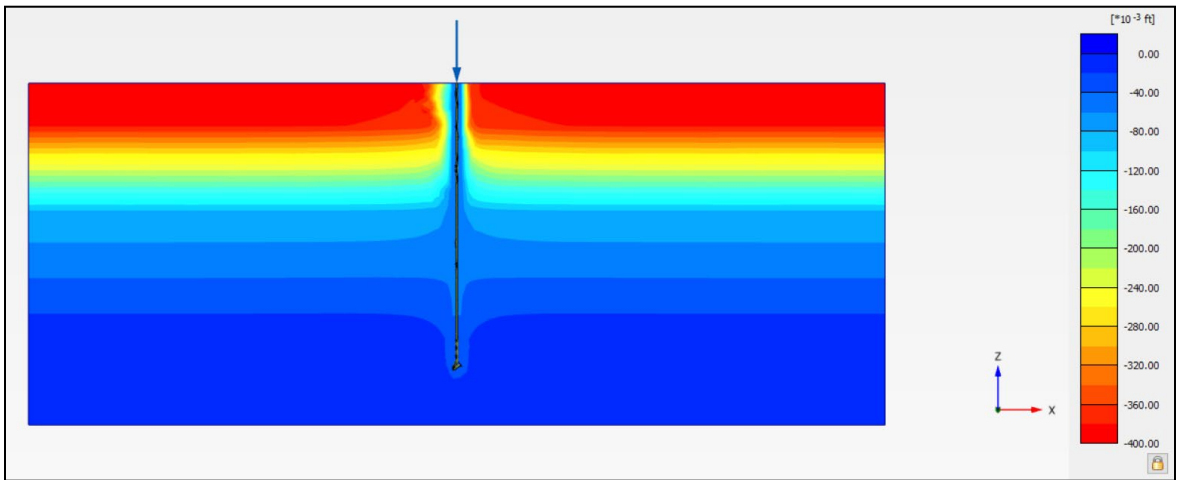

Figure 5.5 Model 1 Phase 3 (pile loading) vertical displacement with 400-kip load applied

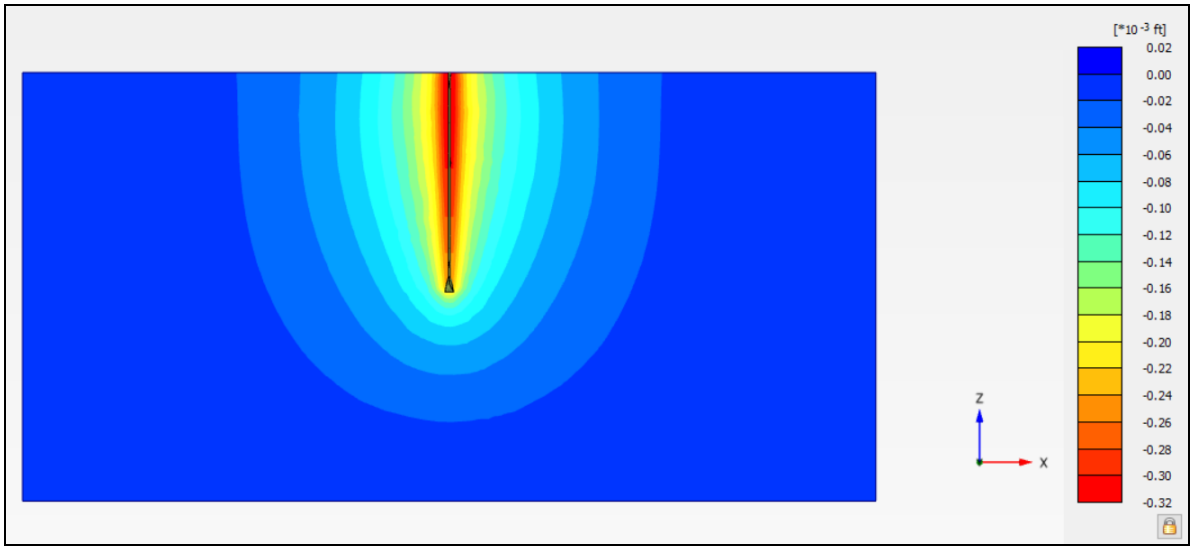

Figure 5.6 Model 2 Phase 1 (pile installation) vertical displacement

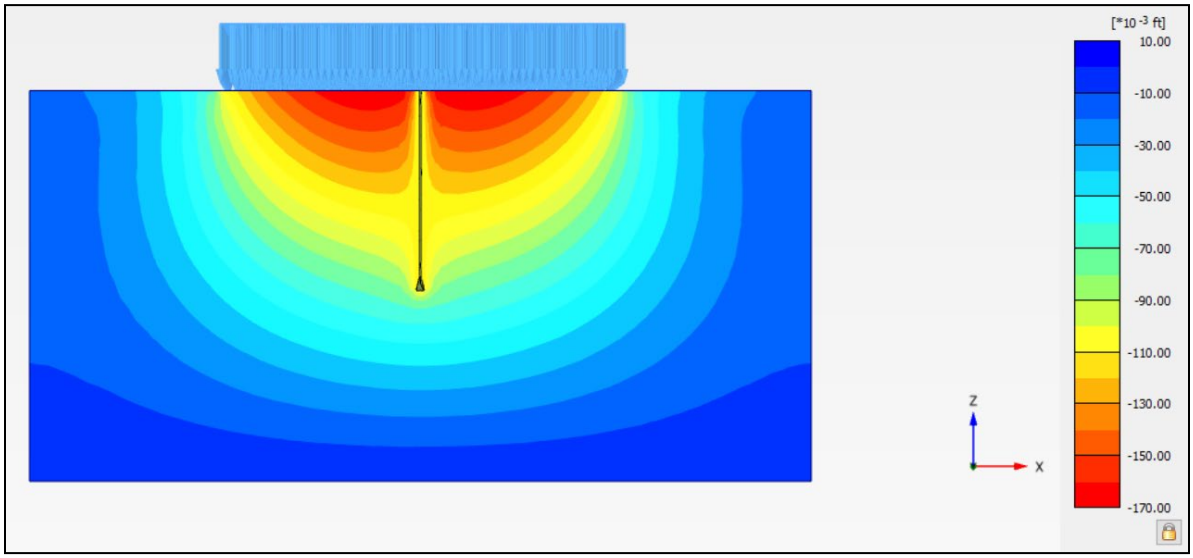

Figure 5.7 Model 2 Phase 2 (fill placement via surcharge pressure) vertical displacement with 1800-psf surcharge pressure applied

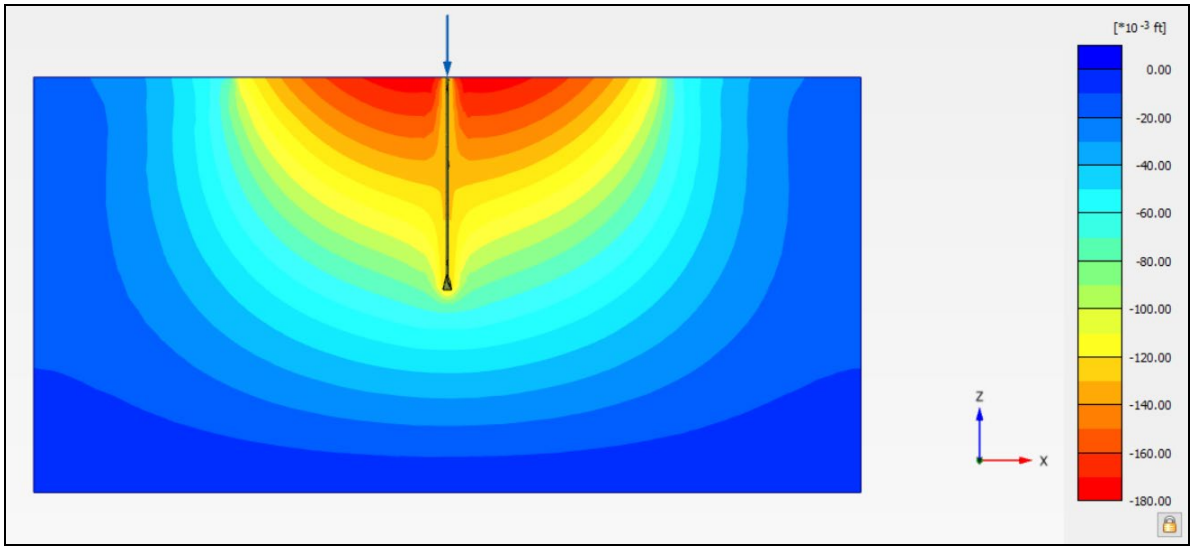

Figure 5.8 Model 2 Phase 3 (pile loading) vertical displacement with 1800-psf surcharge and 300-kip load applied

5.2.7 Assumptions and Limitations

The pile was assumed as cast-in-place since installation effects are ignored within the software. The modeling of installation effects of driven piles is being investigated by others.

Phuong et al. (2015) investigate the material point method (MPM) as a means of simulating pile installation effects in sand. MPM is a complex extension of FEM and can be computationally expensive. Engin et al. (2015) present a displacement-controlled "Press-Replace" technique to simulate pile penetration. The major advantage of this method is that the mesh does not undergo distortion. This simplified analysis, however, does not properly account for the soil wedge underneath the pile tip. Tehrani et al. (2016) model the effects of pile jacking in both loose and dense sands with both the Press-Replace technique and MPM.

Modeled profiles were simple, and layers were perfectly horizontal; soil profiles encountered in the field are heterogenous. It is important to obtain representative soil properties to output higher quality results from programs such as PLAXIS 3D. The soil profiles were chosen to represent both floating pile and end-bearing pile conditions, the former for a boundary condition comparison exercise.

5.3 Phase II Modeling Full Bridge Bents

The Paseo Al Mar Blvd bridge site was modeled with the entire footprint of the embankment and all 16 piles in the bent. Model space was set to be 3 times wider and 3 times longer than the embankment dimensions to confirm the limits of the embankment stress influence on the surrounding soil. Figure 5.9 shows the model space (234 ft wide, 600 ft long, and 70 ft deep).

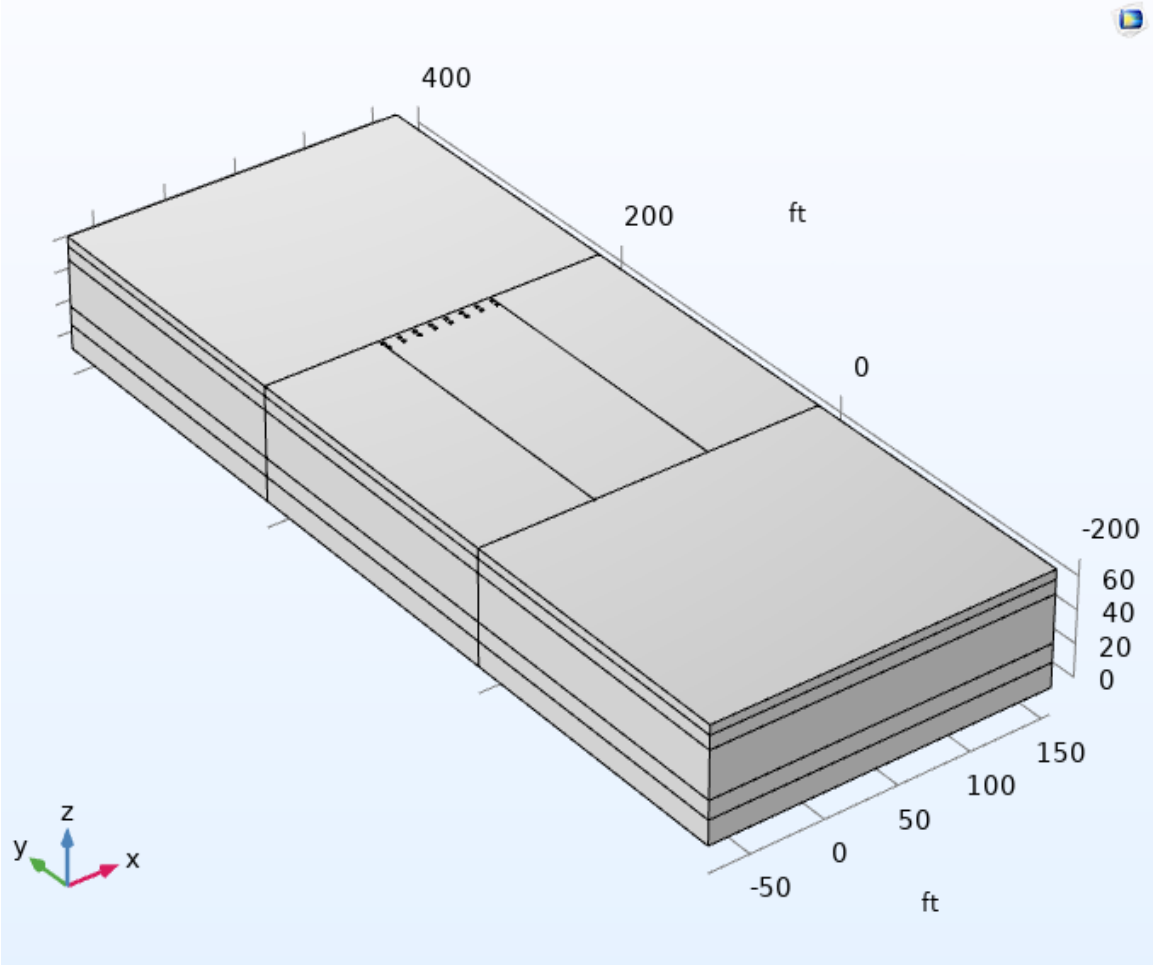

Figure 5.9 Paseo Al Mar model space

Figure 5.9 shows a center rectangular region which represents the location of the embankment. The embankment, while not of uniform height throughout, transitions very slowly matching the vertical curve of the roadway profile. This was assumed to be full height across the 78-ft width of wall and 200-ft length. A clearer image of the center embankment loading region is shown in Figure 5.10. The 16 piles are shown in two rows of 8 piles denoted in the model and plans as piles 1 to 8 in the row closest to the wall and piles 9 to 16 behind the first row of piles. Piles on each edge 1, 8, 9, and 16 were less than 1 ft from the side MSE walls. Both figures indicate five soil layers that correspond to the boring log distribution of loose to dense sand and an underlying limestone. Values assumed for the soil and limestone are given in Table 5.3. Table 5.4 gives pile properties for the model piles.

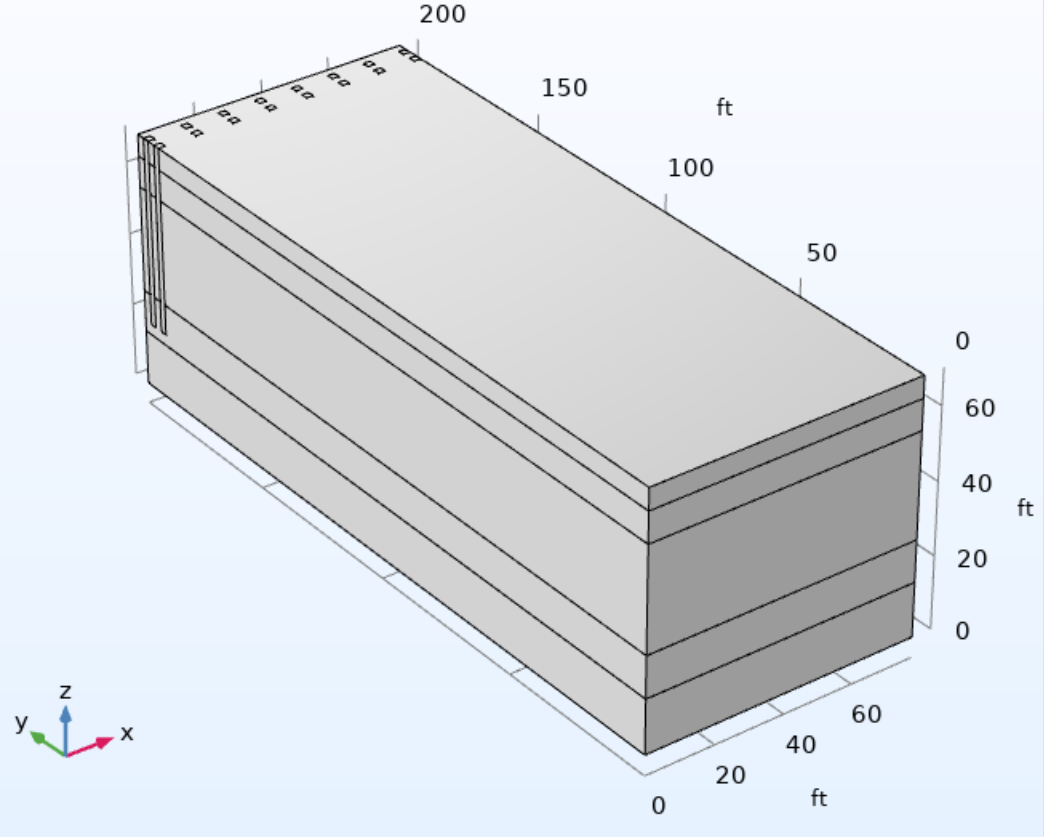

Figure 5.10 Paseo Al Mar embankment loading region

Table 5.3 Paseo Al Mar model parameters

Layer	Depth (ft)	Elastic Modulus (ksi)	Cohesion	Friction Angle (degree)	Density (lb/in^3)
1	6	6.2	0	33	0.0723
2	8.50	8.6	0	35	0.0740
3	29	3.3	0	30	0.068
4	11.5	1800	0	33	0.0763
5	15	1800	0	41	0.0810

Table 5.4 Pile details

No. of piles	Spacing (ft)	Size (ft^2)	Length (ft)	Young's Modulus (psi)	Poisson's ratio	Density (kg/m^3)
1-16 piles	8.85	4	52	6000000	0.2	2300

Results of the surcharge load are shown in Figure 5.11 where the effects of the piles can be seen to have less settlement around the piles. Taking a slice like that shown in Figure 5.12 through the two rows of piles the zone of influence outside the embankment edges can be seen (Figure 5.13). Figures 5.14 and 5.15 show the front row (piles 1 – 8) and back row (9 – 16) of piles, respectively. The study pile was pile 12 adjacent the centerline of the back row.

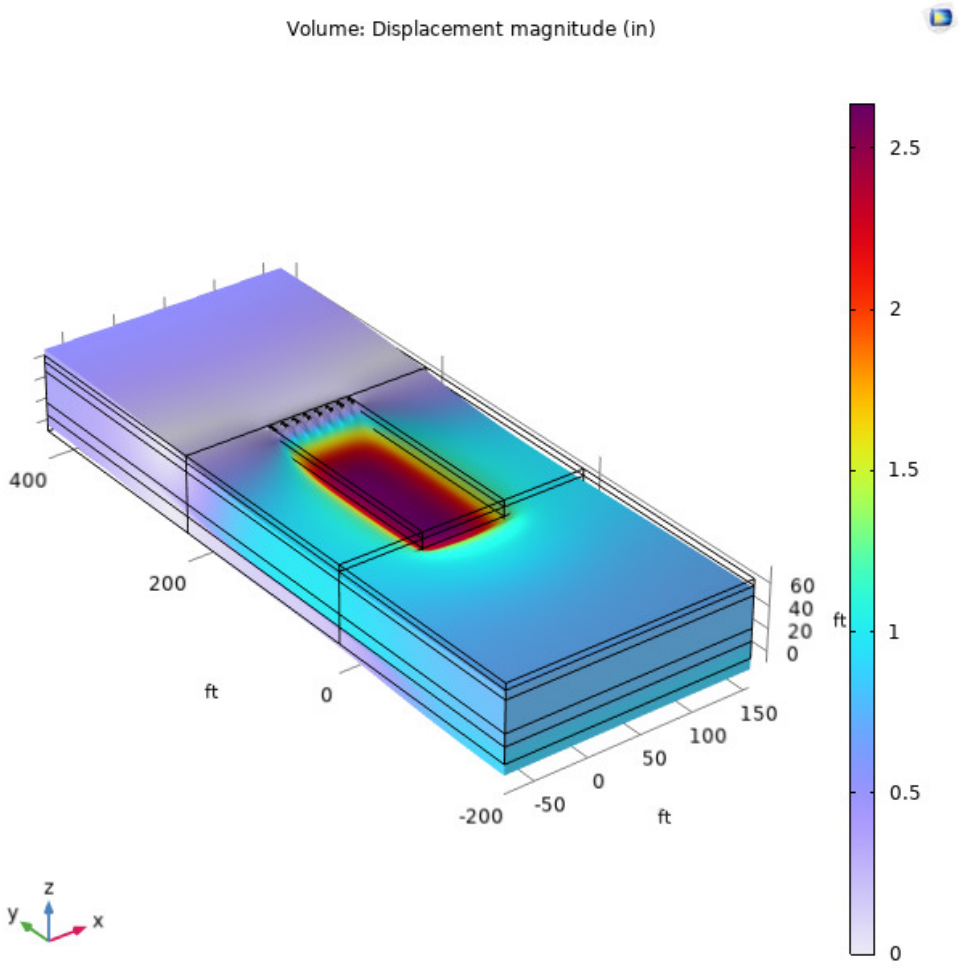

Figure 5.11 Spatial effect of surcharge on the overall settlement

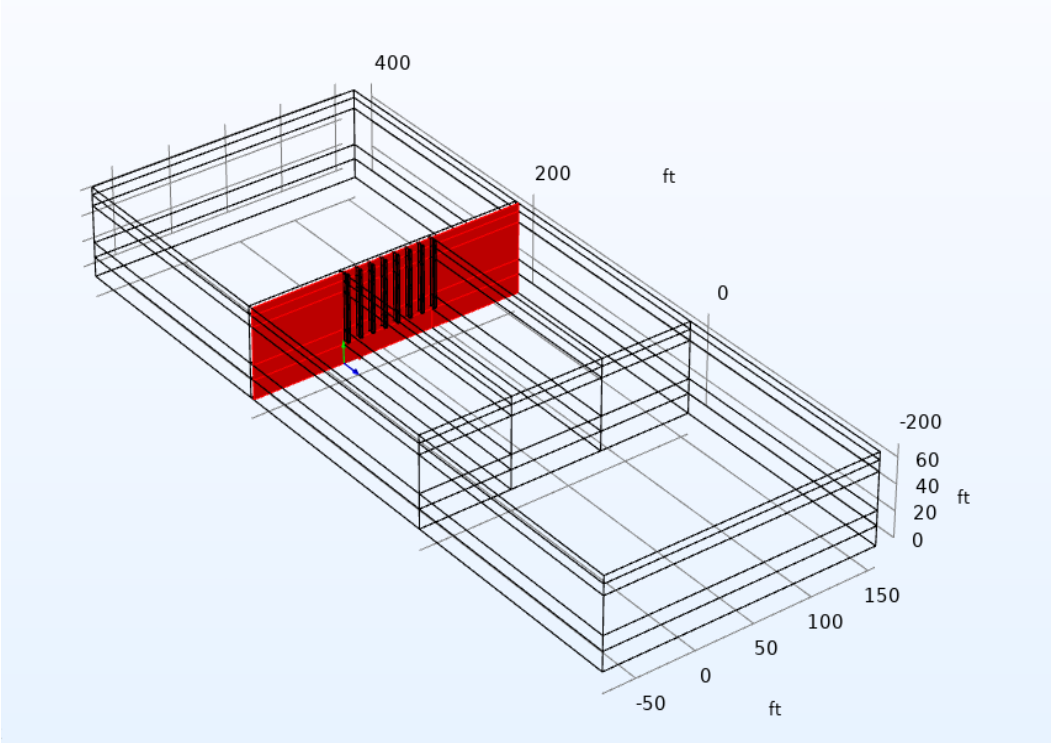

Figure 5.12 Lateral slice through the model

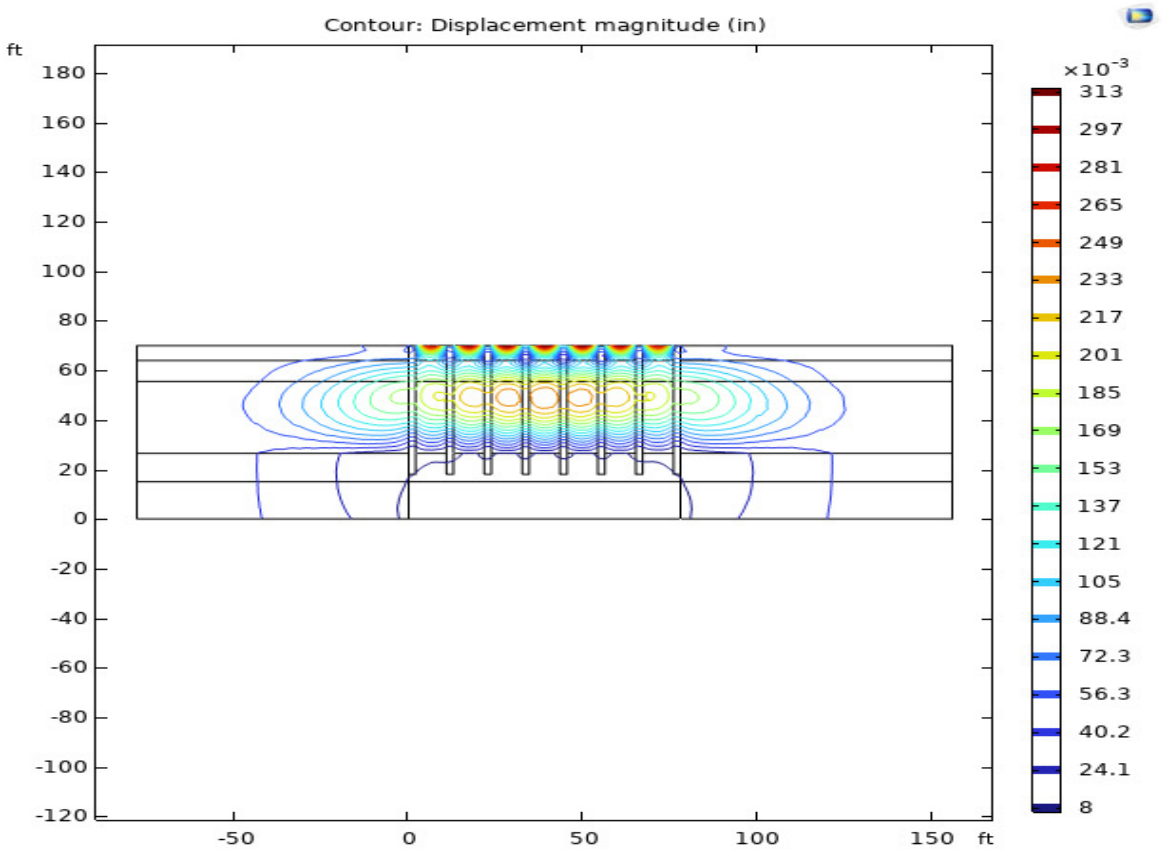

Figure 5.13 Zone of influence beside the embankment

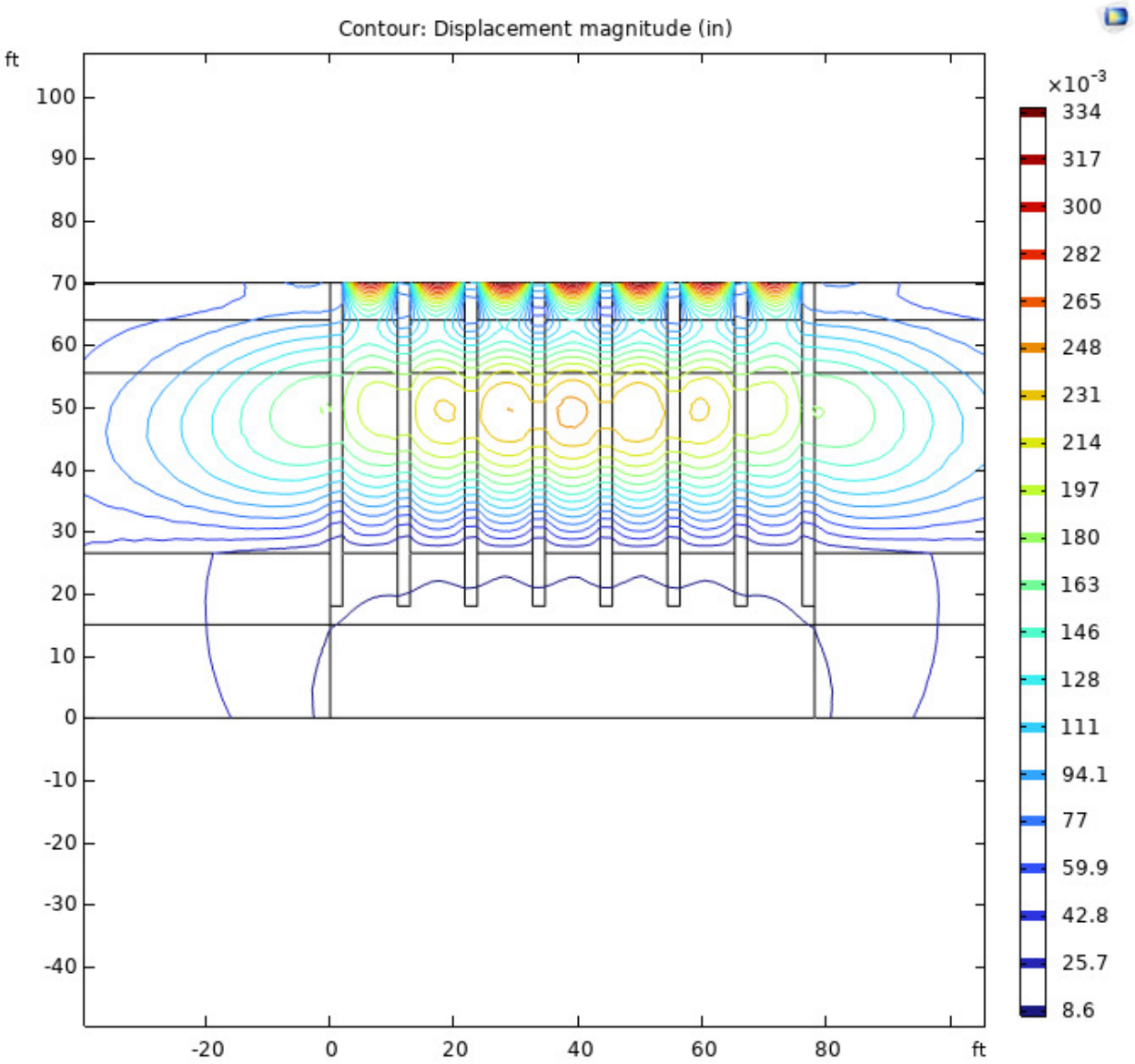

Figure 5.14 Close-up of the front row of piles (0.3-in max settlement)

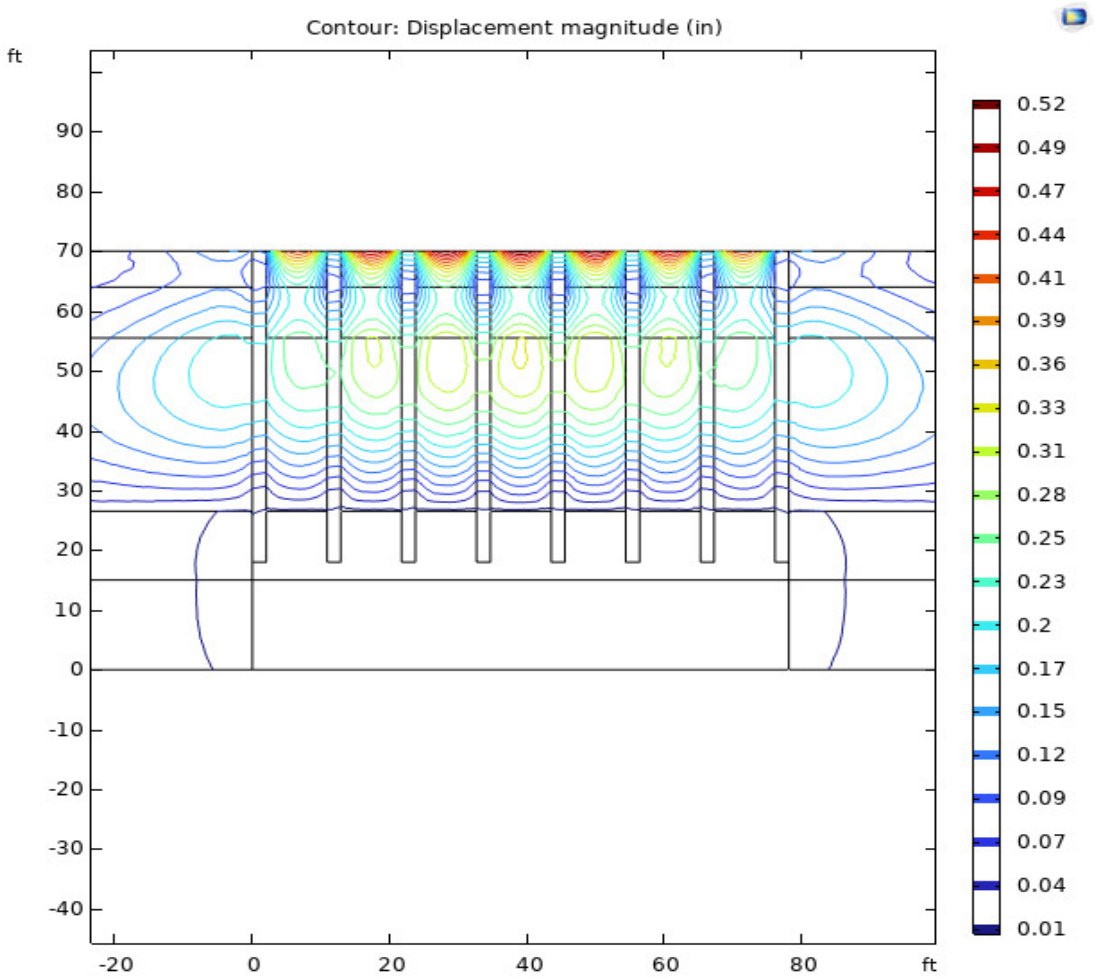

Figure 5.15 Lateral slice through the back row of piles (0.5-in max settlement)

A longitudinal slice through the model space is shown in Figure 5.16 that crosses through piles 4 and 12. Figure 5.17 shows the placement of the settlement gauges 15 ft behind the piles falls within the influence zone of the piles reinforcing the soils and may in part explain the disparity between the measured and predicted settlement.

Model results also show the effect of pile position in the bent where piles closest to the edge of the embankment were less loaded by the embankment (Figure 5.18). Figure 5.19 shows a more rigid end bearing condition attracts more load when compared to the pile lengths as-used at the Paseo Al Mar Blvd bridge site. The measured Pile 12 load compares well with the model results.

The effect of end bearing fixity on the neutral plane is also shown in Figure 5.20 where the 41-ft Paseo Al Mar pile was embedded an additional 11 ft into the limestone. In this case, the neutral plane essentially moves to the top of rock.
Figures 5.21-5.23 show the lateral movement of the soil under the embankment. Lateral forces on the back of the piles in part can be another possible explanation for the bending stresses recorded at Henley Rd. However, the model does not incorporate the compaction effort of the embankment fill process.

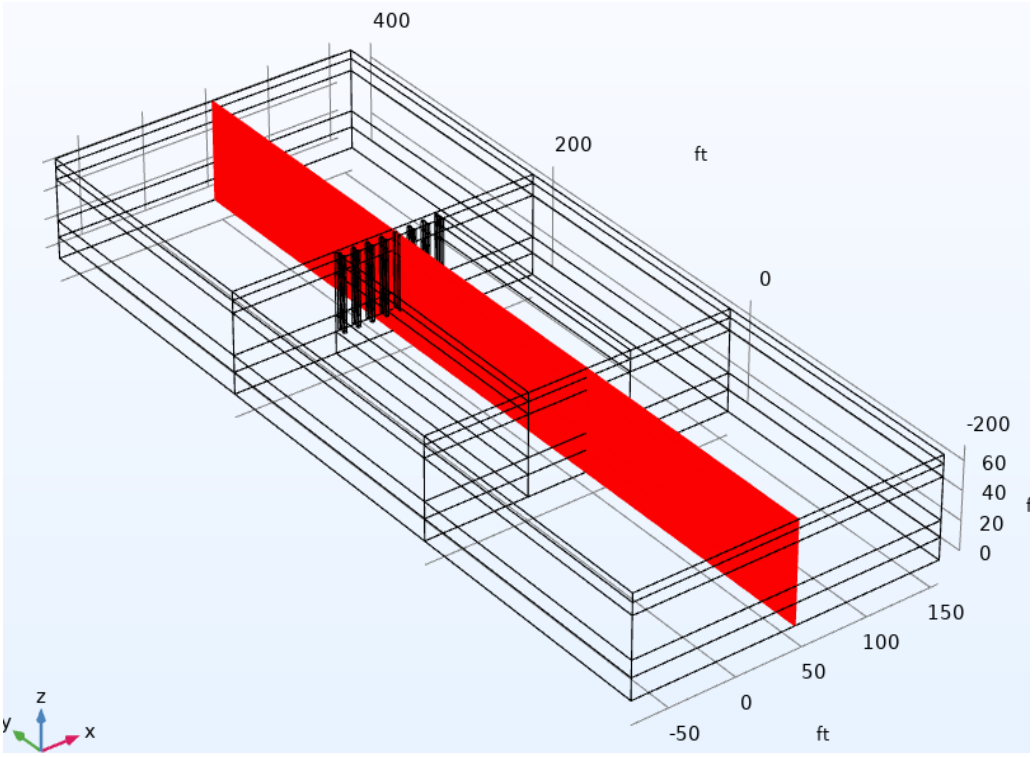

Figure 5.16 Longitudinal slice through piles 4 and 12

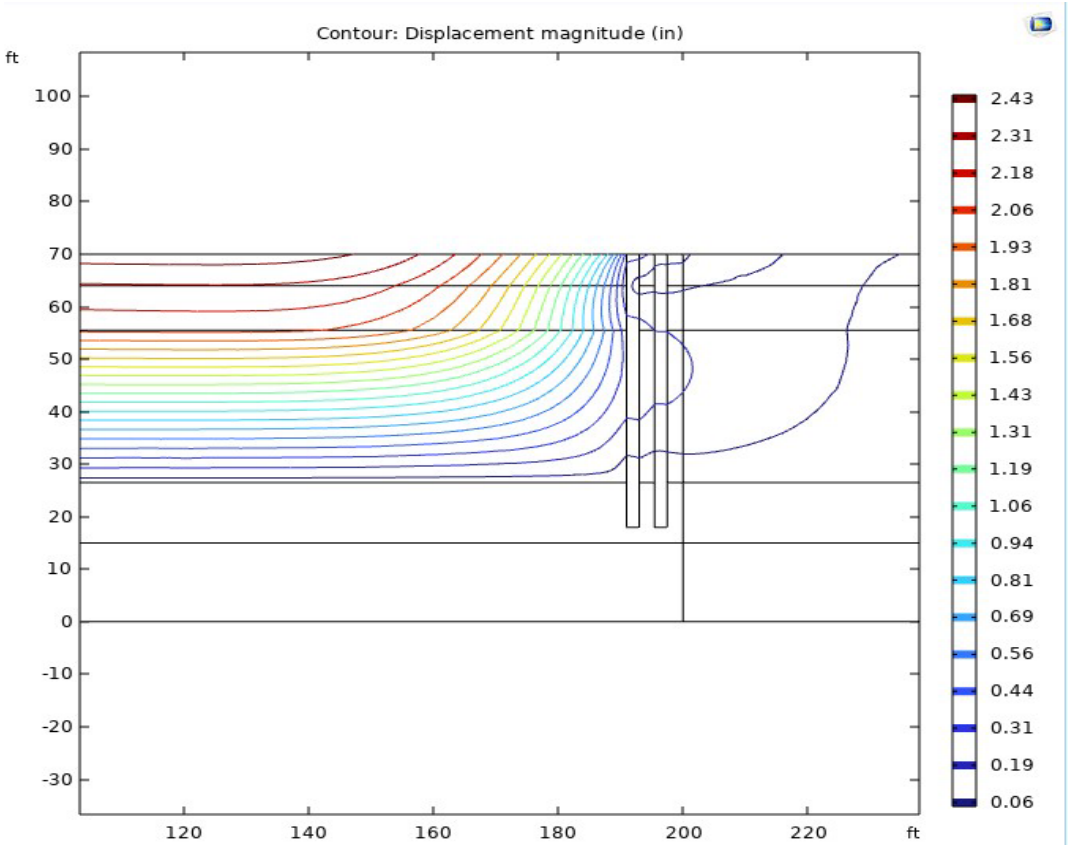

Figure 5.17 Displacement contours from longitudinal slice through piles 4 and 12

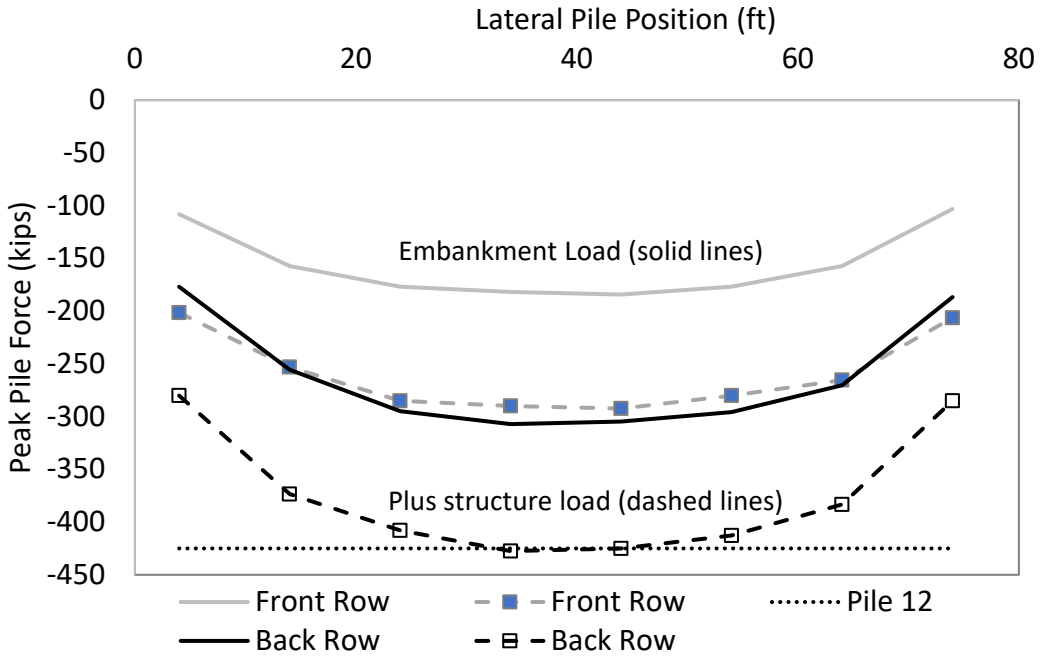

Figure 5.18 Max pile forces vs position in bent with and without 174k structure load (41 ft long; as- constructed at Paseo Al Mar)

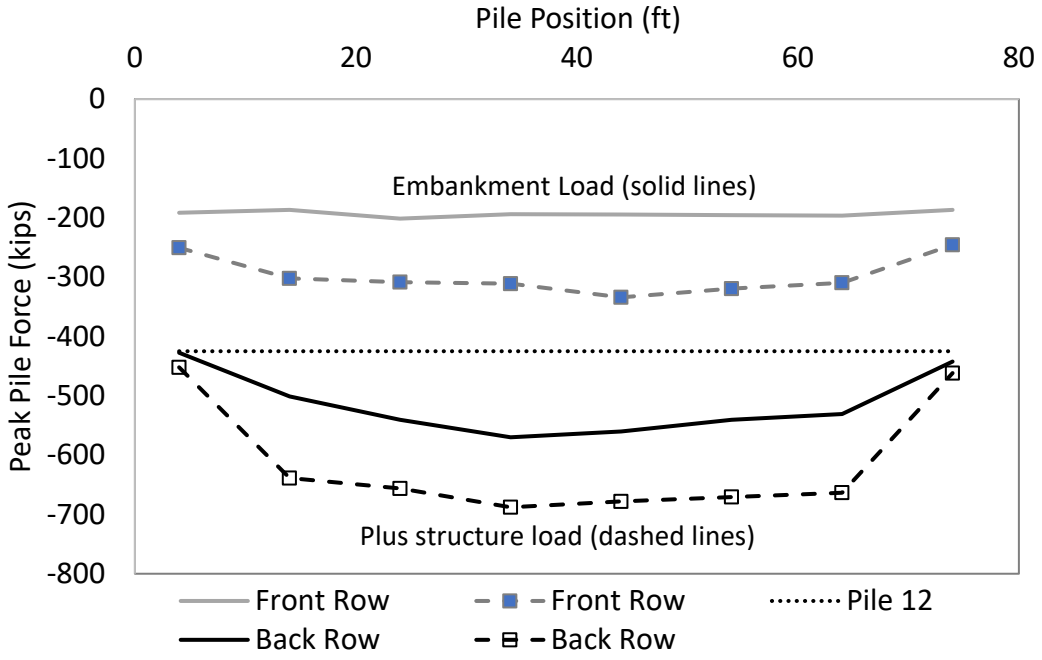

Figure 5.19 Max pile forces vs. position in bent with and without 174k structure load (52 ft long; 11-ft additional limestone embedment)

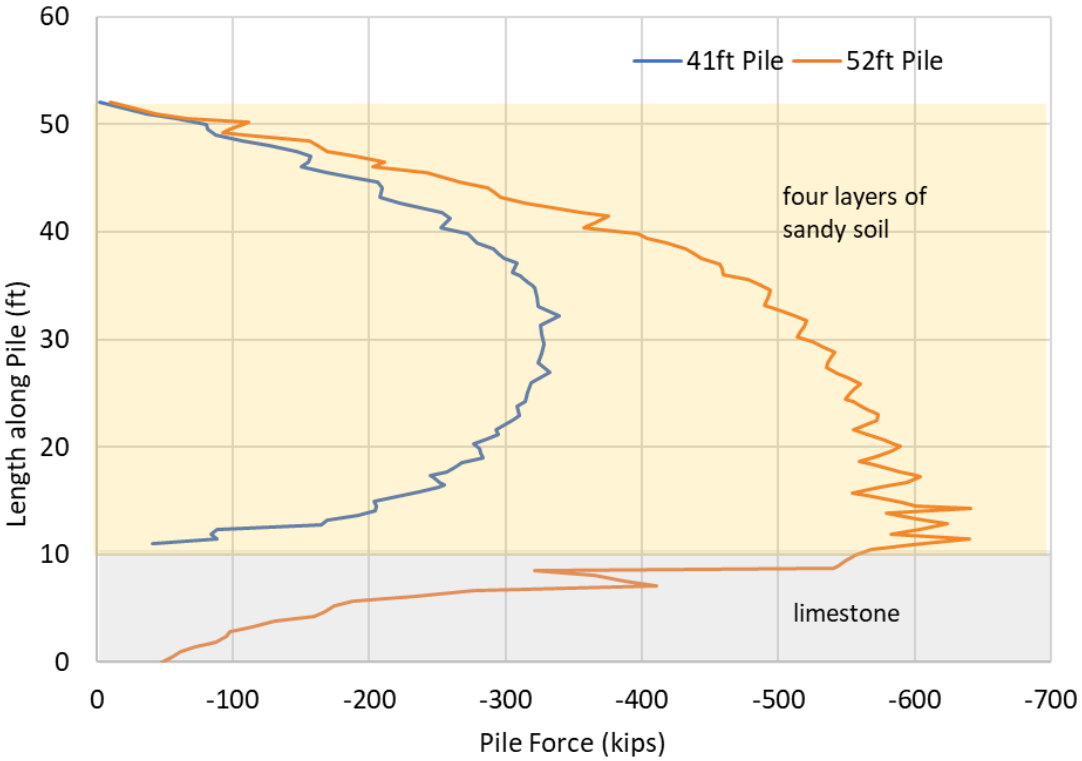

Figure 5.20 Effect of pile length and tip embedment on neutral axis

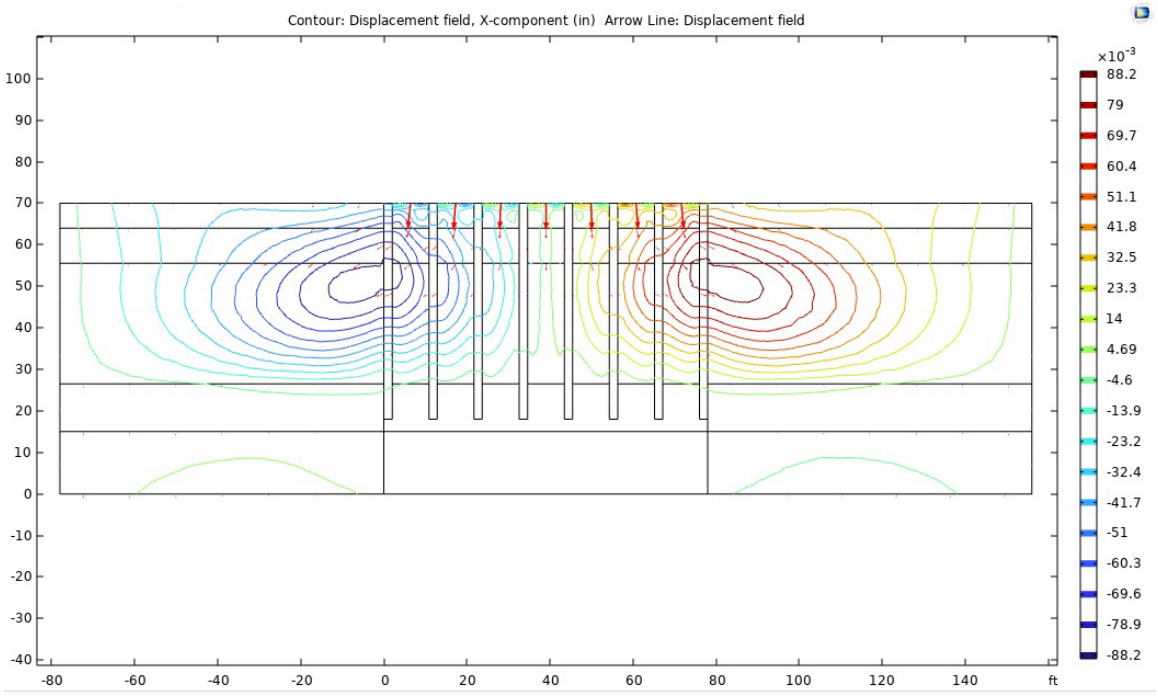

Figure 5.21 Lateral soil movement (~0.1 in highest near edges of embankment)

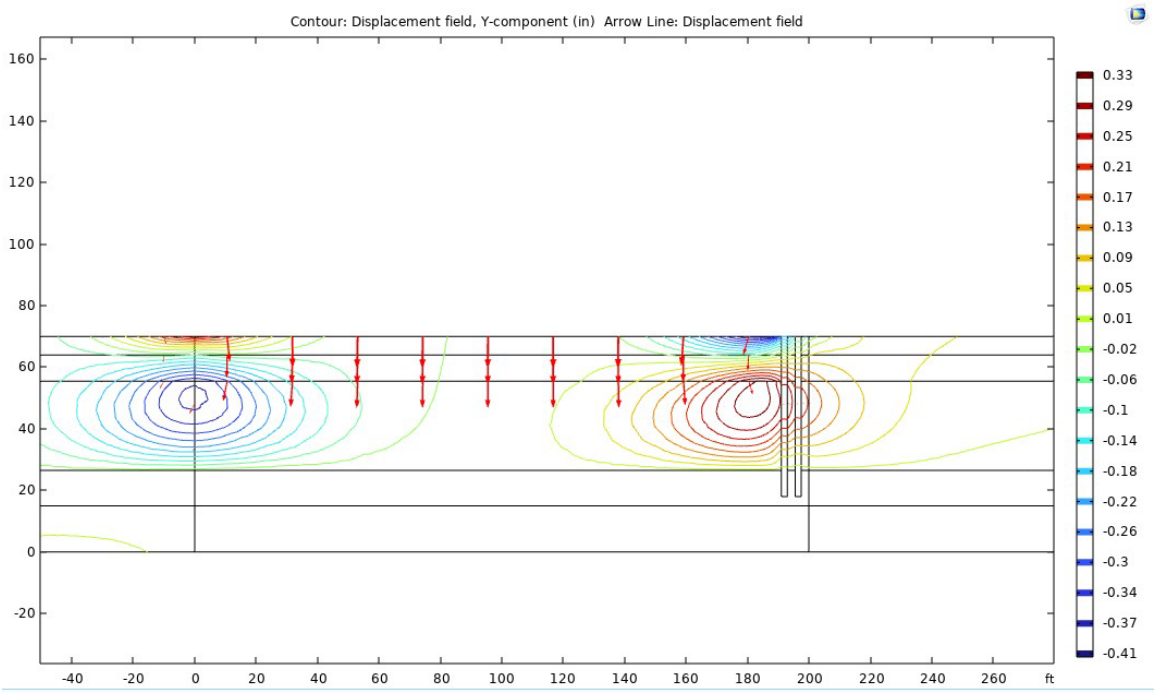

Figure 5.22 Longitudinal soil movement (cut plane through piles 4 and 12)

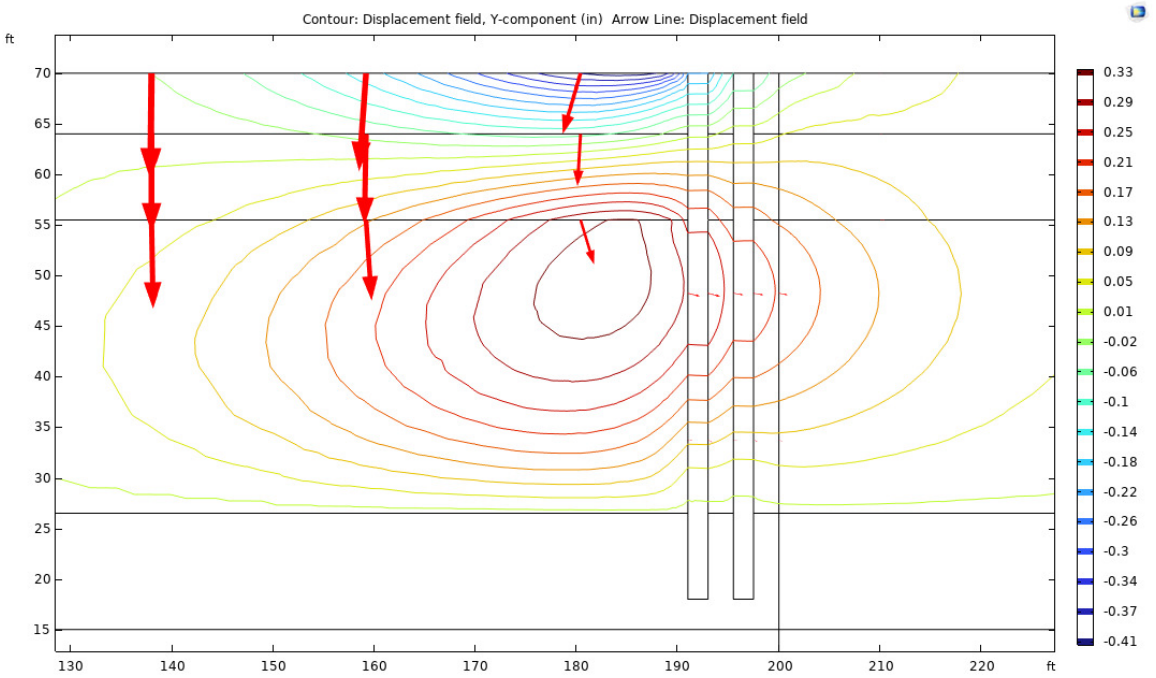

Figure 5.23 Longitudinal soil movement pushing against back of piles (~0.25 in highest)

5.4 Chapter Summary

Numerical modeling of single piles and pile groups was conducted where the field conditions measured in the pile groups were replicated compared to the values from the Paseo Al Mar site where the road is finished and in service. Piles in two rows do not share downdrag uniformly rather, the row of piles closest to the wall experiences half the load of the piles closest to the embankment downward movement. Settlement behind the wall in the embankment was shown to be affected by the presence of the piles which in part might explain the difference between predicted and measured settlement values 7.5 diameters of the pile behind the wall. In fact, settlement values did not become uniform until approximately 20 pile diameters behind the pile bent. The location of the neutral plane was found to follow literature noted conditions where piles tipped in a firm bearing stratum register the highest downdrag forces.

Chapter Six: Recommendations and Conclusions

6.1 Overview

This project monitored the internal pile forces within the end bents at three bridge sites along with the soil settlement caused by embankment fill loads. Forces were shown to increase in the piles at depths far below the ground surface prior to structural bridge loads. This is consistent with settlement induced downdrag when piles are installed prior to embankments for end bent type piers. Project plans from all three sites noted downdrag forces to be zero (Table 6.1) presumably on the basis that the predominant soil type was cohesionless.

Table 6.1 Pile data table showing no anticipated downdrag (Sandridge Rd).

PILE DATA TABLE																					Table Date 01/01/16
INSTALLATION CRITERIA								DESIGN CRITERIA								PILE CUT-OFF ELEVATIONS					
PIER or BENT NUMBER	PILE SIZE (in.)	NOMINAL BEARING RESISTANCE (tons)	NOMINAL UPLIFT RESISTANCE (tons)	MINIMUM TIP ELEVATION (ft.)	TEST PILE LENGTH (ft.)	REQUIRED JET ELEVATION (ft.)	REQUIRED PREFORM ELEVATION (ft.)	FACTORED DESIGN LOAD (tons)	FACTORED DESIGN UPLIFT LOAD (tons)	DOWN DRAG (tons)	TOTAL SCOUR RESISTANCE (tons)	NET SCOUR RESISTANCE (tons)	100-YEAR SCOUR ELEVATION (ft.)	Ø COMPRESSION	Ø UPLIFT	PILE 1	PILE 2	PILE 3	PILE 4	PILE 5	PILE 6
End Bent 1	18	267	N/A	N/A	95	N/A	N/A	173	0	0	N/A	N/A	N/A	0.65	N/A	95.6	95.5	95.3	95.2	95.0	94.9
End Bent 2	18	267	N/A	N/A	95	N/A	N/A	173	0	0	N/A	N/A	N/A	0.65	N/A	95.9	95.8	95.6	95.5	95.3	95.2

At the time of this report, one of the bridges had been opened to traffic, another was largely complete serving as a haul road to transport fill and road base to other portions of the ongoing construction efforts, and the third had girders in place but the concrete deck was not yet poured.

The load distribution along the length of all instrumented piles (one at each of three sites) clearly indicated the presence of a neutral plane where load was maximum when loaded with both permanent structural load and settlement induced downdrag (e.g.,. Figures 4.6, 4.11, and 4.19). A commonly cited aspect of downdrag considerations is that transient loads (live loads) do not add to highest pile load at the neutral plane. For this study, truck loading events were performed on one bridge site where both static and dynamic loads were registered. Figure 6.1 shows the effect of a 70-kip load parked near the instrumented end bent where an 11 kip change in top of pile load was detected. Recall Level 5 is the top of pile load and Level 1 is the pile toe. A reduction in the top of pile load effect can be seen with depth. The additional load caused a 3-kip increase at the neutral plane, 27% of the additional top of pile load but not zero (Figure 6.2). For this site the unfactored live load used for design was 81 kips per pile so perhaps an additional 22 kips could be expected at the neutral plane under full design load.

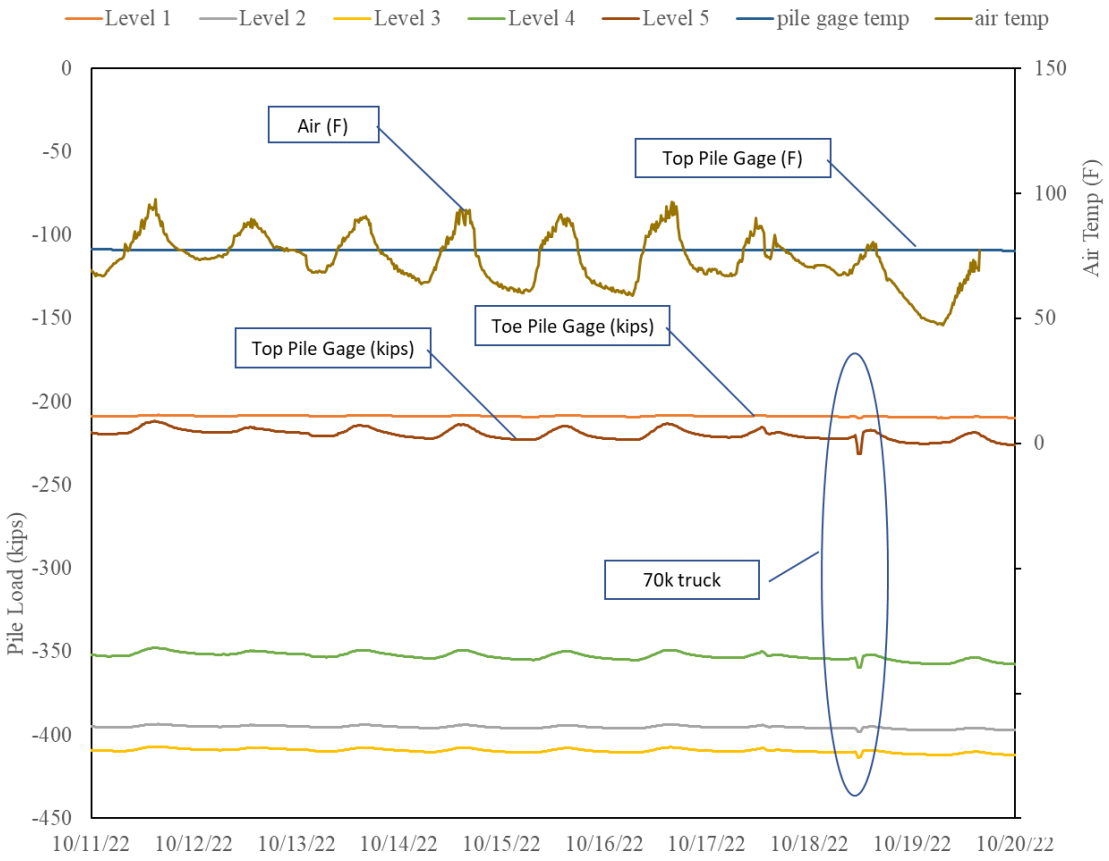

Figure 6.1 Load attenuation with depth from static 70-kip truck load

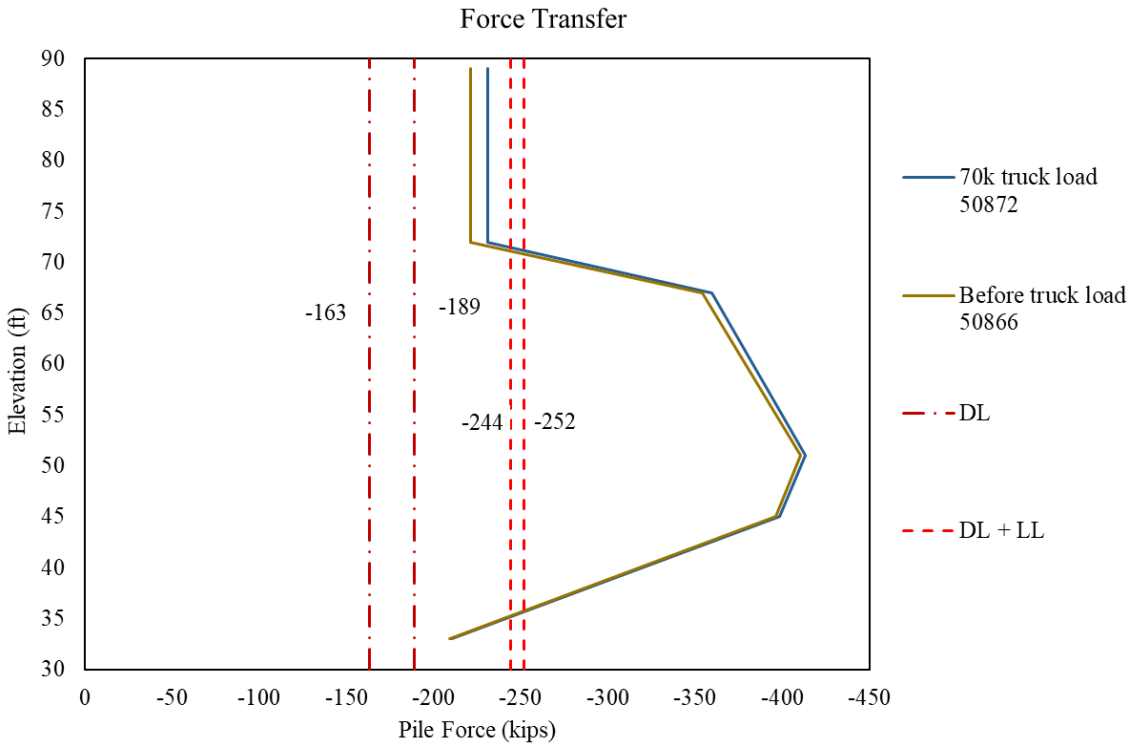

Figure 6.2 Effect of 70k truck load on load distribution (Sandridge Rd)

6.2 Dynamic Live Loading Events

To date, dynamic load tests have been limited to slow moving trucks hauling fill and roadway base to other parts of the SR23 construction corridor. Over a nine-day period, 541 truck loading events were recorded as shown in Figure 6.3. Fluctuations in the baseline pile force again followed changes in air temperature. While slow speed sampling continued with15-minute intervals, high speed monitoring of the eight pile strainmeters simultaneously occurred sampled at 20-Hz. Events were triggered by monitoring the standard deviation of the top of pile strain which averaged 0.015ue over any 15-minute interval within a 15-day period with no truck load. If the one second standard deviation exceeded 0.05ue an event was collected (trigger-on), data for the previous second was retrieved and high-speed sampling continued until the standard deviation fell below 90% of the trigger threshold. Five seconds of additional data was also collected post trigger-off.

To provide further insight into the dynamic aspects of the truck loading events four events were videoed and synchronized with the recorded data (Figure 6.4). For the report only an image is shown with the load traces superimposed (Figures 6.5 – 6.8). However, the synchronized videos can be viewed using the following links: Event 1 gif file Event 2 gif file Event 4 gif file Event 5 gif file. Dynamic loads ranged from 4 kips per pile (~24 kips end bent load) to 14 kips per pile (~84 kips end bent load) for empty and fully loaded trucks, respectively.

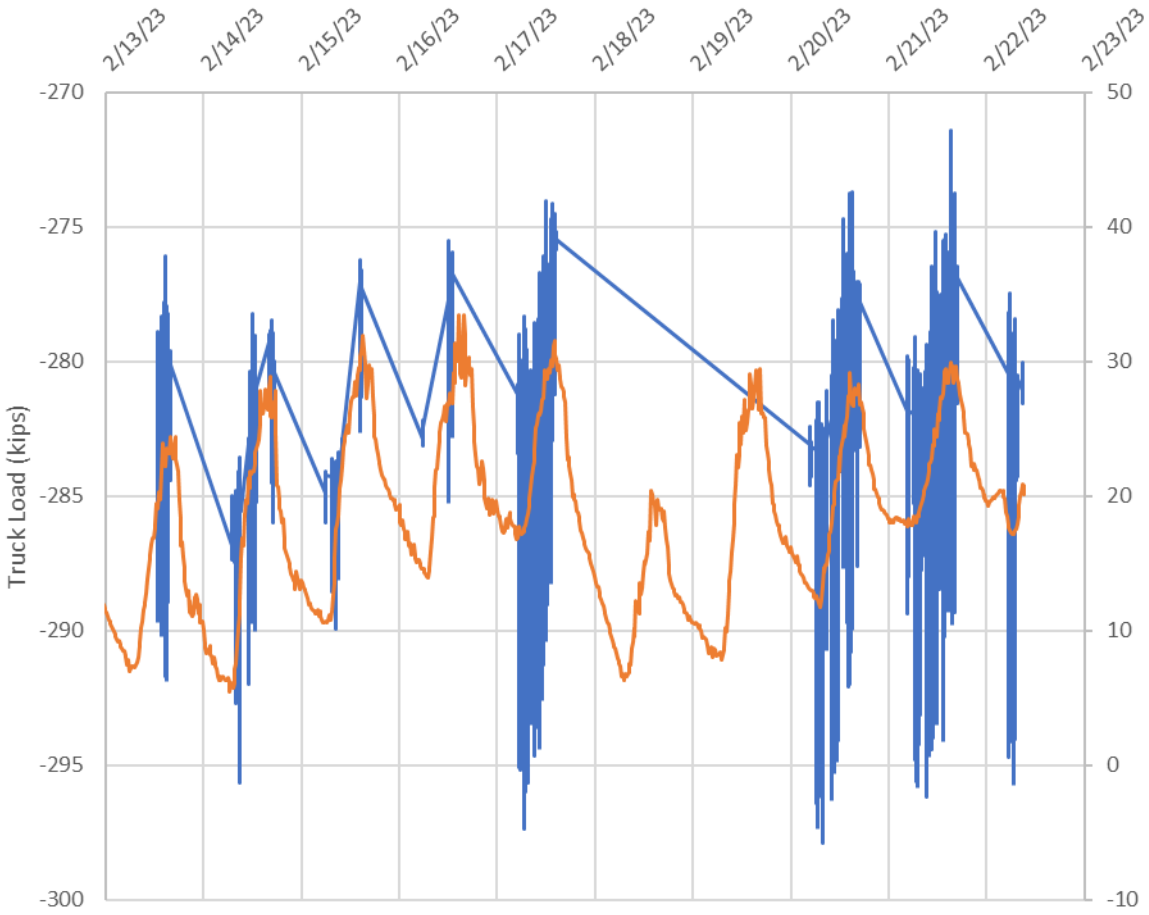

Figure 6.3 High speed sampling of top of pile force from truck loading events (air temperature in orange)

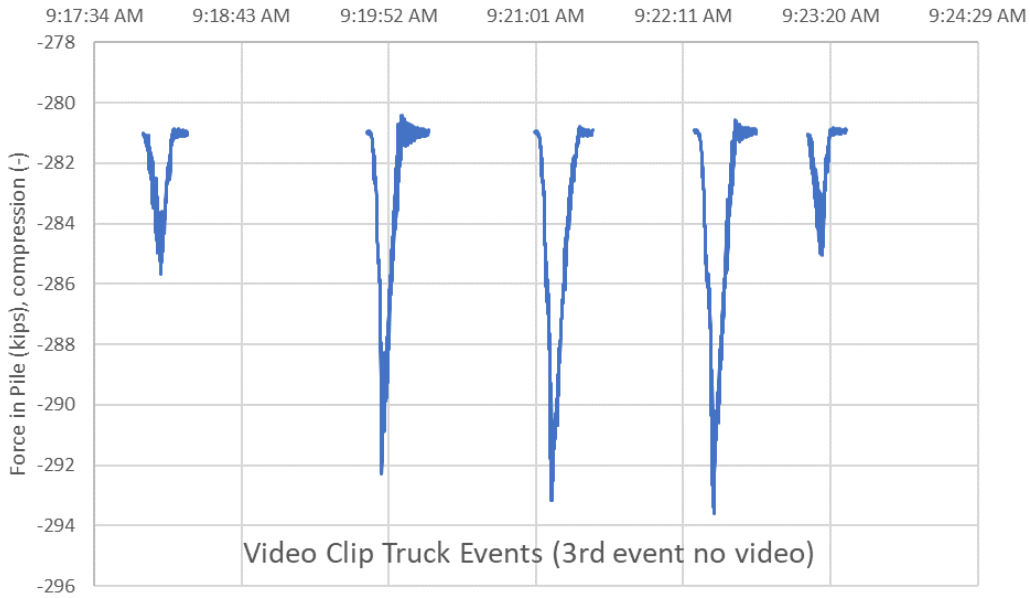

Figure 6.4 Truck events that were also videoed.

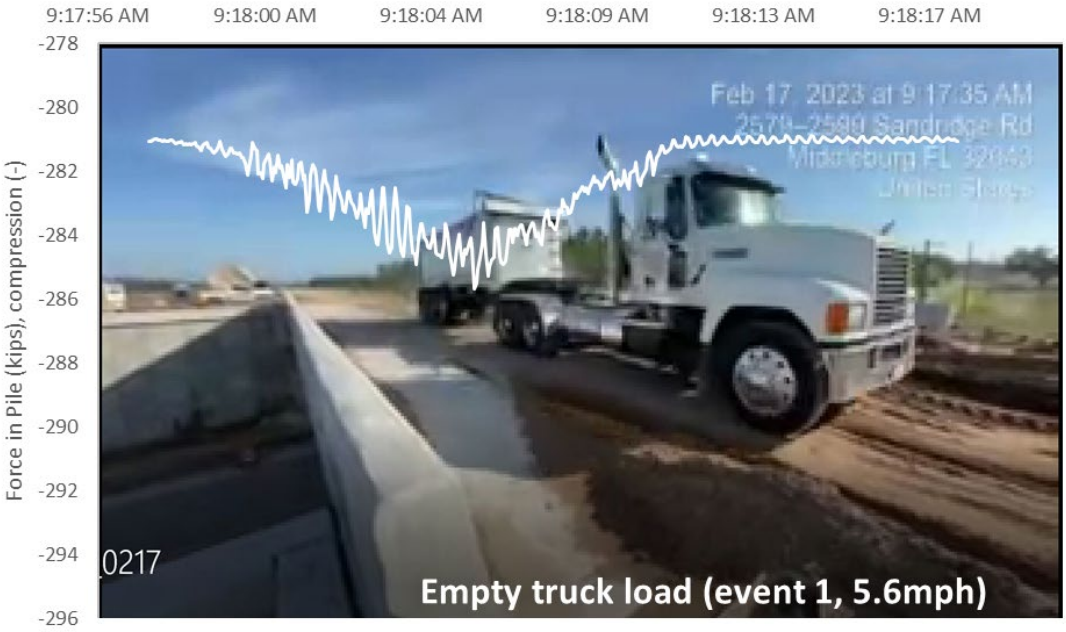

Figure 6.5 Truck-loading event 1 with an empty truck.

Figure 6.6 Truck-loading event 2 with a full truck.

Figure 6.7 Truck-loading event 4 with a full truck.

Figure 6.8 Truck-loading event 5 with an empty truck.

Truck speed was estimated using the duration of the event (10.6 to 17 seconds) and the length of the single span bridge (114 ft). The truck speed during videoing ranged from 4.6 to 7.3 mph. The drivers appear to have exercised caution while a bystander was present taking the videos as the speed was slightly lower when compared to other events not videoed. Figure 6.9 shows a

considerable change in the dynamic response from two fully loaded trucks at speeds of 5.6 and 9 mph. At these speeds there was little change in force magnitude but the time required to dampen the vibrations was noticeably increased. Data collection is planned to continue after the completion of the study to see the effects of highway speeds and truck loading on pile loads. Where sampling rates were 20 Hz for the above events, rates as high as 400 Hz are possible with the existing systems which can be adjusted via remote access.

The effects of transient truck loads down the length of the pile show approximately 33% of the top of pile force was transferred to the neutral plane where the highest pile forces occur. As the full load was not detected at the neutral plane, an exchange of reduced downdrag with the additional live load can be offered as the reason for only 33% of the new load reaching the peak pile force location. Figure 6.10 shows the effect of the 5.6-mph fully loaded truck also shown in Figures 6.6 and 6.9 at all gauge levels down the pile. For clarity all loads are expressed as change in load and not the actual load at those levels.

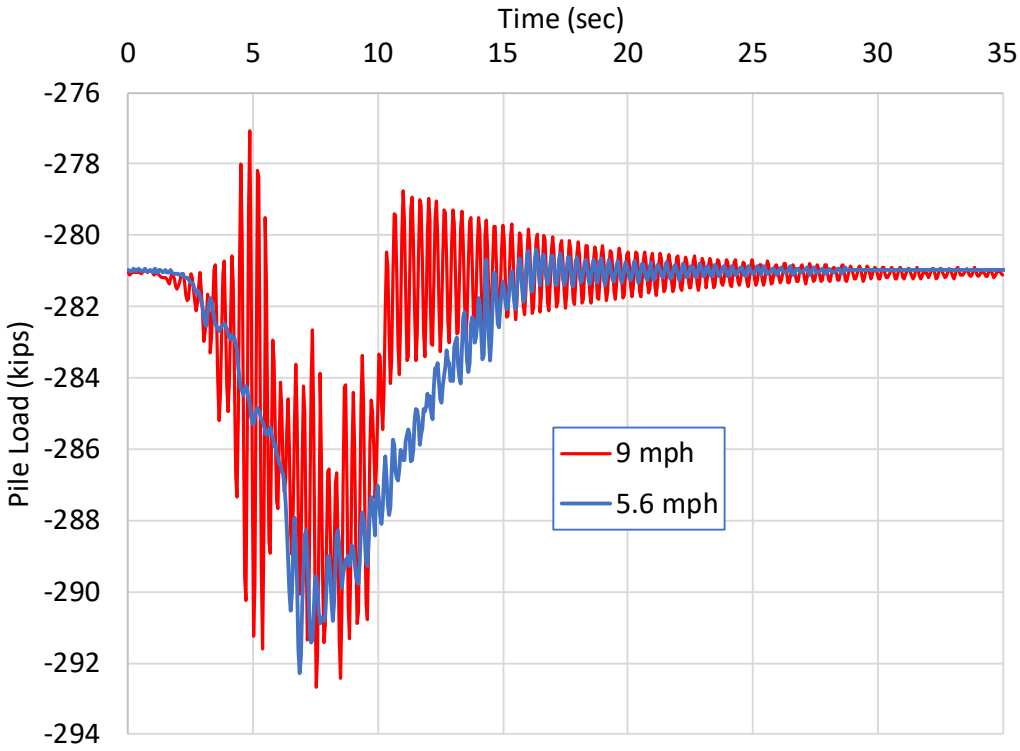

Figure 6.9 Effect of truck speed on load response (Sandridge Rd)

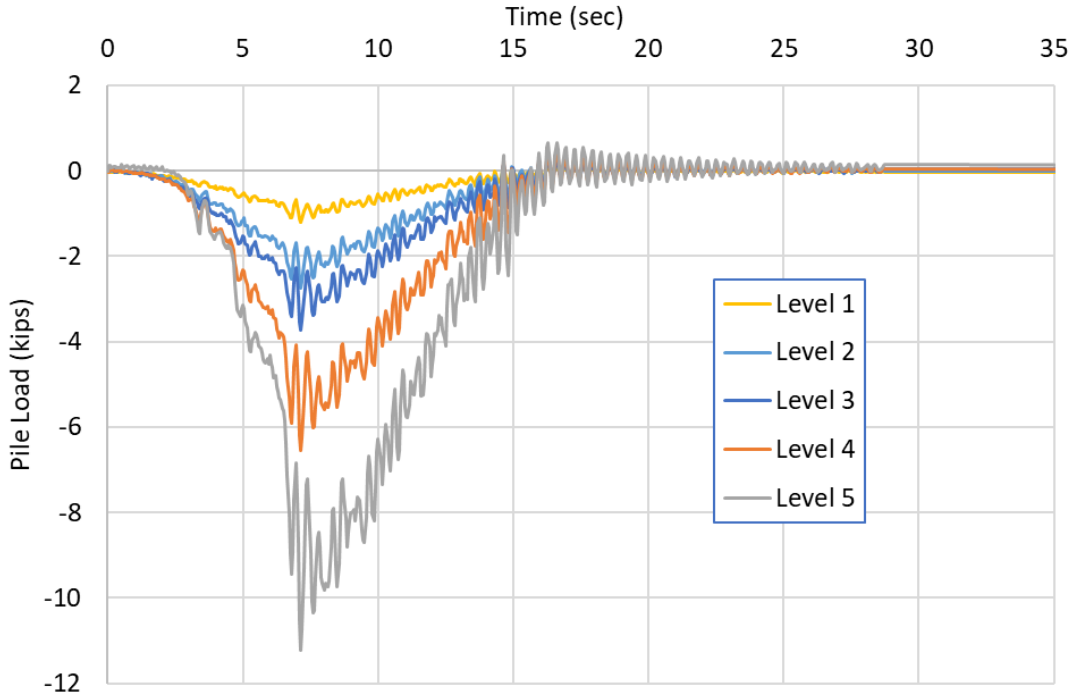

Figure 6.10 Effect of truck loads down the length of the pile (5.6 mph, fully loaded truck)

6.3 Seasonal Changes in Loads

Hourly, daily, and seasonal changes in temperature were shown to affect the magnitude of the top of pile and neutral plane loads. To provide context, the Sandridge Rd factored design load was 173 tons with a nominal bearing resistance of 267 tons (Table 6.1). Without precise knowledge of the unfactored load values a DL/LL ratio can be estimated to be between 2 and 3 making the range of DL values 163 to 189 kips; the range of total service load would then be 244 to 252 kips. Figure 6.11 shows the change in top of pile and neutral plane forces caused by seasonal temperature change and the estimated range in structural loads. No live loads were present at the time of the measurements. Measured permanent loads in general exceed the estimated loads and approach the total service load.

A 56-kip top of pile force variation is shown in Figure 6.11 (185 to 241 kips); the change at the neutral plane force was 12 kips (401 to 413 kips), 21% of the top of pile load which is similar to the static truck load effect (27% discussed earlier). The downdrag magnitude at any time is the difference in the force measured at the neutral plane and the top of pile. The change in downdrag caused by new top of pile loads is similar regardless of the source (permanent or transient). Figure 6.12 shows the downdrag magnitude versus top of pile load over the duration of the project where construction milestones are called out.

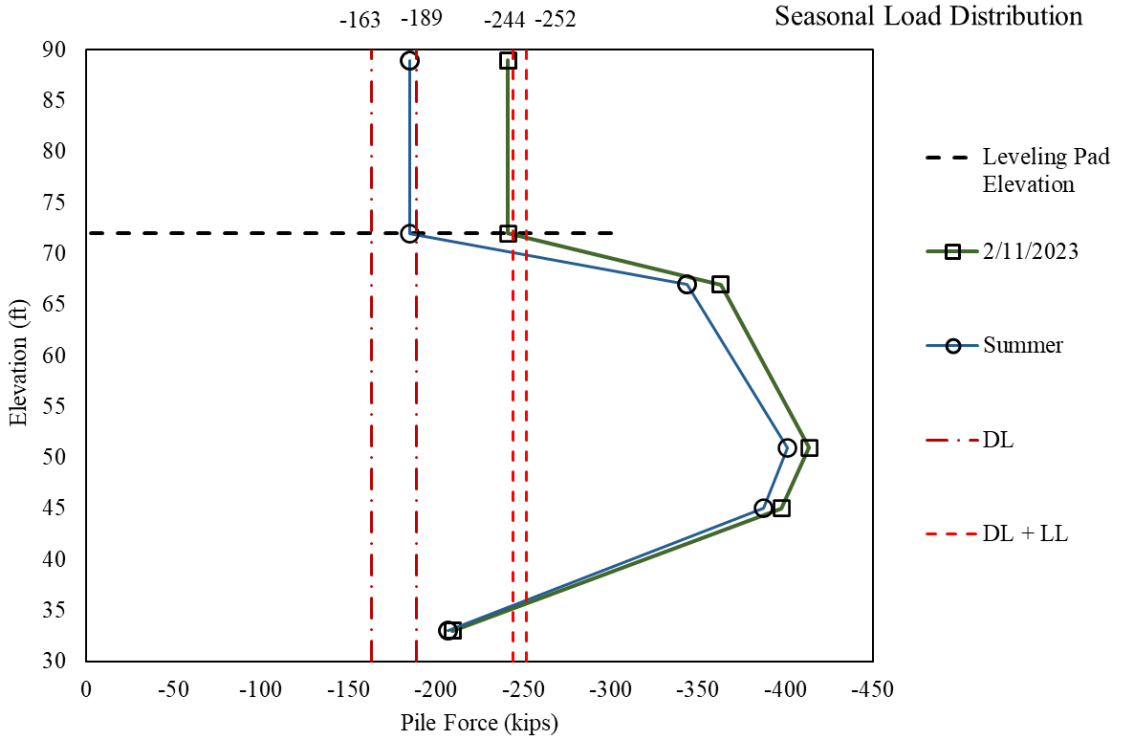

Figure 6.11 Effect of seasonal temperature change on load distribution (Sandridge Rd.)

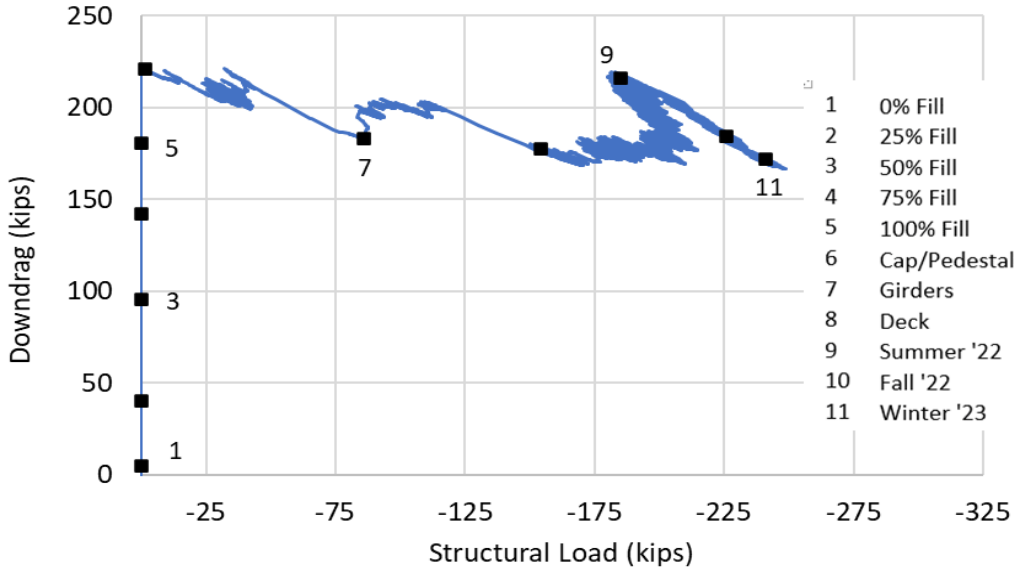

Figure 6.12 Effect of structural load on downdrag (Sandridge Rd)

With any significant increase in load (e.g., girder or deck slab weight) a reduction in downdrag can be seen. These trends shown as diagonal linear responses provide insight into how additional load will be transferred into the pile and the load distribution. Seasonal loads have the same effect of an approximate 1 to 1 relationship, 70k reduction in downdrag with a 70k increase in structural load. However, peak pile loads do not reduce with additional structural load, rather in this case 21 to 27% of new top of pile structural load was added to the neutral plane loads. Hence, the peak pile force of 413k with only DL could be expected to increase to 435k with the additional 81k LL (all service loads). Factored load at the neutral plane would then be 616 or 598k for DL/LL ratios of 2 or 3, respectively.

6.4 Effect of Neglecting Downdrag in Design

Given the factored design load for a project is 346k (173T) and the nominal bearing resistance is 532k the following shows the effect if downdrag is disregarded. These values assumed no downdrag at the time of design. The above measured loads were shown to exceed expected loads, but without this knowledge a designer might look to *The Soils and Foundations Handbook* (*SFH*, FDOT 2020) equation from Appendix C which is evaluated below for this pile.

$$\text{DOWNDRAG} = R_{dd} + (\text{Driving Resistance of soil contributing to } R_{dd})$$
$$R_n = (\text{Factored Design Load} + \text{Net Scour} + \text{Downdrag}) / \varphi$$
$$R_{dd} = 143\text{k estimated by office calculations; } 200\text{k measured}$$
$$\text{Driving Resistance of } R_{dd} = 0.75R_{dd}$$
$$\text{Factored Design Load} = 346\text{k}$$
$$\text{Net Scour} = 0$$
$$\varphi = 0.65$$
$$\text{NBR} = 532\text{k; } 557\text{k max Ru from CAPWAP}$$

$$346\text{k} + 143\text{k} + 0.75\,(143\text{k}) \leq 0.65\,(557\text{k})$$
$$596\text{k} \not\leq 362\text{k} \quad (\text{fails design criterion})$$

Moving forward, three observations for consideration include: downdrag should always be considered even if shown to be small. (2) Even if downdrag is considered, the measured downdrag was higher than estimated and a downdrag load factor is not provided in the *SFH* equation. This is not surprising given that methods to predict side shear are often conservative when considering positive side shear resistance. This same level of underprediction then is unconservative when determining negative side shear forces. AASHTO Table 3.4.1-2 (Table 6.2 herein) recommends DD load factors based on the method used for clay, not sand. (3) Even with the additional capacity offered by CAPWAP predictions in this case, there is no resistance factor large enough to satisfy the inequality.

Table 6.2 AASHTO recommended load factors for downdrag forces

Type of Load, Foundation Type, and Method Used to Calculate Downdrag		Load Factor	
		Maximum	Minimum
DC: Component and Attachments		1.25	0.90
DC: Strength IV only		1.50	0.90
DD: Downdrag	Piles, α Tomlinson Method	1.40	0.25
	Piles, λ Method	1.05	0.30
	Drilled shafts, O'Neill and Reese (2010) Method	1.25	0.35

6.5 Explicit vs. Neutral Plane Methods

The FDOT Soils and Foundations Handbook (SFH) recommends a methodology to assess the effects of downdrag which parallels AASHTO and references FHWA HI 97-013 (Hannigan et al., 1998) pile design documents. Therein, a 10-mm (0.4 in) differential settlement between the soil and pile ($w_{soil} - w_{pile} \geq 0.4$) is required to activate negative side shear. The *SFH* adopted a 0.5-in threshold. Discussions[a] with authors of the most recent FHWA design manual (Hannigan et al., 2016) indicate the origins of the 0.4 in criterion are unknown perhaps based on Cheney and Chassie (1982), Vesic (1969) or on FHWA past experience. The 10-mm value does show up in Briaud and Tucker as a post construction settlement value indicating where downdrag may occur (Table 6.3).

Table 6.3 Indicators to know when to consider downdrag (Briaud and Tucker 1997)

1.	The total settlement of the ground surface is larger than 100 mm
2.	The settlement of the ground surface after the piles are driven is larger than 10 mm
3.	The height of the embankment to be placed on the ground surface exceeds 2 m
4.	The thickness of the soft compressible layer is larger than 10 m
5.	The water table is drawn down by more than 4 m
6.	The piles are longer than 25 m

WARNING: Downdrag can occur even if the above conditions are not met.

FHWA has since superseded their recommendations by adopting the explicit or neutral plane methods (Hannigan et al., 2016) largely based on studies showing only 2 mm (0.1 in) of differential settlement is required to develop full side shear, positive or negative. Interestingly, the same table from Briaud and Tucker reappears in 2001 but with different pre and post construction ground surface settlement values (Table 6.4). Neither of these tables refers to a differential pile to soil movement threshold.

Table 6.3 Changes in ground surface settlement criteria (FHWA HI-98-032, 2001)

1	Total settlement of the ground surface > 10 mm
2	Settlement of ground surface after pile driving > 1 mm
3	Height of embankment filling on ground surface > 2 m
4	Thickness of soft compressible layer >10 m
5	Water table drawn down >4 m
6	Piles length > 25 m

WARNING: Downdrag can occur even if the above conditions are not met.

[a] Mullins, G. (2023). "Personal communications with Brent Robinson and Patrick Hannigan," January 27, 2023 and March 5, 2023, respectively.

Briaud and Tucker (1997) present a straightforward approach to computing the force balance equilibrium for a pile with structural and downdrag forces where a *neutral point* is defined as the depth where both the pile and soil displacement are the same. This corresponds to the depth where the negative side shear becomes positive (Figure 6.13). This is perhaps the most usable computation method based on force equilibrium (Eqn 6.1) which assumes the relative moment to activate side shear is so small that side shear is either positive or negative with no transitions for very small relative displacements on either side of the neutral point.

$$Q_t + F_n = F_p + Q_p \qquad \text{Eqn 6.1}$$

where,

Q_t = structural loads
F_n = force caused by downdrag or negative side shear
F_p = positive side shear, and
Q_p = end bearing force, pile tip force.

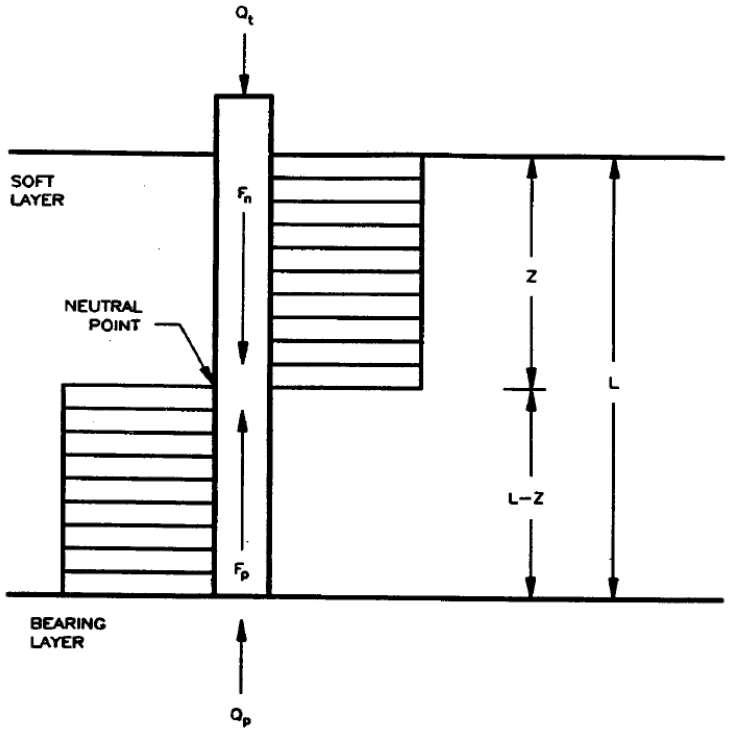

Figure 6.13 Static equilibrium for a pile subjected to structural and downdrag (Briaud and Tucker, 1997).

Regardless of the downdrag determination method, the soil settlement profile must be determined and compared to the pile displacement profile. The explicit method described by Briaud and Tucker (1997) computes a pile neutral point movement envelope where Equation 6.1 is solved at all depths assuming the neutral point were to exist at each depth. This requires the unit side shear to be known in each soil layer which lends itself well to the depth increments from a boring log and the side shear that is computed from any rational design method. Going back to the Research

Bulletin 121 by Schmertmann and updates to that work, side shear is easily computed using the SPT blow count and the soil type.

Equation 6.2 solves Equation 6.1 for Q_p and again any rational Q-z relationship can be used to determine the pile tip movement required to mobilize that level of end bearing resistance. The settlement at the neutral point (w_{np}) is determined by adding the pile tip movement to the elastic compression in the pile from between the pile tip to the assumed neutral point. Figure 6.14 shows the end bearing response to loading for the Paseo Al Mar pile. Where the equation solves as a negative end bearing or a value that exceeds ultimate, this indicates the equation cannot be satisfied and that condition is impossible. However, only one pile neutral point movement will coincide with the soil settlement profile. This process is usually performed where the soil settlement is only calculated to the tip of the pile. If the overall soil settlement is used, the pile tip movement must be added to the soil settlement value at the depth of the pile tip.

$$Q_p = Q_t + F_n - F_p \qquad \text{Eqn 6.2}$$

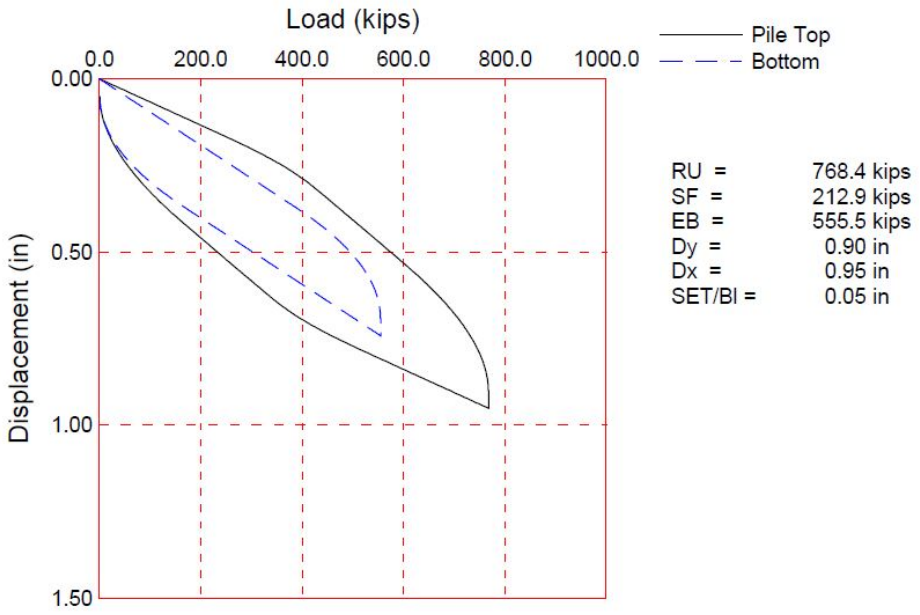

Figure 6.14 CAPWAP-modeled pile resistance for Test Pile 3 at Paseo Al Mar End Bent 3.

Figure 6.14 shows the maximum end bearing to be 556k and the overall pile capacity to be 768k. These values must be known either by estimated capacity or in this case from pile test results.

Using the top of pile load from the Paseo Al Mar site (162k measured), pile tipped at 53 ft, and the end bearing response from Figure 6.13, the displacement at the neutral point (w_{np}) was calculated for all depths to produce the w_{np} envelope and is shown in Figure 6.14. The w_{np} value again was computed by adding the elastic shortening between the tip of the pile and the assumed neutral point locations added to the end bearing movement $w_{piletip}$ required to mobilize the Equation 6.2 value for Q_p.

$$w_{np} = w_{pile\ tip} + \sum_{i=1}^{n} F_i L_i / (A_{pile} E_c) \qquad \text{Eqn 6.3}$$

At depths shallower than 30 ft, the computed end bearing using equation 6.2 gave negative values; this translates into no pile tip displacement but there is still elastic shortening which shows up as a non-zero but very small values in Figure 6.14. However, the neutral point must be below that depth. When equation 6.2 was solved at the toe of the pile the resulting value was 569k; hence if the neutral point is not found between these two limits the equilibrium solution does not exist. The solution is determined where the w_{np} envelope values intersect the soil settlement profile which in this case was at approximately 42.5 ft (Figure 6.15). Detailed computations for worksheet applications are provided in the Appendix for this case which are immediately adaptable to other sites.

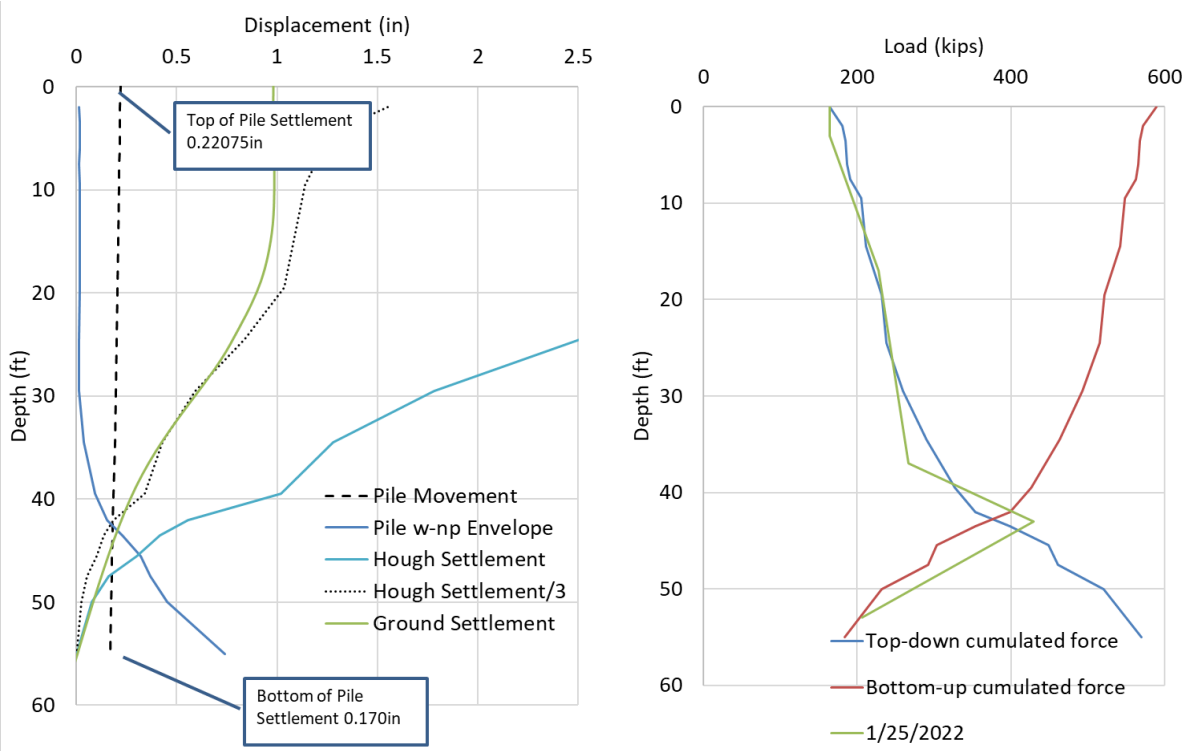

Figure 6.15 Neutral point located (left); neutral plane located (right) which agree with field results.

The neutral plane shown in Figure 6.15 (right) not only agrees with the location of the field measured depth but also the positive and negative force distribution and strain gauge measured end bearing force. An estimated soil settlement profile is typically used in determining the neutral point. In this case both field measurements and calculated values are shown. As noted earlier, calculated settlement values in sand often overestimate the magnitude of settlement by a factor of 2 to 3. The effect of overestimating settlement pushes the neutral point deeper (Figure 6.15, left), in this case by about 2ft. Using the calculated settlement divided by 3, values agree with the field values and the neutral point is very close to the field measured location.

The neutral plane method is very similar to the explicit method demonstrated above with the exception that the end bearing mobilization is often estimated at 0, 50, or 100% of the ultimate computed end bearing where the effect between 50 and 100% is minor (Seigel, 2013). This is where most applications tend to fall. The 100% end bearing case represents the worst-case structural loading in the pile. The end bearing movement required to mobilize a given force

equilibrium condition must be iteratively compared to ensure strain compatibility between the side shear and end bearing. However, unlike Briaud and Tucker (1997), no concise examples are provided to show how the user should precisely determine the percentage of end bearing. Figures 6.16 and 6.17 show the neutral plane method applied to the Paseo Al Mar and Sandridge Rd bridge site data. The effect of increasing top of pile and end bearing loads into the cumulated top-down and bottom-up side shear values is shown as structural load increased. The top-down curve incorporates the measured top of pile load while the bottom-up curve includes the measured end bearing force. The last curve (right) in each figure depicts the final loading condition with all permanent dead load as-measured.

In Figures 6.16 and 6.17 the pile tip movement required to mobilize the measured load was added to the measured soil settlement at the depth corresponding to the tip of the pile rather than zeroing the settlement at that depth. In general, the neutral plane from measured forces and neutral point from measured settlements agree. The shape of the predicted load distribution for both sites also agreed with the measured load distribution. However, the Sandridge Rd loads were approximately 25% higher than predicted.

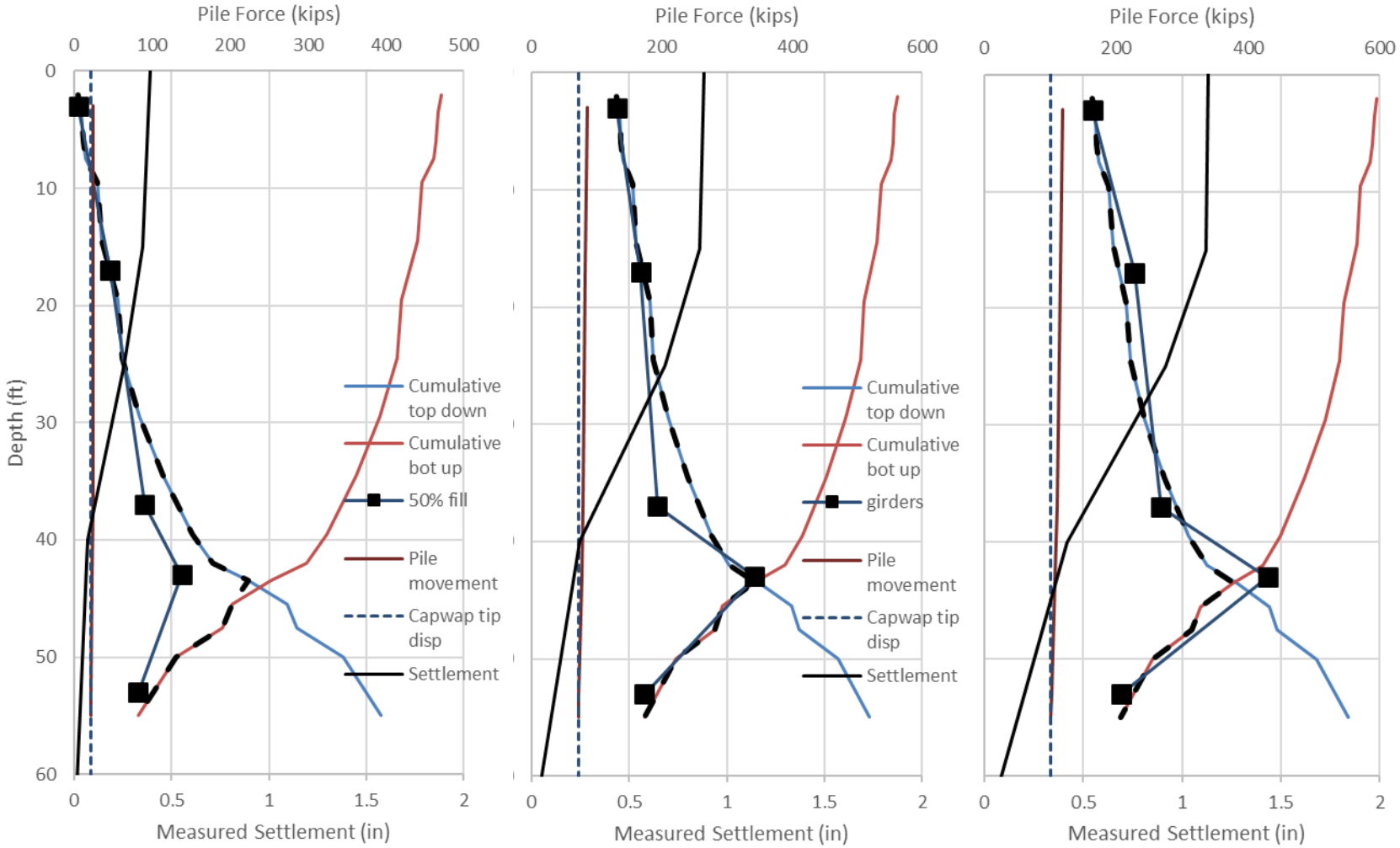

Figure 6.16 Predicted neutral plane versus measured pile load distribution (Paseo Al Mar Blvd)

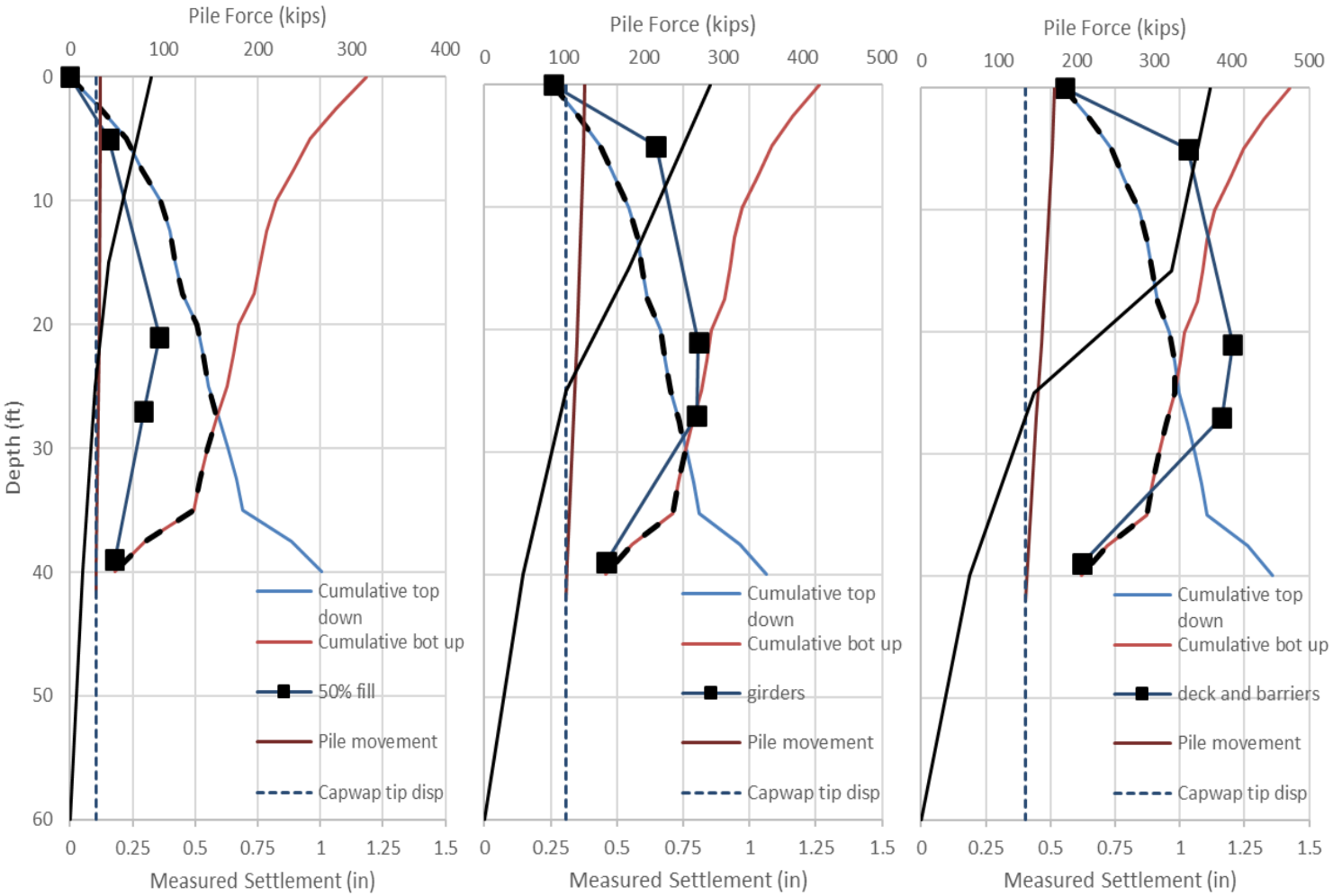

Figure 6.17 Predicted neutral plane versus measured pile load distribution (Sandridge Rd)

6.6 Recommendations

There are two prevailing approaches to assessing the effects of downdrag on the geotechnical and structural limit states. The first ignores DD in the geotechnical strength limit state where only the factored DL + LL is compared to the ultimate geotechnical pile capacity. The rationale there is a that DD and LL will not coexist in the pile at the neutral plane, and if the pile is pushed deep enough, it will eliminate negative side shear and regain that force as positive side shear. However, preliminary findings from this study showed approximately 21%-33% of non-permanent top of pile load was transferred to the neutral plane where the highest pile forces are experienced. This percentage only increases with more firmly embedded pile tips. Factored DL + DD is however checked in the limit states governing the pile structural capacity. Presently there is no load factor for sandy soils transferring DD forces into a pile.

In the second approach, DD is added to factored structural loads and must be resisted by the positive side shear and end bearing capacity. This approach is presented in AASHTO and is used by FDOT where the net pile resistance, R_{net}, subtracts the downdrag force, R_{dd}, from the ultimate pile capacity, R_{ult} (FDOT, 2020).

$$R_{net} = R_{ult} - R_{dd} \qquad \text{Eqn. 6.4}$$

and

$$NBR = (Factored\ Design\ Load + Net\ Scour + DOWNDRAG)\ /\ \emptyset \qquad \text{Eqn. 6.5}$$

The nominal bearing resistance, NBR, at the time of driving must provide the net capacity plus overcome the driving resistance offered by the downdrag soil layers, which are assumed to resist only 75% of the side shear that develops after driving and the soils have setup. Hence, the plan value for DOWNDRAG is $1.75R_{dd}$. The second approach is perhaps more appropriate given large amounts of settlement would be required to reverse the effects of the downdrag soil layers. The separation of the strength limits state from service limits state controlled by settlement is an unrealistic overlay from structural engineering that should be avoided in soil mechanics. For example, pile capacity from SPT analysis restricts end bearing to 1/3 ultimate to better match the displacement required for ultimate side shear. Unfortunately, this debate is likely to persist. Again, a pile with a firmly embedded tip will not allow the displacement required to reverse negative side shear strain and provide positive side shear resistance.

The original motivation for this study stemmed from the notion that compressible loose sandy soils do not pose a danger of overloading a pile due to the immediate nature of sand settlement. This is supported in part by the omission of a downdrag load factor in the AASHTO LRFD Bridge Design Specifications for piles in sand; hence, it has not been considered to be important. This study showed that downdrag from compressible sandy soil layers contributed significant loads to the pile which would cause Equation 6.5 to require far more nominal bearing resistance than any of the three sites noted in the respective plan sets.

Unless there is an FDOT change in philosophy regarding geotechnical strength limit states which might then disregard downdrag in the geotechnical limit state, the study findings support

computation of downdrag forces for all embankment end bent piles as force will always be transferred from settling soils. All studies reviewed herein note only a small relative movement between the pile and soil is required to engauge full side shear. The origins of the present 0.4 in (AASHTO) or 0.5-in (FDOT) differential soil-to-pile-movement criterion is unclear based on discussions with the authors of the most recent FHWA pile design guidelines (Mullins, 2023). Excluding portions of the piles that did not reach the 0.5-in threshold, for example, would have reduced the predicted Sandridge Rd downdrag force from 130k to 30k when compared to the measured downdrag force which reached 200k. This also supports the need for a downdrag load factor for piles in sandy soils; a 1.25 factor was suggested by Seigel (2013). The ongoing NCHRP 12-116A study is said to be addressing this.

The method of computing downdrag forces in piles outlined by Briaud and Tucker (1997) is the most rational design approach when considering downdrag as a top of pile load. It makes no distinction as to the magnitude of differential pile/soil movement but can be easily adapted to incorporate that parameter. The recommendation of this research is to adopt this methodology without a relative movement threshold which again is outlined in detail in the appendix. Further, a load factor is recommended for DD but with only limited data the 1.25 factor used for DL is reasonable. The load combinations considering DL and DD only was shown to be incorrect as transient loads are transferred to the neutral plane, but it is reasonable to use a reduced LL load factor when considering LL, DL, and DD together. Hence two load combinations to determine the worst-case loading might include:

$$1.25DL + 1.75LL + scour \leq \emptyset\, NBR \qquad \text{Eqn. 6.6}$$

$$1.25DL + 0.5LL + 1.25DD + scour \leq \emptyset\, NBR \qquad \text{Eqn. 6.7}$$

where

DD = 1.75 R_{dd} as outlined in the Soils and Foundations Handbook (FDOT, 2020)
and 0.5LL stems from 21 to 33%LL (27% avg) transmitted to peak pile force 0.27*1.75LL

6.7 Closing

At the time of this final report, one of the three bridges was complete and the other two were not in service. Limited live loading events were available to prove or disprove the claim that transient live loads do not add to maximum pile load when downdrag is present. The results from one bridge show the transient loads do add to the worst-case loads in the piles by 33%. Data collection systems continue to monitor and store data from the three sites which are uploaded hourly to USF. Live load events which could not be performed within the contract timeline of this study should be considered as a future project to fully implement the study outcomes. An extended monitoring period is recommended to capture highway speed events and verify long-term effects from seasonal changes in loads. Figures 6.18 - 6.20 show the latest state of the bridges.

Figure 6.18 Henley Rd bridge with girders but no deck in place


Figure 6.19 Sandridge Rd (study bridge right) used as haul road

Figure 6.20 Paseo Al Mar Blvd bridge in service

References

AASHTO (2017). "LRFD Bridge Design Specifications." American Association of State Highway and Transportation Officials, Washington, D.C.

Allen, T. M. (2005). *Development of Geotechnical Resistance Factors and Downdrag Load Factors for LRFD Foundation Strength Limit State Design*, U.S. Department of Transportation Federal Highway Administration, Washington, D.C.

Bakholdin, B. V., and Berman, V. I. (1974). "Investigation of Negative Skin Friction on Piles and Suggestions on Its Calculations." *Soil Mechanics and Foundation Engineering*, 11(4), 238-244.

Bozozuk, M. (1972). "Downdrag Measurements on a 160-Ft Floating Pipe Test Pile in Marine Clay." *Canadian Geotechnical Journal*, 9(2), 127-136.

Brand, E., and Luangdilok, N. (1975). "A Long-Term Foundation Failure Caused by Dragdown on Piles." *4th Southeast Asian Conference on Soil Engineering* Kuala Lumpur, Malaysia, 4-15 to 4-24.

Briaud, J. L., and Tucker, L. (1997). *Design and Construction Guidelines for Downdrag on Uncoated and Bitumen-Coated Piles NCHRP Report 393*, Transportation Research Board, Washington, D.C.

Budge, A. S., Dasenbrock, D. D., and Mattison, D. J. (2015). "A Synthesis of Pile Performance Monitoring Projects in Downdrag Environments in Minnesota." *IFCEE 2015*, 457-471.

Campbell Scientific (2020). "SP50-L, SP90-L, and SP305-L Solar Panels." https://s.campbellsci.com/documents/us/manuals/sp50-sp90.pdf. (January 27, 2021).

Campbell Scientific (2021a). "GRANITE VWIRE 305 8-Channel Dynamic Vibrating-Wire Analyzer." https://www.campbellsci.com/vwire305. (January 27, 2021).

Campbell Scientific (2021b). "CR6 Measurement and Control Datalogger." https://www.campbellsci.com/cr6. (January 27, 2021).

Campbell Scientific (2021a). "31315 Bulkhead Surge Protection Installed in Enclosure, Type N to SMA, 700 to 2700 MHz." https://www.campbellsci.com/31315. (January 27, 2021).

Campbell Scientific (2021b). "32262 2 dBd 4G/3G Multiband Omnidirectional Antenna with Mounting Hardware." https://www.campbellsci.com/32262 (January 27, 2021).

Campbell Scientific (2021c). "RV50X Industrial 4G LTE Cellular Gateway." https://www.campbellsci.com/rv50x (January 27, 2021).

Campbell Scientific (2021d). "COAXNTN-L RG8 Antenna Cable with 2 Type N Male Connectors." https://www.campbellsci.com/coax-ntn. (January 27, 2021).

Campbell Scientific (2021e). "ENC14/16 Weather-Resistant Enclosure, 14 x 16 inches." https://www.campbellsci.com/enc14-16 (January 27, 2021).

Campbell Scientific (2021f). "PS84 84 Ah Power Supply with 14 x 16 in. Enclosure." https://www.campbellsci.com/ps84. (January 27, 2021).

Campbell Scientific (2021g). "CM106B 7 to 10 ft Galvanized-Steel-Tubing Tripod with Grounding Kit." https://www.campbellsci.com/cm106b. (January 27, 2021).

Campbell Scientific (2021h). "SP50-L 50 W Solar Panel." https://www.campbellsci.com/sp50-l (January 27, 2021).

Cheney, R. S., and Chassie, R. G. (1982). *Soils and Foundations Workshop Manual*, Federal Highway Administration, National Highway Institute, Washington, D.C.

Cheney, R. S., and Chassie, R. G. (1993). *Soils and Foundations Workshop,* Publication No. FHWA-HI-88-009 (Revised); Federal Highway Administration, U.S. Department of Transportation, Washington, D.C., 382 pp.

Coyle, H. M., and Reese, L. C. (1966). "Load Transfer of Axially Loaded Piles in Clay." *Journal of the Soil Mechanics and Foundations Division*, 92(2), 1-26.
Davisson, M. (1993). "Negative Skin Friction in Piles and Design Decisions." *3rd Conference of the International Conference on Case Histories in Geotechnical Engineering*, University of Missouri--Rolla, Rolla, Missouri, 1793-1801.
Davisson, M., Manuel, F. S., and Armstrong, R. (1983). *Allowable Stresses in Piles*. Federal Highway Administration, Washington, D.C.
Dias, T., and Bezuijen, A. (2018). "Load-Transfer Method for Piles under Axial Loading and Unloading." *Journal of Geotechnical and Geoenvironmental Engineering*, 144(1), 04017096.04017091-04017096.04017099.
Engin, H. K., Brinkgreve, R. B. J., and van Tol, A. F. (2015). "Simplified Numerical Modelling of Pile Penetration – The Press-Replace Technique." *International Journal for Numerical and Analytical Methods in Geomechanics*, 39(15), 1713-1734.
FDOT (2020). "Soils and Foundations Handbook." Florida Department of Transportation.
Fellenius, B. H. (1972). "Down-drag on Piles in Clay due to Negative Skin Friction." *Canadian Geotechnical Journal*, 9(4), 323-337.
Fellenius, B. H. (1989). "Unified Design of Piles and Pile Groups." *Transportation Research Record*, 1169, 75-82.
Fellenius, B. H. (1997). "Piles Subjected to Negative Friction: a Procedure for Design. Discussion." *Geotechnical Engineering*, 28(2), 277-281.
Fellenius, B. H. (2006). "Results from Long-term Measurement in Piles of Drag Load and Downdrag." *Canadian Geotechnical Journal*, 43(4), 409-430.
FHWA (2001). "Load and Resistance Factor Design (LRFD) for Highway Bridge Structures," NHI Course No. 132068, FHWA HI-98-032, Federal Highway Administration, Washington, D.C.
Geokon (2021a). "Rebar Strainmeters (VW) Model 4911 - 4911A." https://www.geokon.com/4911-4911A. (January 27, 2021).
Geokon (2021b). "Rod-Type Borehole Extensometers Model 1150 (A-3), 1200 (A-4), 1250 (A-5)." https://www.geokon.com/content/datasheets/A3_A4_A5_Borehole_Extensometers.pdf. (January 27, 2021).
Geokon (2021c). "Displacement Transducers (VW) Model 4450." https://www.geokon.com/4450. (January 27, 2021).
Hannigan, P., Goble, G. Thendean, G. Likins, G. and Rausche, F. (1998). "Design and Construction of Driven Pile Foundations - Volume 1," FHWA-HI-97-013, Federal Highway Administration, Washington, D.C.
Hannigan, P. J., Rausche, F., Likins, G., Robinson, B., Becker, M., and Berg, R. R. (2016). *Design and Construction of Driven Pile Foundations – Volume I*. National Highway Institute, Washington, D.C.
Indraratna, B., Balasubramaniam, A., Phamvan, P., and Wong, Y. (1992). "Development of Negative Skin Friction on Driven Piles in Soft Bangkok Clay." *Canadian Geotechnical Journal*, 29(3), 393-404.
Jeong, S., Kim, S., and Briaud, J.-L. (1997). "Analysis of Downdrag on Pile groups by the Finite Element Method." *Computers and Geotechnics*, 21(2), 143-161.
Jeong, S., Ko, J., Lee, C., and Kim, J. (2014). "Response of Single Piles in Marine Deposits to Negative Skin Friction from Long-term Field Monitoring." *Marine Georesources & Geotechnology*, 32(3), 239-263.

Johannessen, I., and Bjerrum, L. (1965). "Measurement of the Compression of a Steel Pile to Rock due to Settlement of the Surrounding Clay." *Proc., Soil Mech & Fdn Eng Conf Proc/Canada/,*261-264.
Koerner, R. M., and Mukhopadhyay, C. (1972). "Behavior of Negative Skin Friction on Model Piles in Medium Plasticity Silt." *Highway Research Record* (405), 34-44.
Kuhns, G. (2008). "Downdrag in Pile Design: The Positive Aspects of Negative Skin Friction." *From Research to Practice in Geotechnical Engineering*, Geotechnical Special Publication, https://ascelibrary.org/doi/book/10.1061/9780784409626, 489-506.
Kuwabara, F., and Poulos, H. G. (1989). "Downdrag Forces in Group of Piles." *Journal of Geotechnical Engineering*, 115(6), 806-818.
Lambe, T. W., and Baligh, M. (1978). "Negative Friction" downdrag on a Pile"."
Matyas, E. L., and Santamarina, J. C. (1994). "Negative Skin Friction and the Neutral Plane." *Canadian Geotechnical Journal*, 31(4), 591-597.
Meyerhof, G. G. (1976). "Bearing Capacity and Settlement of Pile Foundations." *Journal of the Geotechnical Engineering Division*, 102(3), 197-228.
Phuong, N. T. V., van Tol, A. F., Elkadi, A. S. K., and Rohe, A. (2015). "Numerical Investigation of Pile Installation Effects in Sand Using Material Point Method." *Computers and Geotechnics*, 73, 58-71.
Poulos, H. G. (2008). "A Practical Design Approach for Piles with Negative Friction." *Proceedings of the Institution of Civil Engineers - Geotechnical Engineering*, 161(1), 19-27.
Samtani, N., and Nowatzki, E. (2006). *Soils and Foundations—Volumes I and II. Publications No.* FHWA NHI-06-088 and FHWA NHI-06-089, Federal Highway Administration, Washington, D.C.
Schmertmann, J. H., Hartman, J. P., and Brown, P. R. (1978). " Improved Strain Influence Factor Diagrams." *Journal of Geotechnical and Geoenvironmental Engineering*, (Tech Note), 104.
Seigel, T., Lamb, R., Dasenbrock, D. and Axtell, P. (2013). "Alternative Design Approach for Drag Load and Downdrag of Deep Foundations within the LRFD Framework," Proceedings of the 38th Annual Conference on Deep Foundations, 2013, Phoenix, AZ, 23-39.
Stanton, K., Motamed, R., Elfass, S., and Ellison, K. (2015). "An Evaluation of T-Z Analysis Methods." *40th Annual Conference on Deep Foundations,* Oakland, CA, September, 2015, 303-312.
Tan, S., and Fellenius, B. (2016). "Negative Skin Friction Pile Concepts with Soil-structure Interaction." *Geotechnical Research*, 3, 1-11.
Tawfiq, K. S. (1994). "Laboratory Investigation on Bitumen Coating and Polyethylene Sheeting for Downdrag Reduction in Piles: A Comparative Study." *Geotechnical Testing Journal*, 17(2), 171-184.
Tehrani, F. S., Nguyen, P., Brinkgreve, R. B. J., and van Tol, A. F. (2016). "Comparison of Press-Replace Method and Material Point Method for analysis of jacked piles." *Computers and Geotechnics*, 78, 38-53.
Vesic, A. S. (1969). "Load Transfer, Lateral Loads, and Group Action of Deep Foundations." *Performance of Deep Foundations*, R. Lundgren, and E. Appolonia, eds., ASTM International, West Conshohocken, PA, pp. 5-14.
Vesic, A. S. (1977). *Design of Pile Foundations. Synthesis of Highway Practice 42.* Transportation Research Board, Washington, D.C.

Wang, R., and Brandenberg, S. J. (2013). "Beam on Nonlinear Winkler Foundation and Modified Neutral Plane Solution for Calculating Downdrag Settlement." *Journal of Geotechnical and Geoenvironmental Engineering*, 139(9), 1433-1442.

Appendices

- Appendix A: Sample spreadsheet to determine the neutral point and neutral plane forces
- Appendix B: Campbell scientific data logger program for low and high-speed data acquisition

Appendix A: Example Neutral Point Determination Spreadsheet

- Spreadsheet requires input shown as bold and outlined cell ranges
- Unit side shear is determined from RB-121, FBDEEP, SPT97, FLPIER Appendix A or similar where pile type and soil type is needed and then multiplied by the SPT blow count.
- Neutral point requires the top of pile load Qt or Qtop be input.
- Soil settlement is input from measured or computed source down to the tip of pile where soil settlement is set to be zero.
- An end bearing vs pile tip displacement relationship should be know. A VLOOKUP function is used in this example from digitized data taken from a CAPWAP end bearing response.
- Equations listed reference cell locations in the provided sheet; adjustments to another spreadsheet layout will require tracking the changes in relative cell positions.
- Plot column A vs Column I and column A vs Column J to show intersection which corresponds to the neutral point where both the soil settlement and pile movement are the same

Neutral Plane Force Plot

- Columns A and E are plotted to give the top down cumulated force curve
- Columns A and L are plotted to give the bottom up cumulated force curve

	A	B	C	D	E	F	G	H	I	J	K	L	M	N	O
6	f'c	**10**	ksi												
7	pile modulu	**5700**	ksi												
8	pile area	**576**	in2												
9	pile size	**24**	in												
10	Qtop	**164**	kips												
11	Pile length	**55**	ft						w-np	Meas. or			Qp max	Pile	Actual
12			Unit						envelope	computed		Qp + Pp	+ Pp	Disp	Pile Force
13	Depth	SPT	side shear	Incr Force	Qt+Fn	Fp	Qp reqd	w-tip	w-np (pile)	w-soil		(kips)	(kips)	(in)	(kips)
14	(ft)	(N60)	(ksf)	(kips)	(kips)	(kips)	(kips)	(in)	(in)	(in)					
15	**0.00**				**164**							589.5	961.6	0.2198	164.0
16	**2.00**	**28**	1.06	17.0	181.0	357.1	-176.1	0.000	0.014	**1.552**		572.5	944.6	0.2185	181.0
17	**3.50**	**9**	0.35	4.2	185.2	340.1	-154.9	0.000	0.017	**1.381**		568.2	940.4	0.2175	185.2
18	**6.00**	**3**	0.10	2.0	187.2	335.9	-148.6	0.000	0.016	**1.326**		566.2	938.4	0.2158	187.2
19	**7.50**	**8**	0.30	3.6	190.9	333.8	-143.0	0.000	0.015	**1.191**		562.6	934.7	0.2148	190.9
20	**9.50**	**24**	0.91	14.6	205.4	330.2	-124.8	0.000	0.016	**1.141**		548.0	920.2	0.2133	205.4
21	**14.50**	**4**	0.15	6.1	211.5	315.6	-104.1	0.000	0.016	**1.088**		541.9	914.1	0.2095	211.5
22	**19.50**	**13**	0.51	20.2	231.7	309.6	-77.9	0.000	0.016	**1.034**		521.7	893.9	0.2055	231.7
23	**24.50**	**4**	0.15	6.1	237.8	289.4	-51.6	0.000	0.015	**0.839**		515.7	887.8	0.2012	237.8
24	**29.50**	**15**	0.56	22.2	260.0	283.3	-23.3	0.000	0.014	**0.594**		493.4	865.6	0.1966	260.0
25	**34.50**	**20**	0.76	30.3	290.4	261.1	29.3	0.023	0.037	**0.427**		463.1	835.3	0.1916	290.4
26	**39.50**	**24**	0.91	36.4	326.7	230.7	96.0	0.080	0.094	**0.340**		426.7	798.9	0.1860	326.7
27	**42.00**	**36**	1.36	27.3	354.0	194.3	159.7	0.141	0.155	**0.186**		399.4	771.6	0.1829	354.0
28	**43.50**	**99**	3.76	45.1	399.2	167.1	232.1	0.214	0.228	**0.139**		354.3	726.4	0.1809	354.3
29	**45.50**	**82**	3.13	50.1	449.3	121.9	327.4	0.305	0.320	**0.101**		304.1	676.3	0.1785	304.1
30	**47.50**	**20**	0.76	12.1	461.5	71.8	389.7	0.355	0.367	**0.054**		292.0	664.2	0.1763	292.0
31	**50.00**	**78**	2.98	59.6	521.1	59.6	461.5	0.443	0.452	**0.026**		232.4	604.5	0.1739	232.4
32	**55.00**	**32**	1.21	48.5	569.6	0.0	569.6	0.738	0.738	**0.000**		**183.8**	556.0	0.1701	183.8

Equation Listing by Cell

C16: =0.0002639*B16*144
D16: =A16*$B$9/12*4*C16
E16: =E15+D16
F16: =IF(A16>$B$11,error,IF(A16=$B$11,0,D16+F17))
G16: =E16-F16
H16: =IF(G16<0,0,VLOOKUP(G16,$AH$12:$AI$42,2))
I16: =($B$11-A16)*(G16+AVERAGE(F16:$F$31))/$B$8/$B$7*12+H16
L15: =L16+D16
M15: =M16+D16
N15: =N16+(O15+O16)/2/$B$8/$B$7*(A16-A15)*12
O15: =IF(E15<=L15,E15,L15)
All above equations copy down

Single Cell Values below
L32: Interpolate to get Qp required at neutral point using column A depth
And Column G Qp reqd values
E15: =B10
B6: input concrete strength f'c in ksi
B7: =57000*SQRT(B6*1000)/1000
B8: =B9^2 (assumes square pile)
B9: input pile size in inches (square in this case)
B10: input top of pile load in kips
B11: input pile length in feet

Array Values
A15:A32 depth inputs from boring log in feet
B15:B32 SPT blow counts converted to SPTN60 if automatic hammer
J15:J32 soil settlement data computed elsewhere from SPT depth increments else add depth column that corresponds to the settlement data at hand
AH12:AH42 input end bearing load response data or equation with relative fine disp increments
AI12:AI42 input displacement that corresponds to end bearing from column AH

	AH	AI
10	PDA	
11	Load (k)	Disp (in)
12	7.853403	-2E-05
13	28.79581	0.022896
14	49.73822	0.041965
15	65.44503	0.057229
16	89.00524	0.080125
17	107.3298	0.095369
18	136.1257	0.125916
19	154.4503	0.14116
20	178.0105	0.167902
21	206.8063	0.190757
22	230.3665	0.213653
23	256.5445	0.240375
24	280.1047	0.26327
25	303.6649	0.28232
26	321.9895	0.305256
27	342.9319	0.324325
28	358.6387	0.339589
29	376.9634	0.354833
30	397.9058	0.373903
31	416.2304	0.392992
32	439.7906	0.419734
33	460.733	0.44265
34	479.0576	0.469432
35	500	0.496194
36	513.089	0.523017
37	526.178	0.545993
38	541.8848	0.584333
39	552.356	0.622714
40	557.5916	0.65729
41	560.2094	0.691885
42	562.8272	0.738019

Appendix B: Example Data Collection Programming Code

```
'======= EXAMPLE PROGRAM =======
'GRANITE VWIRE 305 vibrating-wire analyzer
'Program to read 20 Hz dynamic data from one GRANITE VWIRE 305 analyzer measuring one channels
'Declare Public Variables

  Public DGage_Disp(3), DGage_Digits(3), DGage_DgC(3)
  Public DGage_Digits0(3) =  {         2357,           2357,           2357}
  Public DGage_DgCo(3)    = {          23.4,           23.4,           23.4}
  Public DGage_LGF(3)     =  {   0.0002335,    0.0002335,    0.0002335} 'inches per digit
  Public DGage_K(3)
  Dim    CR6VW(3,6)
' Alias  CR6VW(x,1)'Frequency_Hz
' Alias  CR6VW(x,2)'Amplitude_mVrms
' Alias  CR6VW(x,3)'SNR
' Alias  CR6VW(x,4)'NoiseFreq_Hz
' Alias  CR6VW(x,5)'DecayRatio
' Alias  CR6VW(x,6)'Thermistor_DgC
  Dim    iGage As Long

Public Freq(8)         'Dynamic Frequencies
Public Diag(8) As Long 'Diagnostic Code
Public StaticFreq(8)   'Static (1 Hz output) frequencies
Public Therm(8)        'Thermistor readings
Public DynStdDev(8)    'Std Deviation of dynamic freq during the most recent one-second

Const CPIAddress As Long = 1
Const SysOptions As Long = 0

'The following arrays are used to configure the GRANITE VWIRE 305. Refer to the CDM_VW300Config
'instruction used below

'                                    CH1         CH2         CH3         CH4         CH5         CH6         CH7         CH8
Dim ChanEnable(8) As Long = {          1,          0,          0,          0,          0,          0,          0,          0}
Dim ResonAmp(8) =           {     0.0020,     0.0020,     0.0020,     0.0020,     0.0020,     0.0020,     0.0020,     0.0020}
Dim MinFreq(8) =            {       1400,        290,        290,        290,        290,        290,        290,        290}
Dim MaxFreq(8) =            {       3200,       6000,       6000,       6000,       6000,       6000,       6000,       6000}
Dim OutFormat(8) As Long =  {          1,          1,          0,          0,          0,          0,          0,          0}
Dim Mult(8) =               { 3.54e-04,          1,          1,          1,          1,          1,          1,          1}
Dim Offset(8) =             { -2.752e+03,        0,          0,          0,          0,          0,          0,          0}
Dim SteinA(8) =             { 1.4051e-03, 1.4051e-03,        0,          0,          0,          0,          0,          0}
Dim SteinB(8) =             {  2.369e-04,  2.369e-04,        0,          0,          0,          0,          0,          0}
Dim SteinC(8) =             {  1.019e-07,  1.019e-07,        0,          0,          0,          0,          0,          0}
Dim RF_MeanBins(8) As Long =  {       10,         10,         10,         10,         10,         10,         10,         10}
Dim RF_AmpBins(8) As Long =   {       10,         10,         10,         10,         10,         10,         10,         10}
Dim RF_LowLim(8) =          {       290,        290,        290,        290,        290,        290,        290,        290}
Dim RF_HighLim(8) =         {      6000,       6000,       6000,       6000,       6000,       6000,       6000,       6000}
Dim RF_Hyst(8) =            {      1.00,       1.00,       1.00,       1.00,       1.00,       1.00,       1.00,       1.00}
Dim RF_Form(8) As Long =    {         0,          0,          0,          0,          0,          0,          0,          0}
```

```
'Configure the CDM-VW300 series device
CDM_VW300Config(VWIRE305,CPIAddress,SysOptions,ChanEnable, _
            ResonAmp,MinFreq,MaxFreq,OutFormat,Mult,Offset,SteinA,SteinB,SteinC, _
            RF_MeanBins,RF_AmpBins,RF_LowLim,RF_HighLim,RF_Hyst,RF_Form)

'Define Data tables

  DataTable(_1Hr,True,-1)
  DataInterval(0,1,Hr,10)
  Maximum(3,DGage_Disp(),IEEE4,False,False)
  Minimum(3,DGage_Disp(),IEEE4,False,False)
  Average(3,DGage_Disp(),IEEE4,False)
  StdDev (3,DGage_Disp(),IEEE4,False)
  Maximum(8,Freq()      ,IEEE4,False,False)
  Minimum(8,Freq()      ,IEEE4,False,False)
  Average(8,Freq()      ,IEEE4,False)
  StdDev (8,Freq()      ,IEEE4,False)
  EndTable

  DataTable(CRVW_Diagnostics,True,86400/5)
  Sample(3*6,CR6VW(1,1),IEEE4)
  EndTable


DataTable(DynamicFreq, true, -1)
  Sample(8, Freq(), IEEE4)          'Dynamic Frequency (20 Hz output)
  Sample(8, Diag(), IEEE4)          'Diagnostic code for the current dynamic reading
EndTable

DataTable(OneSecData, true, -1)
  Sample(8,StaticFreq(),IEEE4)      'Static Frequency reading (1 Hz output)
  Sample(8,Therm(),IEEE4)           'Thermistor reading : Ohms or DegC
  Sample(8,DynStdDev(),IEEE4)       'Std Deviation of dynamic freq (one second)
EndTable

'Define the program
BeginProg

  CpiSpeed(250)           '250 kbps, how fast the datalogger will operate the CPI bus.
                          'This value may need to be adjusted based on the number of
                          'VWIRE 305 modules and the total cable length.  Refer to the
                          'VWIRE 305 quick start guide for more information.

  Scan(50, msec, 500, 0)    '20 Hz / 50 msec scan rate

    CDM_VW300Dynamic(CPIAddress, Freq(), Diag())   'Get dynamic readings
    CallTable DynamicFreq

    If TimeIntoInterval(0,1,Sec) Then ' Process static data only once per second
      CDM_VW300Static(CPIAddress, StaticFreq(), Therm(), DynStdDev()) 'Get static data
      CallTable OneSecData
    EndIf

    CallTable(_1Hr)

  NextScan
```

```
  SlowSequence'#1

    Scan(5,Sec,3,0)

'\\3 each Geokon displacement gages:

  VibratingWire(CR6VW(),3,U1,1200,2800,1,0.01,"",60,1.4051E-3,2.369E-4,1.019E-7)

  For iGage= 1 To 3

    DGage_Digits(iGage)=CR6VW(iGage,1)^2/1000
    DGage_DgC(iGage)=CR6VW(iGage,6)
'\  Calculate thermal coefficient: K=((R1*M)+B)*G
'    For 12 inch Model 4420 displacement gage:
    Const M=  0.000424
    Const B= -0.6778
    DGage_K(iGage)=((DGage_Digits(iGage)*M)+B)*DGage_LGF(iGage)
'/
    DGage_Disp(iGage)=                (DGage_Digits(iGage)-DGage_Digits0(iGage))*DGage_LGF(iGage)
    DGage_Disp(iGage)=DGage_Disp(iGage)+(DGage_DgC(iGage)-DGage_DgCo(iGage))*DGage_K(iGage) '<--
Applies the temperature correction.

  Next

  CallTable(CRVW_Diagnostics)

'//

    NextScan

  EndSequence'#1

EndProg
```